

Tectonics

COMMISSIONED MANUSCRIPT

10.1029/2018TC005365



Key Points:

- We discuss current challenges in implementing and interpreting geologic and geomorphic data typically used in modern PSHA
- Topics include slip rates, earthquake recurrence, fault complexity, fault-scaling relations, topography, and enigmatic faults
- Creative new methods and advances in fundamental science behind triggering, complex rupture, earthquake clustering, fault scaling are needed

Correspondence to:

K. D. Morell,
kmorell@ucsb.edu

Citation:

Morell, K. D., Styron, R., Stirling, M., Griffin, J., Archuleta, R., & Onur, T. (2020). Seismic hazard analyses from geologic and geomorphic data: Current and future challenges. *Tectonics*, 39, e2018TC005365. <https://doi.org/10.1029/2018TC005365>

Received 30 AUG 2019

Accepted 24 SEP 2020

Accepted article online 2 OCT 2020

Seismic Hazard Analyses From Geologic and Geomorphic Data: Current and Future Challenges

Kristin D. Morell¹ , Richard Styron² , Mark Stirling³, Jonathan Griffin^{3,4} , Ralph Archuleta¹ , and Tuna Onur^{5,6}

¹Department of Earth Sciences, University of California, Santa Barbara, CA, USA, ²Global Earthquake Model Foundation, Pavia, Italy, ³Department of Geology, University of Otago, Dunedin, New Zealand, ⁴Community Safety Branch, Geoscience Australia, Canberra, ACT, Australia, ⁵Onur-Seemann Consulting, Inc., Victoria, British Columbia, Canada, ⁶The University of Victoria, Victoria, British Columbia, Canada

Abstract The loss of life and economic consequences caused by several recent earthquakes demonstrate the importance of developing seismically safe building codes. The quantification of seismic hazard, which describes the likelihood of earthquake-induced ground shaking at a site for a specific time period, is a key component of a building code, as it helps ensure that structures are designed to withstand the ground shaking caused by a potential earthquake. Geologic or geomorphic data represent important inputs to the most common seismic hazard model (probabilistic seismic hazard analyses, or PSHAs), as they can characterize the magnitudes, locations, and types of earthquakes that occur over long intervals (thousands of years). However, several recent earthquakes and a growing body of work challenge many of our previous assumptions about the characteristics of active faults and their rupture behavior, and these complexities can be challenging to accurately represent in PSHA. Here, we discuss several of the outstanding challenges surrounding geologic and geomorphic data sets frequently used in PSHA. The topics we discuss include how to utilize paleoseismic records in fault slip rate estimates, understanding and modeling earthquake recurrence and fault complexity, the development and use of fault-scaling relationships, and characterizing enigmatic faults using topography. Making headway in these areas will likely require advancements in our understanding of the fundamental science behind processes such as fault triggering, complex rupture, earthquake clustering, and fault scaling. Progress in these topics will be important if we wish to accurately capture earthquake behavior in a variety of settings using PSHA in the future.

Plain Language Summary Growing infrastructure and increasing population have caused significant loss of life due to recent large earthquakes, with the 2008 M_w 7.9 Wenchuan and 2005 M_w 7.6 Kashmir earthquakes each causing greater than 50,000 deaths. These earthquakes highlight the need for the development of building codes designed to withstand the strong ground shaking caused by earthquakes, as reinforced infrastructure is one of the most important factors for preventing fatalities due to ground shaking from earthquakes. Identifying the seismic hazard of a region, or the likelihood of ground shaking at a site due to potential earthquakes over time, is a key ingredient for informing a defensible building code. Here, we focus on current and future advances in how data from the fields of geology and geomorphology contribute to the most widely used type of seismic hazard model. These geologic data represent vital components to seismic hazard models, as they can provide information about the location and types of earthquakes that can occur over long, thousands of years, time periods, that cannot be obtained using other methods. We discuss some of the most pressing scientific issues about these data that are important for the development of seismic hazard models and defensible building codes.

1. Introduction: The Need for Seismic Hazard Analyses

Growing infrastructure and increasing population have led to significant loss of life and billions of dollars in damages as a consequence of large earthquakes throughout the past several decades. The two largest events to occur recently have been devastating (2011 M_w 9.1 Tohoku, 16,000 deaths; and 2004 M_w 9.1 Sumatra, 230,000 fatalities), primarily because of the tsunamis they generated. However, smaller seismic events near populated regions have been similarly destructive, largely due to the effects of ground shaking

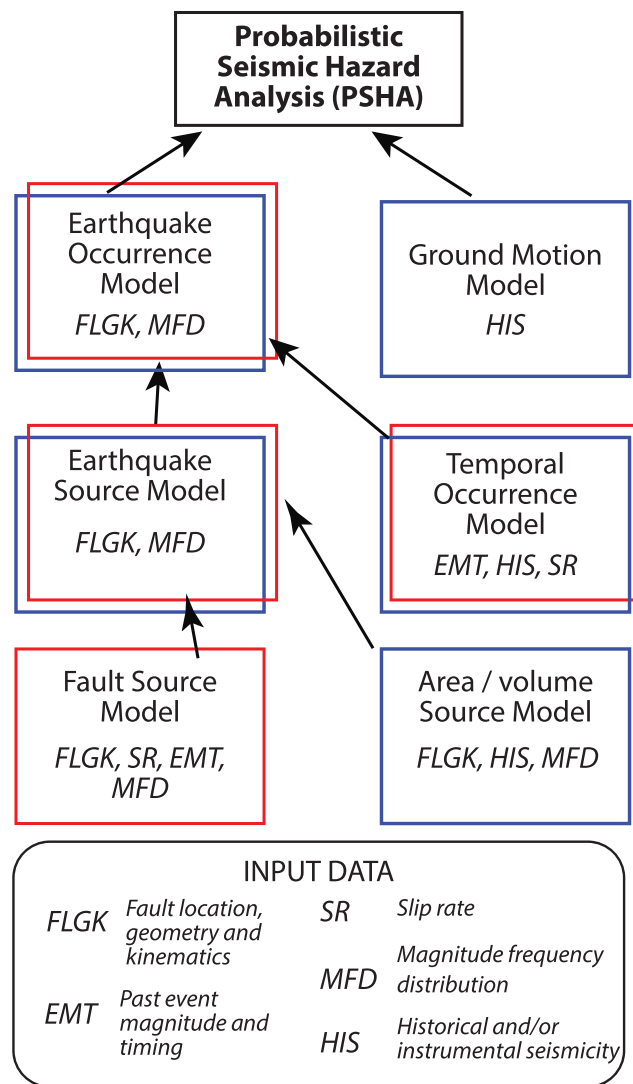


Figure 1. Schematic diagram illustrating common components of a probabilistic seismic hazard analysis (PSHA) model as used for seismic risk analysis and typical types of data sets that inform each component of the model. Blue boxes represent models with historical or instrumental seismicity data inputs. Red boxes represent models with geologic data inputs, the focus of this contribution.

(e.g., 2005 M_w 7.6 Kashmir, 90,000 deaths; 2008 M_w 7.9 Wenchuan, 69,000 deaths; and 2010 M_w 7.0 Haiti, 230,000 deaths). These latter examples highlight the need for seismically informed building codes, as reinforced infrastructure is often credited as one of the most important factors for preventing loss of life due to seismic events in populated regions (e.g., Bilham & Gaur, 2013). The quantification of seismic hazard is a key ingredient for informing a building code, because it is not cost effective to make structures entirely damage free at all levels of earthquake shaking.

An earthquake occurrence model, which provides the expected location, magnitude, and frequency of future earthquakes in a region, is an essential building block of a probabilistic seismic hazard analysis (PSHA) model, the most widely used type of seismic hazard model (Figure 1). Geologic or geomorphic data are vital components to PSHAs, as they can provide information about the magnitudes, locations, and types of earthquakes associated with long recurrence intervals (spanning thousands of years) that are largely absent from most historical, geodetic, or seismicity records (spanning tens to hundreds of years). Typical geologic or geomorphic data used to develop earthquake occurrence models include the location, kinematics and geometry of active faults; estimates of recurrence interval and slip rate; and estimates of previous rupture magnitude and timing (e.g., Field et al., 2014; Petersen et al., 2015). Paleoseismic trenching (e.g., Behr et al., 2010;

Sieh, 1978), the use of well-dated deformed geomorphic markers (e.g., Sieh & Jahns, 1984), and/or the application of fault-scaling relationships to offset features (e.g., Leonard, 2010; M. Stirling et al., 2013) remain the gold standard with which to obtain these geologic data, as they can provide information about fault slip rates and paleoearthquake magnitude, timing and recurrence interval over long (thousands of years) periods. However, several recent earthquakes and a growing body of literature have begun to challenge some of our long-standing assumptions surrounding the methods and types of geologic data sets that are frequently used in PSHA (e.g., S. Stein et al., 2012). In this paper, we begin with a brief introduction to PSHA and then discuss some of the most significant challenges in the use of geologic and geomorphic data in PSHA models. We also include our thoughts on the future directions these topic areas are, or may be, taking. This review paper is intended to be accessible to a broad audience of earth scientists, who may be interested in how paleoseismic and geomorphic data can be used in PSHA models.

2. Introduction to PSHA

PSHA quantifies the likelihood of earthquake-induced ground shaking at or above a specified intensity for a specific return period or probability, whereas seismic risk defines the likelihood of losses exceeding a value defined in the PSHA model. A typical PSHA model is constructed by combining earthquake occurrence models together with ground motion models (Figure 1). A ground motion model is usually developed by application of a ground motion prediction equation that quantifies the ground motions produced by a given earthquake and the surrounding crustal properties. An earthquake occurrence model is one of three major components of a seismic risk model. The other two components are (1) exposure models (e.g., Yepes-Estrada et al., 2017), which include databases of building stock and population, and (2) fragility models (e.g., Lovon et al., 2018), which describe the damages and losses expected for each class of item in the exposure model to different levels of ground shaking.

In a PSHA model, the probabilities or return periods of strong ground motions at a site or region are based on all potential earthquakes and their frequencies (Cornell, 1968; McGuire, 2004). One advantage of the PSHA method over other simpler methods (the “deterministic” approach; e.g., Bommer, 2002) is the ability to consider both the epistemic (model or knowledge) uncertainty in any parameter involved, as well as the aleatory variability (stochasticity or randomness) of earthquake occurrence and ground motions. The outputs of a typical PSHA model describe the frequencies or probabilities of exceeding a level of ground shaking (e.g., peak ground acceleration or velocity) in a given time period and are commonly framed in terms of ground motion exceedence probabilities or return periods. Hazard maps derived from these analyses show the level of ground shaking for a particular probability or return period, while hazard curves show the annual frequencies, probabilities, or return period for all computed ground shaking levels at a single site. Below we briefly describe each of the components that are typically used in the development of an earthquake occurrence model in a PSHA, emphasizing those that rely on geologic or geomorphic data sets (Figure 1).

2.1. Earthquake Source and Fault Source Models

An “earthquake source model” within a PSHA framework is usually constructed using both a “fault source model” derived from seismic, geologic, and/or geodetic data and an “area/volume source model” derived from geodetic and/or seismicity data sets (Figure 1). An area/volume source model is typically developed from the historical seismicity record and is used to account for the distributed earthquakes that can occur in the crustal volumes between known seismogenic faults, the possible presence of unmapped and/or unmodeled faults, and allowing for earthquakes to occur on unknown faults. A good example is the occurrence of the M_w 7.1 2010 Darfield, New Zealand, earthquake (Gledhill et al., 2011), which occurred on a previously unknown fault. This earthquake was effectively accounted for in the distributed seismicity model of the 2010 New Zealand National Seismic Hazard Model, which had a maximum magnitude set at 7.2 (M. Stirling et al., 2012).

Typically, there are two main components of a fault source model used in PSHA. The first is a 3-D surface that represents the fault through the seismogenic portion of the crust. The simplest method for the creation of this fault surface is the projection of a mapped fault trace to depth at a constant dip, although more complexity can be incorporated if warranted. The second main component is a magnitude-frequency distribution, which describes the range of potential earthquakes that can be generated on the fault and the occurrence rates of those earthquakes. Commonly used magnitude-frequency distributions include the characteristic distribution (Youngs & Coppersmith, 1985), where the majority of seismic moment release occurs on the

largest earthquakes that rupture the full fault surface, and the truncated Gutenberg-Richter distribution, where seismicity follows the Gutenberg-Richter relation (Gutenberg & Richter, 1944) up to some maximum magnitude (e.g., Wesnousky et al., 1984). In the absence of more definitive data (such as a major historical earthquake), a fault's maximum earthquake magnitude is often estimated using fault-scaling relationships, which are empirical regression equations that relate fault dimensions to earthquake magnitude (e.g., M. Stirling et al., 2013; Wells & Coppersmith, 1994). The rates of earthquakes of a given magnitude are generally determined using paleoearthquake data when available, or fault slip rates if paleoearthquake data are unavailable.

Although there are many approaches for this analysis, fault slip rates are often translated into earthquake occurrence rates through seismic moment balancing:

$$\mu A \dot{D}(f_s) = \dot{M}o = \int_{M_{\min}}^{M_{\max}} r(M) Mo(M) dM.$$

$\dot{M}o$ is the seismic moment release rate. On the left-hand side of the equation, μ is the shear modulus, A is the area of the fault, and \dot{D} is the slip rate; these parameters determine the rate of strain energy release as slip on the fault. f_s is the fraction of the total moment rate that is released seismically, as aseismic processes such as creep and afterslip contribute to fault displacement, but not as hazardous, energetic seismic moment release; this parameter is challenging to estimate if not actually observed (e.g., some subduction zones and specific faults in California) and therefore not always incorporated. On the right-hand side, $r(M)$ is the annual occurrence rate of earthquakes of magnitude M , and $Mo(M)$ is the seismic moment for an earthquake of magnitude M . In the common case that the magnitude frequency distribution is discretized to finite magnitude “bins,” the integral is replaced by a summation of the bins.

2.2. Earthquake Occurrence and Temporal Occurrence Models

The final earthquake occurrence model, which describes the location, size, and frequency of potential earthquakes, incorporates the information from the earthquake source model together with a temporal occurrence model (Figure 1). A temporal occurrence model describes the statistical distribution of the interevent times of earthquakes of a given magnitude. In other words, the temporal occurrence model describes how earthquakes of various sizes are temporally distributed on a fault over time. The most commonly used temporal occurrence models are the Poisson model, in which earthquakes are modeled as occurring randomly in time with no memory of previous occurrences, and at a fixed mean rate; and a quasiperiodic model, in which earthquakes occur more regularly in time. Poisson occurrence models provide “time-independent” hazard, because the probability of the next event occurring at any time in the future is independent of the elapsed time since the previous event, whereas other temporal occurrence models are “time dependent.” These are described in more detail in section 4.

2.3. Outstanding Questions and Future Directions

Although PSHAs have relied on geologic data for quite some time (e.g., Cornell, 1968), questions and challenges remain in how to properly use, interpret, and/or incorporate geologic and geomorphic data sets into earthquake occurrence models. In the following sections we discuss some of these important topics and outstanding issues, including new developments and uncertainties in slip rate estimation, understanding and modeling the temporal distribution of fault activity, the implications of rupture complexity, the development and use of fault-scaling relationships, and the identification and characterization of enigmatic faults using topography and geomorphology. Making progress in these topics will in turn contribute to the development of defensible building codes.

Other important components of PSHA that will not be treated in this paper include the shape of the magnitude-frequency distribution on faults (e.g., Field et al., 2017; Kagan et al., 2012; M. W. Stirling et al., 1996; Wesnousky, 1994), future directions in seismic attenuation relations and ground motion prediction equations, and the statistical evaluation of hazard models. We also do not discuss the large variety of geological (e.g., Korup, 2012), biological (e.g., Yang et al., 2018), and anthropological processes (e.g., Rodríguez Pascua et al., 2013) that are impacted by seismic events or the study of hazards due to tsunamis (e.g., Grezio et al., 2017), earthquake-induced landsliding (e.g., Gallen et al., 2015), or liquefaction (e.g., Obermeier, 1996). These topics are all areas of active research, and advances in understanding earthquakes and seismic hazard will help push investigations in those areas.

3. Fault Slip Rates and Seismic Hazard

Fault slip rates are primary quantities used in creating fault sources for PSHA and one of the areas in which geologic study greatly contributes to the understanding and mitigation of seismic hazard and risk (see section 2). In the context of PSHA, the utility of a slip rate estimate depends primarily on how accurately the slip rate estimate forecasts seismicity on a fault over the next several decades. Slip rates are currently estimated over a great range of timescales, roughly 10^1 (e.g., Bendick et al., 2000) to 10^7 years (e.g., Friedrich et al., 2003), and via a wide variety of methods. These methods all estimate slip rates by measuring the distance of fault offset (ideally in the direction parallel to the slip vector of earthquakes on the fault), divided by the time over which that offset accumulated.

Hazard modelers are often tasked with selecting a slip rate and associated uncertainties to include in the PSHA model by synthesizing available fault slip rates, which may be derived from a range of methods. Currently, there is no single accepted method of synthesizing slip rates taken by different methods, over different time intervals. Generally, the hazard modeler must evaluate the accuracy and uncertainties associated with each slip rate estimate and decide whether they are mutually exclusive or not. Here, we first briefly review the most common techniques for slip rate estimation over time periods of interest for seismic hazard (i.e., early Quaternary to present), with a focus on recent advances, and their sources of uncertainty. We then discuss the utility of each method in PSHA. Although this contribution is focused generally on geologic and geomorphic data sets, we also include a discussion of geodetic techniques in slip rate estimation, because they are frequently combined or considered jointly with geologic data in PSHA (e.g., Bird, 2009; Bormann et al., 2016; Loveless & Meade, 2011; Osokin et al., 2007; Penarubia et al., 2019; Wesnousky et al., 2012).

3.1. Geodesy: GNSS and InSAR

Geodetic measurements from Global Navigation Satellite Systems (GNSS) and synthetic aperture radar interferometry (InSAR) can provide a decadal rate of slip on a fault and are frequently used in conjunction with other slip rate methods in PSHA. GNSS-derived slip rates are generally computed from single-point velocity measurements relative to a fixed reference frame (Argus et al., 2010; Dixon, 1991) using either a 1-D velocity profile across a fault (e.g., Bendick et al., 2000; Franco et al., 2012) or a 2-D block model (e.g., Evans et al., 2015; Prawirodirdjo et al., 1997). One-dimensional profiles are simpler to construct but may not fully account for the effects of nearby faults, strain partitioning, or any vertical axis rotation that are usually included in block models (Minster & Jordan, 1987; Meade et al., 2002). However, the slip rates derived from GNSS block models can be sensitive to the geometry and configuration of blocks, as well as the spatial distribution of GNSS data points. This effect can be diminished if the location and geometry of the faults derived from other methods can be incorporated into the model (Flesch & Bendick, 2007; Herbert, Cooke, & Marshal, 2014).

InSAR is used to quantify decadal-scale interseismic fault slip rates by measuring variations in the returned phase of satellite-based radar signals sent at different times (J. R. Elliott et al., 2008; Massonnet & Feigl, 1998; Rosen et al., 2000). InSAR produces a fairly continuous 2-D deformation field spanning tens of kilometers and therefore offers a wider spatial coverage than GNSS. This wider coverage can illuminate along-strike changes in fault behavior over large areas (Wright, 2004), facilitate the identification of creeping faults (e.g., Barnhart, 2017; Shirzaei & Brägmann, 2013), and quantify fault geometry at depth (e.g., Lindsey & Fialko, 2013). Although InSAR is sensitive to surface and atmospheric perturbations that can remove the spatial coherence of the signals (J. R. Elliott et al., 2008; Massonnet & Feigl, 1998), these effects can be mitigated by using a large number of interferograms from multiple satellites with varying look angles, sophisticated processing techniques (e.g., Hetland et al., 2012; Jolivet et al., 2014), and identifying consistently identifiable features in otherwise incoherent interferograms (i.e., “persistent scatterers” Hooper, 2008).

Because geodetic techniques provide decadal-scale measurements, the slip rates derived from them can be considered instantaneous surface slip rates that span only a fraction of the earthquake cycle on a given fault. Thus, geodetic slip rates may be biased by the position of the geodetic measurement within a complex and incompletely understood earthquake cycle (Cohen & Kramer, 1984; Savage & Prescott, 1978). As we describe below, geologic techniques that can provide records spanning the Quaternary are often required to estimate slip rates over many seismic cycles.

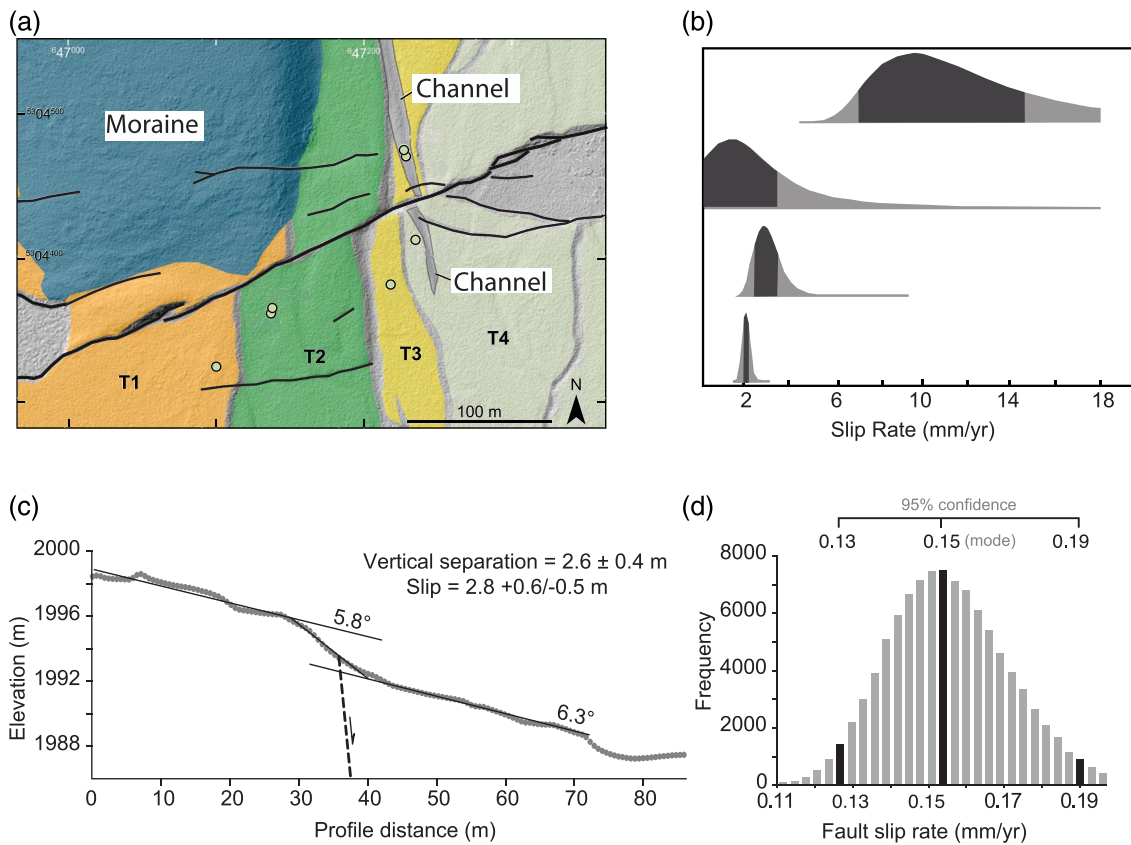


Figure 2. Examples of slip rate calculations based on offset Quaternary geomorphic features from Zinke et al. (2019) and Amos et al. (2010). (a) Interpreted lidar topography from Zinke et al. (2019) showing right-laterally offset fluvial channel and terrace sequence across the Clarence Fault in New Zealand. Green dots denote location of IRSL samples. (b) Incremental fault slip rates calculated based on stratigraphy and IRSL dating of samples and offsets measured by backslipping the lidar topography in (a) (Zinke et al., 2019). Probability distribution functions (gray PDFs) were generated using Monte Carlo simulations (95% confidence interval in black). Parts (c) and (d) show slip rate results from Amos et al. (2010) for the Kern Canyon Fault Zone in Southern California. Part (c) shows a topographic profile of a moraine crest offset by the fault, generated from bare-earth lidar data. Vertical separation was estimated using linear regression of the moraine crest elevations on either side of the fault and was converted to a total slip estimate using a range of constraints on fault dip geometries varying between 60° to 90° in dip. These results, together with CRN surface exposure ages that constrain the moraine to ~ 18 ka in age, were used to compute the vertical slip rate estimates shown in part (d) using a Monte Carlo simulation.

3.2. Quaternary Geologic Slip Rates

A “geologic slip rate” is often referred to in the seismic hazard literature as a slip rate derived from any geologic method (e.g., Petersen et al., 2014); thus, the term can refer to a large array of methods that may estimate slip rates spanning 10^2 to 10^7 years (Friedrich et al., 2003). Here we focus our discussion on slip rates derived from offset Quaternary markers (e.g., Lavé & Avouac, 2000; Sieh & Jahns, 1984; Zielke et al., 2010) and paleoseismic trenching (e.g., Scharer et al., 2007), as these are some of the most common types of geologic slip rate estimates spanning the early Quaternary to present, which is the time period most commonly considered in PSHA.

3.2.1. Offset of Quaternary Markers

Quaternary fault slip rates derived from deformed Quaternary surfaces or features are commonly estimated using (1) coseismic offset measurements of Quaternary geologic unit(s), geomorphic surfaces, or features and (2) numerically derived constraints of the feature or surface (e.g., Sieh & Jahns, 1984). This type of slip rate measurement assumes that the fault was already active at the time the unit was deposited and remains so at the time of measurement and that the offsets record surface displacements caused by faulting processes. Formerly sublinear Quaternary geomorphic markers, such as channel thalwegs, interfluves, moraine crests, debris flow levees, or fluvial terrace risers, are common piercing points used for this type of analysis, as they can be used to provide measurements of both vertical and lateral coseismic fault offset (e.g., Haddon et al., 2016). Originally, subplanar Quaternary geomorphic surfaces, such as fluvial or marine terrace treads, or colluvial, debris flow, or alluvial fan surfaces are also often used (e.g., Amos et al., 2010). The age of the

offset feature can be bracketed by any appropriate Quaternary dating method. Radiocarbon, luminescence, and cosmogenic radionuclide dating are the most common (see section 3.2.3).

The offsets used in these slip rate calculations are increasingly measured with high-resolution topography derived from GNSS surveys (e.g., Lifton et al., 2015), aerially or terrestrially captured light detection and ranging (lidar) measurements (e.g., Frankel et al., 2007; Wilkinson et al., 2015) or photogrammetric techniques such as “structure from motion” derived from digital photography (Bemis et al., 2014; Gao et al., 2017; K. Johnson et al., 2014). These techniques are routinely used to estimate coseismic offsets with submeter or subcentimeter accuracy, by reconstruction of the topography of the former piercing point geometry (e.g., Bi et al., 2018). Offsets are commonly reconstructed by backslipping the current topography along a fault, until the offset piercing point is restored to its original, undeformed geometry (e.g., Frankel et al., 2007). For example, Zinke et al. (2019) computed four increments of late Pleistocene to Holocene right-lateral offset (averaging multiple meters) along the Clarence Fault in New Zealand by restoration of a sequence of offset terraces, channel systems, and other markers to their original positions (Figure 2a).

Vertical separation of originally subplanar or sublinear features are also frequently used to calculate fault offsets as part of a slip rate calculation, using linear regressions of 2-D topographic profiles on either side of a fault scarp (e.g., Thompson et al., 2002). For example, Amos et al. (2010) measure the vertical separation of late Quaternary moraine crests offset across the Kern County fault of Southern California to calculate several meters of normal fault offset since ~18 ka in the southeastern Sierra Nevada region (Figure 2c). However, vertical separation measurements from 2-D topographic profiles can only constrain the vertical component of the fault slip vector, and knowledge of fault geometry and kinematics may be required to compute an offset measurement in three dimensions (Mackenzie & Elliott, 2017; Zechar & Frankel, 2009). If the fault geometry and rake of past fault slip are poorly constrained, Monte Carlo simulations are often used to place bounds on the most probable fault dip and offset amount given the topography of the fault scarp and its intersection with the surrounding surface morphology (e.g., Amos et al., 2010; Mackenzie & Elliott, 2017; Thompson et al., 2002). Constraints on fault geometry and kinematics can also be obtained if combined with structural geologic techniques such as the construction and sequential restoration of balanced cross sections or unfolding folded features (Amos et al., 2007; Jobe et al., 2017; Ren et al., 2013; Veloza et al., 2015).

There are several advantages to using these types of methods in Quaternary slip rate calculations that are relevant to PSHA. First, the offset measurement can include off-fault deformation that may have accumulated at significant distances away from the fault. Off-fault deformation has been shown to potentially account for a significant portion of the total strain within a region (~40% in the eastern California shear zone, USA) (Herbert, Cooke, Oskin, & Difo, 2014). Measurements of fault offsets made on or very close to the fault scarp may not record moderate earthquakes that do not break the surface, but these same earthquakes have been demonstrated to produce surface deformation at distances away from the fault (Fialko et al., 2005; Ryder et al., 2012). Second, so long as there are sufficient piercing points, offset measurements can be sampled at multiple points along strike and can therefore help capture any potential along-strike variability in fault slip and fault kinematics (e.g., Zielke et al., 2012). Third, the method is routinely used to estimate coseismic offsets spanning the Quaternary or longer, which can provide important information about fault slip over several seismic cycles (Sieh & Jahns, 1984).

Despite these advantages, several complications can introduce uncertainties into the fault slip estimate that are difficult to quantify. Postdepositional modifications of the offset marker by faulting, burial, or erosion can inhibit preservation and accurate measurement of offsets (Reitman et al., 2019). For example, Gold et al. (2009) demonstrate that progressive faulting along a strike-slip fault can shelter and preserve offset fluvial terraces on one side of a fault while leaving terraces on the other side susceptible to further fluvial modification (erosion or refreshment) and offer strategies for calculating epistemic uncertainty in such systems. It can often also be difficult to tightly constrain the age of seismic events that produced the faulted feature, and this lack of event timing can introduce uncertainty into the slip rate estimate. For example, the slip rate estimate could be biased if there is a significant time lapse between the age constraints available for the initial formation of the undeformed feature and the time of the earthquake that offset it (i.e., an open interval) (Styron, 2019).

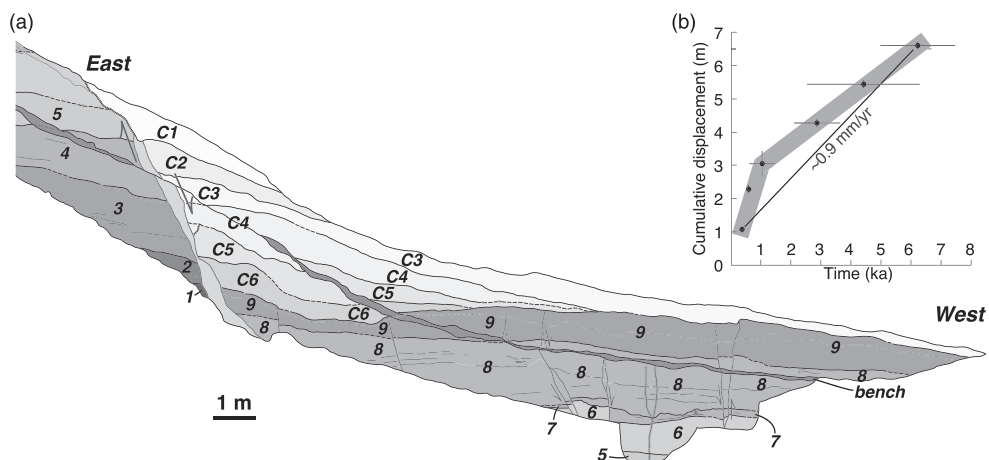


Figure 3. Figure from Bennett et al. (2018) showing simplified log of a paleoseismic trench across the Wasatch Fault in part (a) and slip rate calculated in this study in part (b). Numbers in part (a) refer to trench units, and C1–C6 refer to colluvial wedges associated with ground-rupturing earthquakes on the Wasatch Fault. Part (b) shows event history and cumulative displacement results used to calculate a closed-interval vertical slip rate of ~0.9 mm/year for this portion of the fault, time-averaged over the time period of ~6–0.5 ka. Event timing constrained by OxCal model (Bronk Ramsey, 2009) incorporating OSL and radiocarbon dating of trench units, stratigraphy, structure, and other relationships observed in the trench and surrounding region (Bennett et al., 2018).

3.2.2. Paleoseismic Trenching

Paleoseismic trenching can provide valuable data necessary for a robust, multievent slip rate calculation, including numerical ages of previous surface-altering earthquakes, and estimates of per-event and cumulative offset amounts (e.g., Scharer et al., 2007). For the purposes of slip rate estimation for PSHA, a successful trenching campaign will ideally expose diagnostic evidence of multiple paleoearthquakes, piercing points that allow per-event displacement estimates, and an abundance of dateable material that can bracket event ages (McCalpin, 2009). Both incremental and cumulative fault slip rates can be estimated by dividing the measured codisplacements by one or more interevent times associated with that displacement (e.g., DuRoss et al., 2019). Interevent times used in slip rate calculations from paleoseismic trenching are commonly bracketed using the same Quaternary numerical dating techniques as those used to constrain the age of offset Quaternary markers (see section 3.2.3 for more information).

The evidence for paleoearthquakes in a paleoseismic trench varies widely by site and tectonic setting but is usually based on observations such as offset or deformed marker layers (often Quaternary sediments), the presence of scarp-derived colluvial wedges, crosscutting relationships such as upward terminations of fault or unit contacts, and many other observations that are site specific. Although these types of observations are routinely used to identify paleoearthquakes spanning relatively long time periods (from 10^2 to 10^5 years), the technique may not expose all recent events hosted by a fault. Because paleoseismic trenching can only recognize surface-altering events visible within the walls of the trench, it may not record those events that are older than the exposed preserved stratigraphy, those that ruptured on a deeper portion of the same fault but did not rupture to the surface, or those that might have occurred on an adjacent fault strand among a wider fault zone (off-fault deformation) (Biasi & Weldon, 2006; Hemphill-Haley & Weldon, 1999). The records exposed within a trench may also be biased by prior landscape-altering events, such as glaciations, fluvial erosion, or any other erosional events which serve to shorten the stratigraphic record. All of these factors, among others, could lead to an underrepresentation of the number of earthquakes attributed to a single fault and could in turn affect the resultant slip rate calculation used in PSHA.

The exposures revealed in a paleoseismic trench can also be used to measure offsets suitable for a slip rate calculation, using piercing points identified within the trench walls (e.g., Morell et al., 2018). Per-event offset estimates can be directly measured with a tape in the trench walls using piercing points such as a key bed in the stratigraphy, crosscutting relationships between trench units or faults, or other site-specific relationships (Figure 3). If piercing points are not observed, other inferences are frequently employed to provide estimates of total surface rupture associated with an event. For example, the thickness of a scarp-derived colluvial

wedge observed in a paleoseismic trench can be assumed to equal half of the scarp height associated with a ground-rupturing dip-slip earthquake (e.g., Bennett et al., 2018; Swan III et al., 1980).

However, these types of measurements typically only represent minimum estimates of total coseismic fault offset associated with past ground-rupturing earthquakes. Trenches are often not oriented perfectly with respect to the slip vector of a past event, in which case the fault displacement measured in the plane parallel to the trench wall is only a component of the total coseismic displacement (e.g., Sherrod et al., 2016). In strike-slip settings, this problem is often partially addressed if multiple perpendicular trenches are excavated across a fault (e.g., Personius et al., 2014), but the orientation and excavation of trenches are often subject to site-specific conditions that may preclude the excavation of a perfectly oriented trench. Moreover, it is often the case that fault strands exposed within the trench walls may not contain adequate piercing points or other information needed to estimate offset measurement for individual events, in which case cumulative displacements are routinely inferred for more than one event (e.g., Morell et al., 2018).

3.2.3. Common Quaternary Numerical Dating Methods Used in Geologic Slip Rate Calculations

Quaternary numerical methods commonly used in geologic slip rate calculations include radiocarbon, optically and infrared-stimulated luminescence (OSL and IRSL, respectively), cosmogenic radionuclide dating, uranium series, dendrochronology, and many others (Cortés et al., 2012; Lienkaemper & Ramsey, 2009; Tsodoulas et al., 2016). It is generally best practice to obtain as many ages as possible from separate samples of the relevant units, features, or surfaces and to utilize multiple dating methods. However, the local conditions, composition, geometry, or stratigraphy often require that one method is preferred over the others, and important features may be difficult to date with any method. Here we discuss some of the greatest advantages, disadvantages, and sources of uncertainty in the most common dating methods and their application to slip rate calculations.

Radiocarbon dating is perhaps the most commonly used method in Quaternary slip rate calculations, due to its abundance, precision, and utility for establishing dates within the ~45 ka to present time period (McCalpin, 2009). Radiocarbon dating of detrital charcoal samples extracted from sedimentary units is one typical application. For example, paleoearthquake ages are commonly bracketed in paleoseismic trenches by radiocarbon dating of detrital charcoal extracted from preearthquake and postearthquake stratigraphy, and these data are used to calculate interevent times used in slip rate calculations (e.g., Hatem et al., 2019). However, there many ways that radiocarbon dating of detrital charcoal can either overestimate or underestimate the true depositional age of an important unit used in a slip rate calculation. Overestimation of the depositional age of a Quaternary unit (radiocarbon sample age is apparently older than the depositional age) can occur if charcoal from an older deposit is recycled into a younger unit, or if the time of death of the organic matter occurs significantly before the deposition or the unit (Gavin, 2001). Detrital radiocarbon samples can also provide underestimated ages within a deposit (younger age than the depositional age) due to postdepositional mixing from bioturbation or root growth or contamination by modern carbon regrowth (e.g., Busschers et al., 2014).

OSL and IRSL are popular tools used to date Quaternary units, and these techniques are often used in conjunction with radiocarbon in slip rate calculations (e.g., Bennett et al., 2018; Forman et al., 1991; Ortúñoz et al., 2012). The most commonly used luminescence methods rely on dating the last time grains of quartz (in the case of OSL) or feldspar (in the case of IRSL) within the unit were exposed to sunlight and subsequently buried (Aitken, 1998). Luminescence dating is capable of dating sediments beyond the age limit of radiocarbon (i.e. >45 ka) and is most reliable if the targeted deposit is well preserved and contains unweathered quartz or feldspar grains that have been sufficiently exposed to light immediately prior to burial (well bleached). Apparently, old luminescence ages can occur due to partial bleaching during deposition (Gray et al., 2015), and apparently, young luminescence ages can also arise due to postdepositional mixing from burrowing and root growth, similar to radiocarbon.

The continued development of Quaternary dating methods that rely on measurements of the concentration of terrestrial cosmogenic radionuclides (TCN) near Earth's surface has led to increasing accuracy of dated materials used in Quaternary slip rate methods, as well as a broadening of the range of features that can be dated (Gosse & Phillips, 2001; Hidy et al., 2010; Marrero et al., 2016). This dating technique assumes that the concentration of rare nuclides (such as beryllium-10) within grains or clasts near the targeted surface reflects the time that the nuclides have accumulated in situ due to bombardment by cosmogenic rays (Lal, 1991). A

surface exposure age is often calculated using the concentration of the nuclide, a latitudinally adjusted production rate, and assumptions or constraints on the amounts of local shielding, radioactive decay, erosion, bulk density, inheritance, and other factors (see Granger et al., 2013). Surface exposure dating derived from concentrations of beryllium-10 in quartz is one of the most applied techniques and is a particularly popular technique used to estimate the ages of offset Quaternary geomorphic or geologic features used in slip rate calculations (e.g., Amos et al., 2010). However, many other systems such as aluminum-26, chlorine-36, neon-21, and helium-3 could also be used, and all of these systems can be applied in a number of other ways that we do not discuss here (e.g., burial dating, fault scarp dating, or erosion rate estimation) (Balco, 2011; Gosse & Phillips, 2001; Granger et al., 2013; Mitchell et al., 2001; Palumbo et al., 2004).

Although surface exposure dating has led to an explosion of new dating constraints in slip rate calculations (Page et al., 2014), the assumptions and calculations used in this technique can introduce uncertainty into age estimates that could affect the resultant slip rate. For example, the technique assumes that the sampled surface has experienced negligible erosion or surface lowering. Field observations such as the persistence of desert pavement or glacially polished surfaces can help bolster this assumption. However, a review of surface exposure dates on glacial deposits in Tibet suggests that ages could vary by 40% for similar-aged deposits due to the effects of erosion (Granger et al., 2013; Heyman et al., 2011).

Another complication arises due to the potential influence of any residual TCN concentrations on the clasts or grains that may have accumulated prior to deposition (i.e., inheritance). Several techniques are often employed to test for the presence of inheritance in TCN surface exposure age studies. For instance, analysis of multiple clasts from the same deposit can be tested for consistency, and the youngest clasts can be interpreted as containing the least inheritance (van Der Woerd et al., 2002). Or depth profiles can test for inheritance within samples collected below the depth to which cosmogenic rays could currently penetrate. However, new inheritance model estimates by Prush and Osokin (2020) designed to test for the influence of hillslope processes on inheritance in TCN exposure dating suggest that inheritance has caused a systematic older bias in many surface exposure ages.

3.2.4. Incorporating Numerical Constraints Into Slip Rate Calculations

3.2.4.1. Paleoseismic Trenching

Advances in numerical age dating methods together with new easy-to-use statistical software packages are providing more robust ways to constrain paleoearthquake ages and interevent times used to calculate slip rates (Biasi et al., 2002; Scharer et al., 2007). Interevent times are now commonly bracketed using Monte Carlo routines and Bayesian statistics with software such as OxCal (Bronk Ramsey, 2009). OxCal is often used to constrain probability distribution functions of earthquake ages using a variety of constraints, including any type of numerical age, stratigraphic information, trench structure, historic events, and any other relevant timing information (Bronk Ramsey, 2009; Lienkaemper & Ramsey, 2009). Incremental or cumulative slip rates are often calculated by dividing the per-event offsets measured within the trench walls by the interevent constraints from OxCal (e.g., DuRoss et al., 2019). For example, Bennett et al. (2018) use detrital radiocarbon samples ($n = 13$), OSL dating ($n = 13$), and detailed stratigraphy and structure within a paleoseismic trench to tightly constrain the ages of six earthquakes on the Wasatch fault, Utah, USA, using OxCal. They compute both incremental (per-event) and cumulative (multiple event) fault slip rates that range from 0.7–1.2 mm/year for the time period between ~6.2 and 0.4 ka using these data (Figure 3).

It is preferable to compute slip rates using interevent times calculated between two or more well-dated events and to use records that span relatively long time periods. Using interevent times that are constrained by tightly bracketed earthquakes ensures that the slip rate estimate is not biased by including an incomplete portion of the seismic cycle in the calculation (i.e., an open interval). However, the effect of open intervals on slip rate estimates is lessened for slip rates calculated over longer periods of time. Slip rate estimates based on event records spanning long time periods (more than five earthquake cycles) can also record any potential temporal variance in slip rate that may occur due to clustering or triggering of events. Slip rates derived from short paleoseismic records (less than five earthquake cycles) can also be subject to inaccuracies resulting from averaging a very small number of earthquakes from a system that may have high variance (Nicol et al., 2009; Weldon, 2011). This bias is diminished over longer paleoseismic records, as the number of sampled earthquakes increases and the total rate converges toward the mean (Grant Ludwig et al., 2019; Styron, 2019).

Although paleoseismic trenching studies can provide interevent times important for slip rate calculations, the numerous ways that numerical ages can either overestimate or underestimate the true age of a unit can often lead to a mix of sample ages within a single trench unit or sample ages that appear perplexingly out of stratigraphic order. Samples that are obviously out of stratigraphic order are often excluded from OxCal models designed to constrain interevent times (Bennett et al., 2018; DuRoss et al., 2019; Hatem et al., 2019; Morell et al., 2018), but it can sometimes be difficult to decide which ages most reliably represent the depositional age of the deposit and which are outliers that should be excluded from further analysis. These issues can result in varying earthquake ages and interevent times depending on which numeric ages are included in the analysis, and it can be difficult to accurately specify the uncertainty presented by this problem. There is no standard or accepted way to overcome this issue, and solutions tend to occur on a case-by-case basis. However, it is generally best practice to obtain a large population of ages from as many dating methods as possible, in order to identify outliers and to obtain a statistically significant population of ages for each trench unit.

3.2.4.2. Offset Quaternary Markers

The growing availability of high-resolution topography together with advances in dating methods and statistical software has facilitated the expansion of fault slip rate across a variety of timescales and study areas over the past several decades (e.g., Burgette et al., 2020; Frankel et al., 2007). For example, Zinke et al. (2019) calculate four incremental slip rates, varying from $\sim 2\text{--}9.6$ mm/year throughout the Pleistocene to Holocene, across the Clarence Fault, New Zealand (Figures 2a and 2b). This high resolution was achieved by backslipping sequentially offset fluvial terraces using lidar topography, IRSL dating of the stratigraphy of the fluvial terraces, and Monte Carlo simulations to place constraints on the most probable slip rate given the available constraints. Offset markers identified on high-resolution bathymetry data can also yield well-constrained slip rates on offshore faults, assuming they can be dated (e.g., D. S. Brothers et al., 2020; S. Y. Johnson et al., 2018).

However, the open intervals bracketing all of the earthquakes responsible for the observed deformation are not easily quantified and removed from the slip rate estimate in these types of studies. If more than 5–10 mean earthquake cycles have transpired since the creation of the offset marker, the open intervals and variation of earthquake recurrence times will not dramatically affect the resulting slip rate estimate, but shorter-term slip rate estimates may be inaccurate by a large factor and become biased (Styron, 2019).

The uncertainties introduced by Quaternary dating methods can also have an effect on slip rate estimates from offset Quaternary markers. For example, slip rate studies that rely on surface exposure ages that underestimate the amount of inheritance could overestimate the apparent surface exposure age and therefore artificially decrease the slip rate (Prush & Oskin, 2020). In contrast, if erosion at the surface has occurred and is not properly accounted for, it could also artificially decrease the TCN surface exposure age and overestimate the fault slip rate. And the same types of complications that arise in interpreting numerical ages in paleoseismic trenches, such as inheritance or contamination by weathering or erosion processes, can also affect the interpreted age of offset units used in slip rate calculations (Harkins et al., 2010). Nonetheless, advances in the calibrations of nuclide production rates and pathways (Jull et al., 2015; Phillips et al., 2016), the availability of high-quality software for age calculation (Hidy et al., 2010; Marrero et al., 2016), and the increase in usage of all of these methods are likely to increase the precision and reproducibility of Quaternary dating methods and their use for slip rate calculations in the future.

3.2.4.3. Combined Slip Rate Methods

Studies that use several of these types of slip rate methods together (e.g., Behr et al., 2010; Harkins et al., 2010; Thompson et al., 2002) can provide insights into whether apparent changes in slip rate over time are related to natural phenomena or if they represent potential bias in the slip rate calculation (Mouslopoulou et al., 2009, 2012; Nicol et al., 2009). DuRoss et al. (2019) present a number of late Quaternary slip rate estimates for the Teton fault, Utah, USA, using offsets recorded from well-dated postglacial ($<\sim 14$ ka) features (geomorphic slip rate) together with per-event offsets and event timing constrained using radiocarbon and OSL dating from trench exposures (trench slip rate). Their closed-interval incremental trench slip rates are suggestive of a slight decrease in slip rate over the late Quaternary, ranging from 0.7–2.1 mm/year for the time period from $\sim 14\text{--}10$ ka to 0.5–1.1 mm/year for the $\sim 10\text{--}5$ ka time period (Figure 4). Using event times from trenching, and assumptions about average recurrence interval and per-event offset, they calculate a closed-interval geomorphic slip rate of 1.1 ± 2 mm/year for the time period from $\sim 10\text{--}5$ ka, compared with an open-interval geomorphic slip rate of 0.9 ± 0.06 mm/year from 14 ka to present (Figure 4). These results

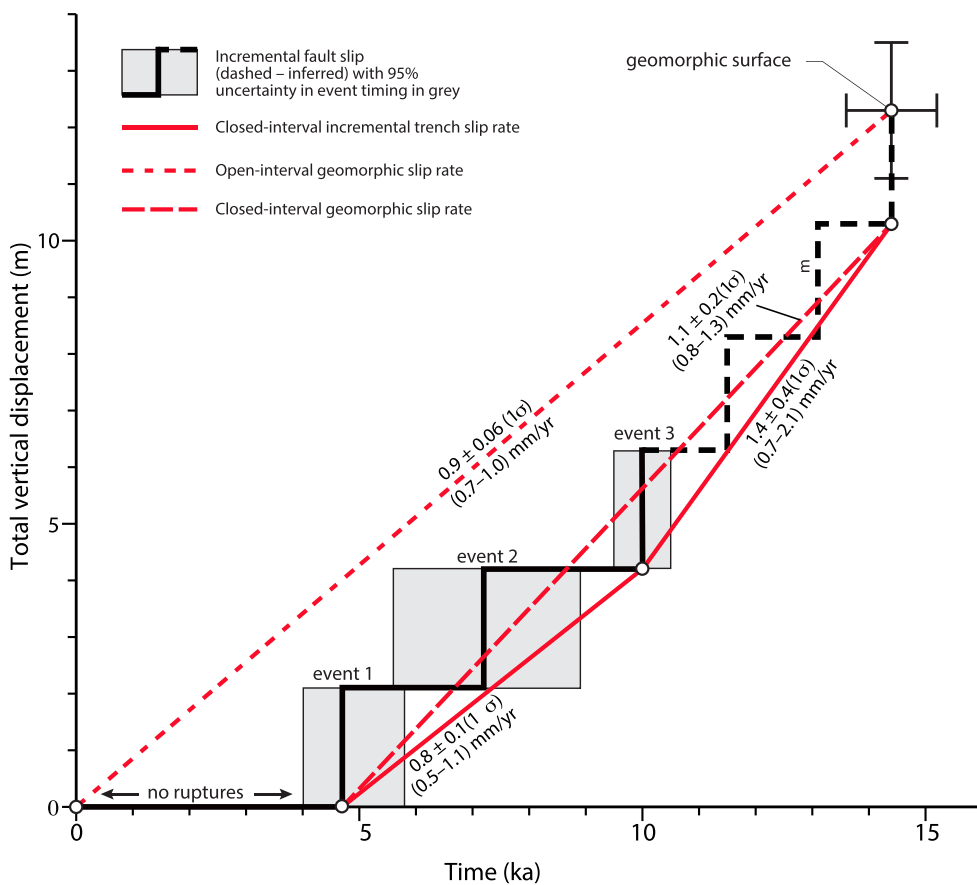


Figure 4. Figure modified from DuRoss et al. (2019) showing measurements of vertical slip rate for the Teton Fault, northern Utah, USA. Event times were constrained by paleoseismic trenching, using radiocarbon dating of charcoal, and OSL methods input into an OxCal model (Bronk Ramsey, 2009). Closed-interval incremental slip rates were calculated using event times and per-event offset measurements from trenching. Geomorphic slip rates were calculated using both open and closed intervals (red dashed lines) based on offset nearby glacial surfaces (Thackray & Staley, 2017).

stand in contrast to previous studies that relied on similar data but used open-interval incremental slip rate estimates with relatively short interevent times (~ 3 kyr) to suggest that the slip rate of the Teton fault at this site decreased by a factor of 10 throughout this same late Quaternary time period (White et al., 2009). The DuRoss et al. (2019) study was able to leverage data from both geomorphic and trench slip rate methods to estimate a closed-interval slip rate that spans approximately five seismic cycles and also provide important information about the magnitude of changes in fault slip rate over time.

3.3. Evaluating Slip Rate Changes Over Time

3.3.1. Combining and Comparing Quaternary Geologic and Geodetic Slip Rates

Slip rates computed from geodetic techniques have commonly been compared with Quaternary geologic slip rates derived from paleoseismic techniques methods in the literature, and both are commonly considered in PSHA (e.g., Cowgill et al., 2009; Mann et al., 2007; Mohadjer et al., 2017). Some of the most extensive comparisons of geodetic and geologic slip rate data were undertaken for the incorporation of geodetic data into the 2014 U.S. National Seismic Hazard Map (Petersen et al., 2014). The results of this work found that block models constrained using only geodetic data predicted slip rates at block margins several (3–10) times higher than rates computed with geologic methods but combined geologic-geodetic models produced results that were fairly compatible. A key facet of the combined geologic-geodetic models was the addition of off-fault strain (Petersen et al., 2014). However, in some areas geologic and geodetic fault slip rates simply do not seem to be easily reconciled, such as in the northern Walker Lane area in California and Nevada, USA (Bormann et al., 2016; Wesnousky et al., 2012).

Slip rates derived from geodetic block models in some instances provide higher estimates than paleoseismic slip rates if intrablock strain is not included, or if the block geometry is oversimplified (Herbert, Cooke, & Marshall, 2014). Both of these effects may result in an overestimation of the amount of strain being allocated onto faults at block margins, even if the total strain across the study region is otherwise consistent between geodetic and geologic data sets. However, incorporating intrablock strain into geodetic block models does not always lower the amount of geodetically determined slip rate, depending on the block model geometry. K. M. Johnson et al. (2007) report that incorporating intrablock strain into geodetic block models in a restraining bend on the San Andreas increased the geodetically derived slip rate to be more in agreement with available paleoseismic and geomorphic data.

In many instances, seemingly discrepant geodetic and Quaternary geologic slip rate estimates can be reconciled by the incorporation of viscoelastic earthquake cycle effects into the geodetic modeling, as the viscoelastic lower crust and upper mantle is predicted to respond more slowly to coseismic stresses imposed by earthquakes compared to the elastic upper crust (e.g., DeVries et al., 2017; K. M. Johnson et al., 2007). Viscoelastic earthquake cycle models and postseismic observations suggest that the instantaneous slip rate of a fault, such as the rate derived from geodesy, will be faster than the long-term average in the postseismic phase following a major earthquake but slower than the long-term average in the late interseismic phase long after an earthquake (Hetland & Hager, 2006; Meade et al., 2002). However, late-interseismic geodetic slip rates are not always lower than longer-term estimates, which implies complex fault behavior such as decadal strain transients, fault network effects, or millennial slip rate variation (Dolan & Meade, 2017).

3.3.2. Evaluating Quaternary Geologic Slip Rate Changes Over Multiple Seismic Cycles

Comparisons of 10^3 -year slip rates versus $\sim 10^4$ – 10^5 -year rates in some cases show consistency (e.g., Nicol et al., 1997) but in other cases reveal discrepancies that are not well understood. These changes have been suggested to result from a wide number of processes, including time-varying fault strength (Dolan et al., 2016), changes in gravitational stress due to sediment or glacial loading and unloading (D. Brothers et al., 2011; Hetzel & Hampel, 2005; Luttrell & Sandwell, 2010), fault interaction (Dolan et al., 2007; Nicol et al., 2010), or earthquake clustering (e.g., Friedrich et al., 2003; Machette, 1984; Mouslopoulou et al., 2009).

Although we discuss the topic of temporal variations in earthquake activity more fully in section 4, a primary challenge is to disentangle the effects of earthquake-cycle fluctuations in an otherwise linearly slipping fault (stochasticity) from longer-term rate “secular” changes that may reflect changes in regional tectonic stress or fault loading. For example, Ferry et al. (2007) used a 45-kyr slip rate history of the Jordan Valley segment of the Dead Sea Fault to document a mean slip rate of 5 mm a^{-1} over that time but also found shorter-term incremental slip rates varied between 3 and 11 mm a^{-1} . In a later study, Fitzenz et al. (2010) found that the entire paleoseismic slip history, on the Dead Sea Fault, including variations in the rate of earthquake occurrence, could be explained by earthquakes with randomly sampled recurrence intervals. This study suggests a degree of randomness and stochastic earthquake cycle processes and implies that incremental slip rate variations observed do not require secular or temporary slip rate changes.

In addition to better constraining earthquake recurrence distributions, the methods used by Fitzenz et al. (2010), which involved generating thousands of synthetic fault displacement histories, could also offer a powerful method of discriminating between secular slip rate changes and earthquake-cycle stochasticity. For instance, if it is difficult to fit synthetic cumulative offset time series to available geologic or paleoseismic constraints based on random sampling, but the same data are easily fit by a change in recurrence and/or per-event slip, this may be taken as strong evidence for a slip rate change. Statistical tools based on information theory may also be useful for determining whether slip rates have changed given ambiguous data. Information criteria, such as the Bayes (Burnham & Anderson, 2004) and Akaike's information criteria (Akaike, 1981), evaluate the statistical likelihood of a model based on its fit to the data, while penalizing a model for its complexity. Information criteria guard against overfitting the model to the data or inferring based on limited information. Information criteria have been used occasionally in evaluating slip rate changes (e.g., Speth et al., 2019) but are used elsewhere in the geosciences (Main et al., 1999; Tamura et al., 1991). A particularly useful form is Akaike's information criterion corrected for small sample sizes (Burnham & Anderson, 2004; Flesch et al., 2018).

3.4. Synthesis

It remains unclear which of the different slip rate estimation techniques should be favored for seismic hazard analysis, although the answer will certainly depend on the context, including the availability of results from

different techniques, uncertainties for each, the degree of disagreement between the different estimates, and the seismotectonic environment. The question of interest may be stated as “Which slip rate technique, over what timeframe, will best predict earthquake activity on a fault in the next few decades?”

Geodetic slip rates are often higher precision than longer-term Quaternary geologic techniques, with almost no uncertainty in the time component of the rate estimation, but they usually span a small fraction of the earthquake cycle on any fault and (particularly with sparse GNSS networks) may also record strain that is released on other structures than the fault in question or is not released in damaging earthquakes. The theoretical effects of viscoelastic relaxation throughout the earthquake cycle should result in an underestimate of slip rate in the late interseismic phase (long after the last earthquake) and an overestimate of slip rate in the postseismic phase.

Quaternary geologic slip rates, as provided by numerical dating of paleoseismic trench units or offset Quaternary markers, can provide essential information about fault slip rates over multiple seismic cycles. Trenching can provide robust closed-interval slip rate estimates for points along a fault but can suffer from relatively short records and often cannot include off-fault deformation. Slip rates derived from offset Quaternary markers can sometimes provide longer estimates of fault slip than trenching and can often include off-fault deformation, but it can be harder to exclude the effects of open intervals on the slip rate estimate. And all of these slip rate methods suffer from sample context uncertainties that are difficult to quantify using any of the popular Quaternary dating methods (e.g., radiocarbon, luminescence, and cosmogenic radionuclide dating (CRN)). Efforts that combine multiple numerical dating and Quaternary slip rate methods together can provide valuable information about fault slip changes over time, and continued advances in geochronology and topographic techniques will likely improve our understanding of how to interpret and calculate fault slip rates spanning multiple earthquake cycles.

Although there are advantages and disadvantages to slip rates spanning short-term (<5 earthquake cycles) and long-term (>5 earthquake cycles) slip rates from any method, longer-term rates should be more accurate than shorter-term estimates (Grant Ludwig et al., 2019; Styron, 2019) unless there is evidence for substantial earthquake clustering or temporal variation in slip rate. Quaternary geologic slip rates based on offset markers can be biased by the unknown duration of open intervals, but this effect is lessened over longer periods of time so long as there has not been substantial variation in fault slip throughout the measurement time. However, if there is evidence for earthquake clustering or changes in slip rates on the fault, shorter-term slip rates may be a better indication of the current state of activity on the fault, rather than a longer-term slip rate that averages over time periods when the fault was potentially behaving differently. Nevertheless, short-term Quaternary geologic slip rates may also fluctuate based on whether those few earthquakes were in sum higher or lower displacement, or more closely or more widely spaced in time, than average.

Most active faults do not have a multiplicity of fault slip rates to choose from. Therefore, the problem of which one to choose is “a nice problem to have” and in the cases where hazard modelers must choose between discrepant rates estimates, the rates should be evaluated on a case by case basis.

4. Understanding and Modeling the Temporal Distribution of Fault Activity

Records of faulting derived from paleoseismic studies are commonly used to estimate long-term slip rates and recurrence rates of large earthquakes on a particular fault, and these values inform earthquake source models for PSHAs (see section 2 and Figure 1). When a new building is constructed, building codes generally assume an average life span for the structure, such as 50 years. Accordingly, PSHAs are usually based on a probability of ground motion exceedence (most commonly 10% and 2%) in 50 years (e.g., Petersen et al., 2015; M. Stirling et al., 2012; Stucchi et al., 2011). Many PSHA models currently in use are time independent in that they do not take into account the time since the most recent large earthquake on the fault of interest. Rather, they only consider any given 50-year period of time. However, if detailed paleoevent magnitude and timing is available, a time-dependent temporal occurrence model (Figure 1) can instead be used that more properly accounts for the time since the most recent large earthquake. Time-dependent models require a statistical representation of the temporal distribution of fault activity, which are ideally informed by long, multievent paleoseismic records.

Most current time-dependent hazard models (e.g., Matthews et al., 2002; Nishenko & Buland, 1987; Ogata, 1999) estimate the probability of rupture within a future time window using a mean recurrence inter-

val or mean rate of fault rupture (with uncertainties) and the time since the most recent large earthquake. This approach assumes that earthquakes occur quasiperiodically and that the mean rate of earthquake occurrence does not change over timescales of interest to the PSHA. These assumptions are consistent with elastic rebound theory (Reid, 1910), the quasi-stationarity of plate motions at the relevant timescales, and paleoseismic results from some plate boundary structures (e.g., the southern San Andreas and Alpine faults Berryman et al., 2012; Cochran et al., 2017; Scharer et al., 2010). However, paleoearthquake studies demonstrate that earthquakes on some faults occur irregularly, with clusters of several earthquakes separated by periods of seismic quiescence, a phenomenon sometimes termed as “supercycles” (Grant & Sieh, 1994; Philibosian & Meltzner, 2020; Sieh et al., 2008; Salditch et al., 2020). Irregular earthquake occurrence is observed in both plate boundary (e.g., Mouslopoulou et al., 2016; Nocquet et al., 2017; Philibosian et al., 2017; Rubin et al., 2017) and stable continental (intraplate) regions (e.g., D. Clark et al., 2012, 2015; Cox et al., 2006; Craig et al., 2016; Crone et al., 1997), but the clustering behavior observed in intraplate regions tends to be less cyclical and to occur over longer timescales than on plate boundaries (Calais et al., 2016; M. Liu & Stein, 2016).

One simple measure of whether earthquakes occur regularly, randomly, or are clustered in time on a fault, is the coefficient of variation (COV) for the interevent time on a fault (standard deviation/mean Goes & Ward, 1994). A value of 0 implies perfectly periodic earthquake recurrences, a COV $\ll 1$ implies quasiperiodic behavior, and COV values $\gg 1$ imply temporal clustering of events. A COV of ~ 1.0 implies random earthquake occurrence, consistent with time-independent hazard models that assume earthquakes are Poisson-distributed in time; that is, each event occurs without any memory of the previous event. Williams et al. (2019) have argued that the majority (58%) of faults for which long-term paleoearthquake records (five or more events) are available have a COV < 1 and hence quasiperiodic earthquake recurrence. Clear exceptions exist, although developing long-term chronologies for faults demonstrating a high degree of clustering is inherently challenging, as long quiescent periods provide time for evidence of older ruptures to be erased.

However, it should be noted that metrics such as the mean earthquake recurrence and its COV, and time-dependent recurrence probability models, are best suited to quantifying the behavior of a single fault without consideration of low- to moderate-magnitude seismicity. Individual fault segments in a fault network may rupture periodically, but this does not mean seismicity over the whole network will be periodic. Consider three adjacent faults that each rupture every 500 years, though the second and third faults consistently rupture 1 and 2 years after the first fault: The individual faults are perfectly periodic, but the fault network as a whole produces clustered seismicity. Likewise, the lower magnitude of seismicity that may be included in recurrence calculations is somewhat arbitrary. In paleoseismological studies, only surface-breaking (or otherwise geologically detectable) earthquakes are considered, which typically places the threshold in the M 5–7 range, depending on tectonic and depositional environment (e.g., D. J. Clark et al., 2020; Biasi & Weldon, 2009), although some quite large earthquakes, such as the 2015 M_w 7.8 Gorkha, Nepal, earthquake, do not surface rupture and are hence unlikely to be recorded in the geological record. In contrast, instrumental seismic catalogs are limited only by instrument sensitivity.

Below, we present examples of long paleoearthquake records to demonstrate the diversity of recurrence behavior observed across tectonic regimes. We point out qualitative differences between regions with strike-slip plate boundary faults, peripheral plate boundary regions, and intraplate faults, but we do not discuss other tectonic settings (e.g., subduction zones, reviewed by Philibosian & Meltzner, 2020) in the interest of space. This section is followed by a discussion of the implications of these results for PSHA and current time-dependent temporal occurrence models that are often used to capture these types of earthquake behavior. We conclude this section with our thoughts on future work required to better understand and model the temporal distribution of fault activity.

4.1. Empirical Evidence of Variable Fault Recurrence Distributions

4.1.1. Strike-Slip Plate Boundary Faults

A number of paleoseismic studies of major strike-slip faults suggest a COV $\ll 1$, implying that quasiperiodic behavior is the norm for large strike-slip plate boundary faults. (e.g., Berryman et al., 2012; T. Rockwell, 2010). A global compilation of strike-slip faults with relatively long paleoearthquake records (>5 events) found COV values ranging between 0.4 and 0.8 (mean of 0.69) for the majority of the faults considered (Yuan et al., 2018). Results from this compilation also suggest that faster slipping faults (>10 mm/year) generally exhibit more periodic (i.e., a lower COV) behavior than those with slower slip rates (<10 mm/year).

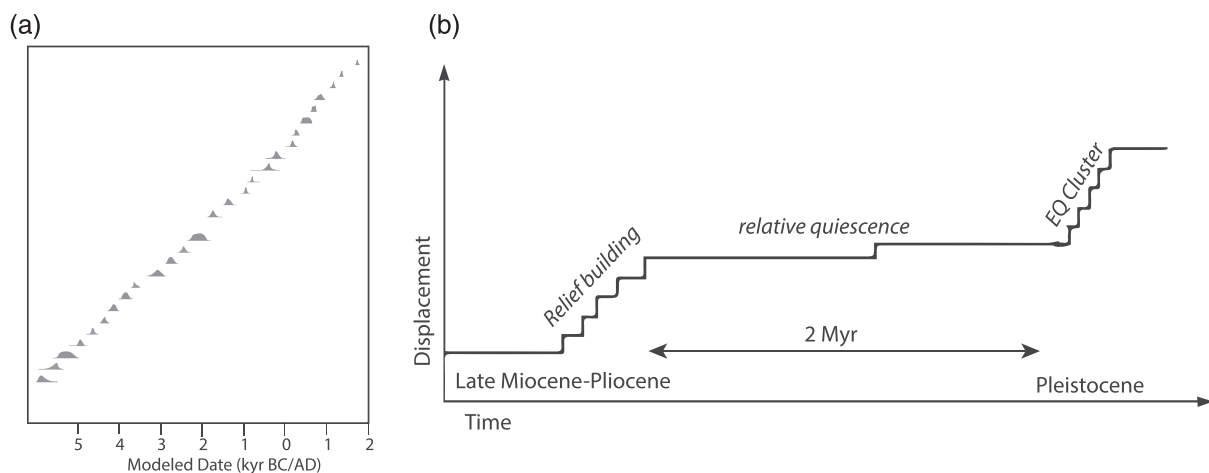


Figure 5. (a) Probability distribution functions (PDF) of ages of paleoearthquakes along the south Westland segment of the Alpine Fault based on combined data from Cochran et al. (2017), Berryman et al. (2012), and K. Clark et al. (2013). Note how earthquake occurrence is highly regular. These data correspond to a recurrence interval of 291 ± 23 years and a COV of 0.41. (b) Generalized model of evolution of the Cadell Fault, southeastern Australia, showing two active periods separated by a long quiescent period. This behavior contrasts with the earthquake record for the Alpine Fault shown in part (a). Figure modified from D. Clark et al. (2015).

The Alpine Fault in southern New Zealand is an end-member example of quasiperiodic earthquake recurrence and demonstrates highly regular behavior in a ~8,000-year, 27-event earthquake chronology developed by Berryman et al. (2012), K. Clark et al. (2013), and Cochran et al. (2017) (Figure 5a). For the southern segment of the Alpine Fault, this chronology yields a COV of 0.41 and a mean recurrence interval of 291 ± 23 years (Cochran et al., 2017). This high degree of regularity has been attributed to the Alpine Fault's high slip rate and the relative isolation of this segment from any nearby faults that may interact with it (Berryman et al., 2012).

Although generally behaving quasiperiodically, studies suggest that large strike-slip faults can also exhibit irregularities in the rate of earthquake occurrence. For example, paleoearthquake records suggest that the Jordan Gorge Fault segment of the Dead Sea Transform Fault hosted significantly more earthquakes (eight events) between the first and seventh centuries CE than in the last millennium (two events) (Wechsler et al., 2014). In Southern California, a 4,000-year-long, 21-event earthquake history on the San Jacinto Fault similarly suggests that the Anza Seismic Gap segment has switched between quasiperiodic and clustered modes of earthquake activity, with a cluster of four earthquakes occurring within a 150-year period (T. K. Rockwell et al., 2015). Finally, precisely dated deformed geomorphic features along the central Altyn Tagh Fault argue for a 400-kyr-long pulse of accelerated earthquake activity among a 16-kyr-long period exhibiting less activity (Gold et al., 2017).

The processes responsible for clustering on these types of systems remains uncertain, but there is some evidence that the aperiodic behavior on these faults may be caused by interactions with neighboring fault segments, fault segmentation, and/or variations in earthquake magnitude. On the Dead Sea Fault, regional paleoearthquake chronologies suggest that the timing and magnitude of earthquakes along the entire length of the fault may have been influenced by activity on nearby smaller fault segments (Wechsler et al., 2014). In the case of the San Jacinto Fault, the 15 largest ruptures observed in the event chronology exhibited a recurrence interval of 254 ± 120 years and a COV of 0.54, whereas the full catalog of events yield a lower recurrence interval of 185 ± 100 years and a higher COV of 0.63.

4.2. Peripheral Plate Boundary Regions

Although the Alpine Fault exhibits quasiperiodic earthquake recurrence, paleoseismic and geomorphological studies argue for aperiodic earthquake occurrence on a number of faults in the Otago basin and range province directly adjacent to it (Figure 6). The Otago region accommodates the remaining ~2 mm/year of convergent plate motion between the Australian and Pacific plates not accommodated on the Alpine Fault, distributed across a series of parallel thrust faults (Norris, 2004). For some faults, such as the Akatore and Titri faults, there are clear quiescent and active periods (e.g., N. Litchfield, 2001; Taylor-Silva et al., 2019),

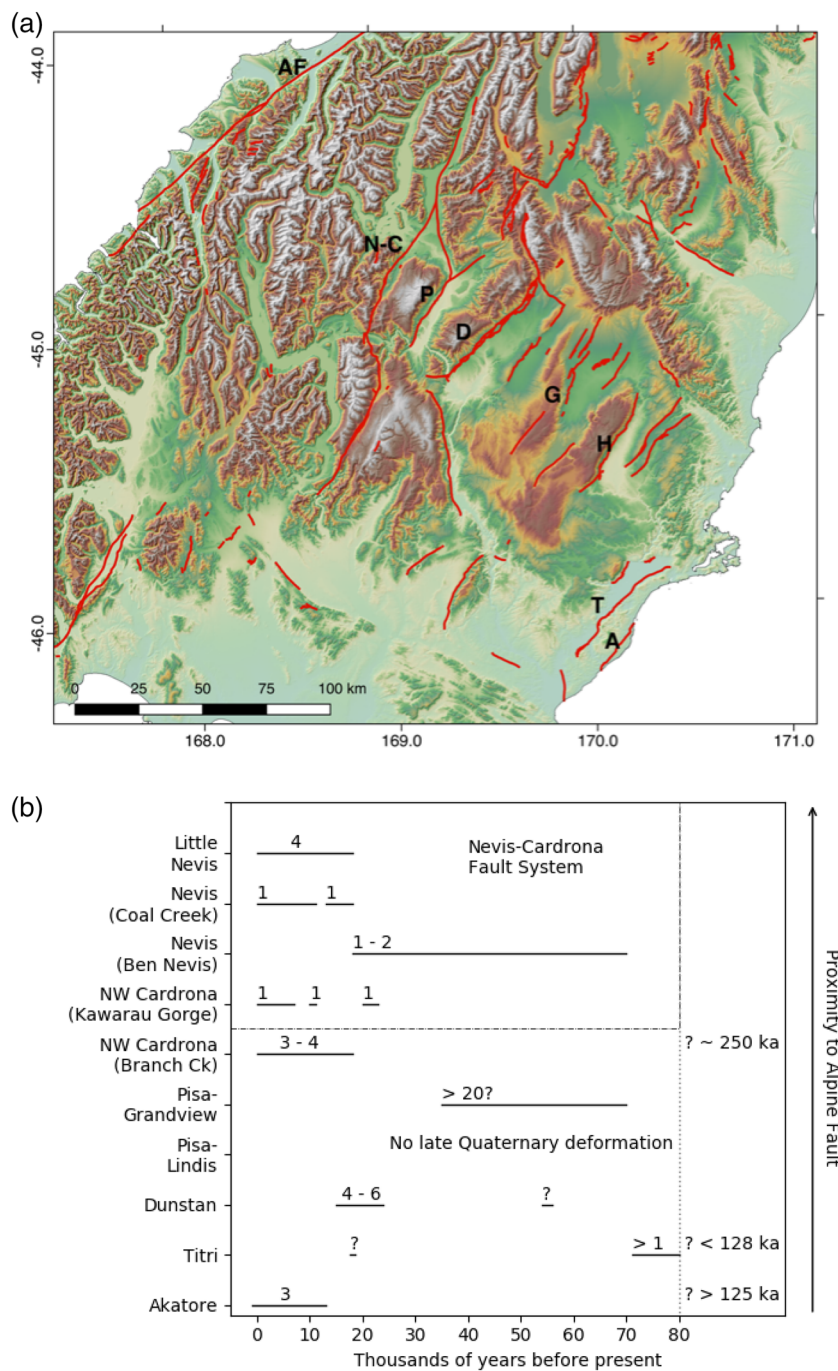


Figure 6. (a) Location of faults (red lines) shown in part (b) relative to the Alpine Fault, overlain on topography. A—Akatore; AF—Alpine Fault; D—Dunstan; G—Gimmerburn; H—Hyde; N-C—Nevis-Cardrona; and P—Pisa. Faults closer to the Alpine Fault are associated with greater uplift and higher long-term slip rates. (b) Timing of active periods on fault within the Otago Basin and Range Province. Known or estimated number of events in each active period is indicated above horizontal lines. Faults closer to the top of the diagram are closer to the Alpine Fault. Data sourced from Beanland and Barrow-Hurlbert (1988), Beanland and Berryman (1989), N. J. Litchfield and Norris (2000), N. Litchfield (2001), Van Dissen et al. (2006), and Taylor-Silva et al. (2019).

while others, such as the Nevis-Cardrona and Pisa Faults, demonstrate apparent migration of slip onto various strands of the fault at different times (Beanland & Barrow-Hurlbert, 1988; Beanland & Berryman, 1989). Figure 6 shows how one or two faults within the system appear to accommodate most of the deformation in the region at any particular time. For example, the Akatore Fault has been more active than any other faults in the Otago region over the Holocene, despite its long-term slip rate being at least an order of magnitude lower (Taylor-Silva et al., 2019). Collated on- and off-fault evidence from a large number of faults in the Basin and Range of the western United States also demonstrate persistent nonstationary slip rates in both time and space with a migration of fault activity similar to the Otago example (Pérouse & Wernicke, 2017; Wallace, 1987). Similar behavior has also been documented in the western United States (Dolan et al., 2007; Oskin et al., 2008; Párouse & Wernicke, 2017), the Central Nevada Seismic Belt (Bell et al., 2004), the Appenines (Benedetti et al., 2013) and elsewhere (e.g., Nicol et al., 2010).

4.3. Intraplate Faults

Many intraplate faults show evidence for strong temporal clustering of earthquakes and very low recurrence rates (10 to 100 kyr) (D. Clark et al., 2008, 2012, 2015; Cox et al., 2006; Crone et al., 1997; Craig et al., 2016; 2003; Gold et al., 2019; Stahl et al., 2016; Vallage & Bollinger, 2019). One intraplate faulting record that clearly demonstrates this behavior is from the Cadell Fault, in southeastern Australia. D. Clark et al. (2015) developed a long-term earthquake chronology showing distinct periods of activity followed by long periods of quiescence, shown in Figure 5b. After a period of tectonic activity in the late Miocene or early Pliocene, only one or two earthquakes occurred in the subsequent ~2 million years. After this period of quiescence, approximately five M_w 7.3–7.5 earthquakes occurred between 70 and 20 ka, with a mean interevent time of ~8 kyr.

In the most distant areas from plate boundaries (cratonic areas), it is possible that single-event (one-time-only) ruptures occur. In cratonic Australia, of the nine surface rupturing events observed in the past ~50 years, none of the causative faults exhibited preearthquake geomorphology that would have allowed them to be identified as active faults, despite occurring in very arid environments characterized by low erosion rates (D. Clark & Allen, 2018; T. R. King et al., 2019). It is unclear whether these events were the first, and possibly only, rupture of the fault in question, or that recurrence times are simply so long that evidence of previous ruptures has been removed from the geologic record (D. J. Clark et al., 2020).

No consensus exists on theories that explains intraplate earthquake occurrence and clustering (e.g., D. Clark et al., 2008, 2012, 2015; Cox et al., 2006; Craig et al., 2016; Crone et al., 1997; Gold et al., 2019), though several, nonexclusive candidates exist. Calais et al. (2016) argue that relatively simple models that can explain earthquake occurrence at plate boundaries, that is, models based on elastic rebound theory, are not applicable to intraplate regions and do not explain earthquake clustering occurring in these regions. Possible mechanisms underlying earthquake clustering include fault system interaction leading to complex migration of seismicity (M. Liu et al., 2011; M. Liu & Stein, 2016), stress changes due to reconfiguration of distant plate boundaries (Sandiford, 2003), and transient stress perturbations triggering the release of strain stored in the crust over million-year timescales (Calais et al., 2016; Craig et al., 2016).

4.4. Implications for PSHA

While the exact mechanisms behind many of these different types of earthquake recurrence behavior remain unclear, these findings nonetheless present challenges and have important implications for PSHA. Strike slip faults with high slip rates and more regular occurrence such as the Alpine Fault have allowed estimation of time-dependent probabilities of future rupture using several different methods (e.g., Biasi et al., 2015; Howarth et al., 2018). But the finding that the average rate of earthquake occurrence on the San Jacinto Fault varies by a factor of 2 over millennial timescales demonstrates that reliance on short paleoseismic records of a few events is not sufficient to accurately characterize earthquake recurrence intervals. Similarly, the aperiodicity and spatial and temporal clustering observed in the Otago region implies that a fault that is in an active state in this type of setting may pose a higher level of hazard than would be estimated from the long-term rate alone, although it is unclear why. Finally, the identification of intraplate faults with such long recurrence intervals requires the use of long paleoseismic records, sometimes much longer than can be obtained by instrumentally recorded seismicity (10 to 100 years) (Vallage & Bollinger, 2019), and these faults can be hard to detect or show little geologic or geomorphic evidence of past rupture. This in turn raises questions as to how informative the spatial distribution of recently observed seismicity is for forecasting future hazard, leading to deep epistemic uncertainty regarding how to characterize seismicity rates for PSHA.

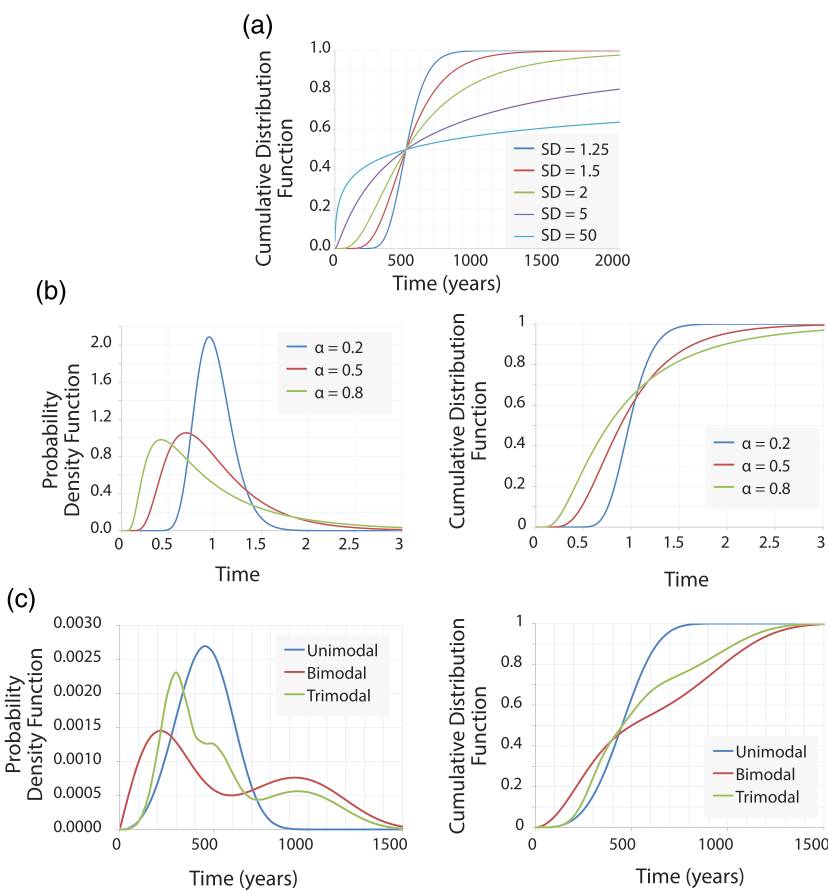


Figure 7. Examples of time-dependent temporal occurrence models used in PSHA (Figure 1). These models can be informed by paleoseismic data such as earthquake recurrence interval and the timing, location, and magnitude of past earthquakes. (a) Cumulative distribution function for the lognormal probability model with an example mean of 500 years and various standard deviation (SD) values. (b) Probability density function and cumulative distribution function for a Brownian Passage Time (BPT) model with a normalized mean of 1 and various aperiodicity values (α). (c) Probability density function and the cumulative distribution function for a Weibull probability model with the time axis normalized to the mean recurrence interval and various shape parameters. The blue unimodal curve has an example mean return period of 500 years. The red bimodal curve is assigned a 300-year return period within the clusters and an overall 1,000-year period as the long-term recurrence rate. The trimodal curve (green) has three concentrations of earthquakes with return periods of 300, 500, and 1,000 years. A different shape parameter was used for each distribution (3.5 for unimodal distribution, 2 and 4 for the bimodal distribution, and 4.5 for each mode of the trimodal distribution).

in stable continental regions (Griffin et al., 2020). Although more work is needed in understanding these types of fault behaviors, below we discuss the most commonly used time-dependent probability models that attempt to capture these recurrence behavior and paleoseismologic data into PSHA.

4.5. Geological Data and Time-Dependent Temporal Occurrence Models in PSHA

Time-dependent temporal occurrence models are probability models used in PSHA to mathematically represent the interevent times of earthquakes of a certain magnitude and can be informed by paleoseismic data such as earthquake recurrence interval and the timing, location, and magnitude of past earthquakes. In practice, PSHAs may utilize a range of probability models within a logic tree framework; mixtures of models may outperform individual models (Rhoades et al., 1994). One of the simplest probability models used to estimate time-dependent probabilistic hazard is the lognormal probability distribution (Nishenko & Buland, 1987). This distribution requires only two parameters, the mean and the standard deviation of the recurrence interval (Figure 7a). It assumes a quasiperiodic recurrence of earthquakes (i.e., $\text{COV} \ll 1$), as would be applicable for the Alpine Fault (Figure 5a), and therefore forces the probability of the next event to reset to 0 after an earthquake and build up again over time. However, a contentious aspect of the lognormal

distribution method is that once a fault system is past its mean recurrence interval, instantaneous rupture probabilities start to decrease instead of increase.

The Brownian Passage Time (BPT), Weibull, and Gamma distributions are other commonly used probability models that can overcome several of the shortcomings of the lognormal method (Figure 7b). The BPT method can quantify the aperiodicity of earthquake recurrence using an aperiodicity parameter and assumes a constant tectonic loading on a fault together with a randomly varying failure threshold (Matthews et al., 2002) (Figure 7b). An aperiodicity parameter of 0 represents completely periodic while 1 represents completely aperiodic. BPT models have enjoyed a wider use in time-dependent PSHA because they are stable for all ranges of time since the most recent event, even after multiple recurrence times. For example, Field (2015) make use of the aperiodicity parameter of the BPT distribution by making it magnitude dependent (the larger the magnitude, the lower the aperiodicity) and assigning weights in a logic tree manner (e.g., for the $6.7 < M < 7.2$ magnitude range, the low-, middle-, and high-range aperiodicity parameters are 0.3, 0.4, and 0.5, respectively). The Weibull and Gamma distributions can also simulate a wide range of probability density function shapes via their “shape” and “scale” parameters. For the Weibull distribution, a shape parameter of 1 yields an exponential distribution, a shape parameter greater than 1 yields a distribution with a thinner tail, while a shape parameter smaller than 1 yields a distribution with a fatter tail.

Although these probability distributions do not have the ability to explicitly account for bimodal (or multimodal) temporal clustering by themselves, multiple distributions can be bootstrapped together with various weighing schemes to simulate temporal clustering. In Figure 7c we show examples of bimodal and trimodal behavior modeled using the Weibull distribution compared to a unimodal distribution with a single return period. It is possible to use any weighting scheme between different return periods. In the example shown in Figure 7c, the return periods were equally weighted in the bimodal and trimodal distributions. This type of probability model could be appropriate for faults with paleoseismic records showing clusters of multiple large earthquakes separated by long periods of quiescence.

In locations where specific information on earthquake recurrence is lacking, alternative approaches can be applied, for example, if the timing of the most recent event is unknown, Field and Jordan (2015) propose to calculate the probability density function for the time since the most recent event as one minus the ratio of the cumulative distribution function of the recurrence interval to the mean recurrence interval. In the case where the timing of the most recent event is known but the timing of previous events is not, Biasi and Thompson (2018) use the long-term fault slip rate and most recent event timing to forecast future rupture probabilities. Information on open intervals at the start and the end of the earthquake record can also be incorporated into model fitting using Bayesian approaches (Nomura et al., 2011; Ogata, 1999).

4.6. Challenges and Future Directions

PSHAs constructed for building codes and other applications are striving to improve on a multitude of fronts, and the development of fault-based, time-dependent probability models based on geological records of past faulting represent a key challenge. We have outlined how diverse earthquake recurrence behavior, such as aperiodic earthquake occurrence and earthquake clustering, can be a challenge to simulate in time-dependent temporal occurrence models in PSHA. Overcoming these challenges will likely require both expanding the evidence base, by obtaining as long and as detailed paleoseismic data as possible, a better understanding of the processes underlying temporal earthquake clustering across a wide variety of settings, and the development of metrics and multivariate probability models to quantify complex fault network behavior.

4.6.1. Expanding the Evidence Base

Robust, detailed, and multievent paleoseismic data sets are ideal to appropriately account for the diversity of earthquake occurrence on many fault systems in time-dependent models. Unfortunately, earthquake records on most faults are generally too short to obtain solid estimates of the earthquake recurrence distribution (Matthews et al., 2002). Conventional paleoseismic trenching methods cannot generally obtain a record longer than a few earthquake cycles from thrust faults, as an earthquake can destroy evidence of earlier earthquakes, and surficial processes can modify the landscape between earthquakes. There are also limits as to what can feasibly be excavated in a paleoseismic trenching investigation.

More diverse methods, capable of providing long-term and detailed paleoseismic records are needed, and will likely require integration of multiple lines of evidence. Off-fault geomorphic evidence such as changes

in drainage (D. Clark et al., 2015; K. Clark et al., 2013; Cochran et al., 2017), indicators of coastal uplift or subsidence (Philibosian et al., 2017; Sieh et al., 2008), turbidite deposits (Goldfinger, 2011; Goldfinger et al., 2012; Moernaut et al., 2018), and paleotsunami deposits (Peterson et al., 2011) have been used to provide long-term earthquake records along a specific fault or within a wider region. Bayesian methods, such as OxCal (Bronk Ramsey, 2009), provide a framework within which to integrate multiple lines of evidence and the often competing interpretations of the data (DuRoss et al., 2011, 2018). Use of such a framework is increasingly important for integrating the results of multiple studies that may use different lines of evidence, subject to varying interpretations and uncertainties.

Studies of fault rocks and geochronologic advances hold promise for developing long-term earthquake records. Williams et al. (2017) developed the longest (400,000-year) on-fault earthquake to date using U-Th dating of coseismic calcite veins on the intraplate Loma Blanca normal fault, in the Rio Grande of southern United States. In a related study, Williams et al. (2019) used radiogenic isotope analysis to infer that a 50,000-year-long cluster of earthquakes on the Loma Blanca Fault was likely facilitated by an increase in pore-fluid pressure due to crystallization within an intrusive magma body beneath the fault.

4.6.2. Probing the Processes Underlying Temporal Earthquake Clustering

Understanding the underlying processes behind temporal earthquake clustering will be important if we wish to accurately capture earthquake behavior in a wide variety of settings using PSHA in the future. Physics-based models may provide insights into the processes behind earthquake clustering both on single fault structures and on networks of faults. Highly clustered seismicity on a single fault may be reproduced in finite element models with randomly varying failure thresholds and a realistic viscoelastic lower crust and upper mantle (e.g., DiCaprio et al., 2008; Kenner & Simons, 2005). In these models, the viscoelasticity acts as a longer-term stress storage, accumulating significant energy during long interseismic loading episodes corresponding to high failure thresholds on the fault. Once failure occurs, frictional weakening of the fault may lead to quickly repeated earthquakes as the lower crust and upper mantle relaxes (DiCaprio et al., 2008). The results from these types of finite element models could be incorporated into temporal occurrence models in the future to account for complex rupture behavior and triggering.

The evidence for spatiotemporal clustering of earthquakes within a larger fault network illustrates that faults do not act independently but are capable of modulating the seismic cycle on other faults in the network. Recent mechanical models have provided insight into these phenomena. The most prominent set is the Coulomb stress change models (G. C. P. King et al., 1994), which describes the instantaneous, static stress changes in crustal volumes and on embedded “receiver” faults transmitted through the elastic lithosphere due to an earthquake’s strain. Coulomb stress changes have long been proposed to be a dominant control on aftershock locations and sequences of mainshocks (e.g., Cocco et al., 2000; Mildon et al., 2017; R. S. Stein et al., 1997; Walters et al., 2018). However, the success of this model has also been questioned. Hardebeck (2004) and Townend and Zoback (2006), among others, have noted that the magnitude of the stress changes on receiver faults (often in the kPa range) is small relative to the background stress levels, even considering the disparity of estimates of tectonic stress (Hardebeck & Hauksson, 2001; Townend & Zoback, 2006). Additionally, when Meade et al. (2017) compared a suite of elastic stress change metrics (including Coulomb stress change, maximum shear stress change, stress change tensor invariants, and dozens of others), they found that Coulomb stress changes predicted aftershock locations better than random only in about half of the 238 mainshocks studied, while other elastic stress change metrics performed significantly better.

Perturbations to the regional stress field from mechanisms other than the static, elastic coseismic stress changes may play a large role in modulating the rates and timings of earthquakes. Dynamic, transient stress changes caused by the passage of seismic waves may cause changes in seismicity rates well after the transients have passed (Kilb et al., 2002). Postseismic processes such as afterslip (e.g., Perfettini & Avouac, 2007) and pore fluid diffusion (e.g., Walters et al., 2018) may continue to modify the crustal stress field after an earthquake. Viscoelastic relaxation of the uppermost asthenosphere can be a much greater contributor to stress changes on receiver faults than the elastic coseismic stress changes (e.g., Lynch et al., 2003), especially over distances greater than a few kilometers. Viscoelastic stress changes have been invoked to explain decades-long clusters of earthquakes in areas of moderate to low strain rates, such as Mongolia (Chery et al., 2001; Pollitz et al., 2003). A better understanding of the role of viscoelasticity in the lower crust and upper mantle, gained by studies of earthquake sequences, will also yield insight into longer-term processes,

such as the development and evolution of fault networks and orogens (e.g., Heimpel & Olson, 1996; Koehn et al., 2010; M. Liu et al., 2000; Lyakhovsky et al., 2001; M. Roy, 1998).

The range of potential causes of temporal clustering of seismicity highlights the need to investigate the problem using rigorous physical and statistical analysis. While studies that evaluate a single mechanism (e.g., static and elastic Coulomb stress changes) are numerous, studies that model the full crustal stress tensor field, and incorporate the various known physical processes that operate over the earthquake cycle are more rare. Comprehensive studies that evaluate competing physical mechanisms against paleoseismological and seismological data are critical to disentangle the influences of the mechanisms on evolving seismicity, which is necessary to effectively and efficiently use these mechanisms to forecast future earthquake sequences. Given the breadth of scope and depth of technical expertise required, it is likely that progress is contingent upon deep collaboration between geologists and geophysicists.

4.6.3. Quantifying Seismic Recurrence in a Fault Network

Though the evidence for fault interaction has been growing for decades (as described throughout this section), our efforts toward a deeper understanding of fault network behaviors such as stress triggering and earthquake clustering, and the incorporation of these phenomena into PSHA, are hampered by our relative inability to *measure* these behaviors, that is, to quantify the important characteristics rather than simply observe or describe them. The issue is not that we cannot measure the time between earthquakes but that we lack the proper statistical tools to properly characterize and quantify earthquake recurrence. As discussed previously in this section, earthquake recurrence metrics such as the mean and COV of interevent times, and typical univariate probability distributions such as the lognormal and BPT distributions, do not distinguish between different magnitudes of earthquakes or between different earthquake sources. However, these distinctions are critical for understanding and modeling earthquake processes.

The necessity of including magnitude dependence in an earthquake recurrence metric or probability distribution can be illustrated by consideration of an area with seismicity that follows a standard Gutenberg-Richter distribution with a b value of 1 and faults that are capable of producing earthquakes of at least $M \geq 8$. Given the Gutenberg-Richter relation, $M \geq 6$ earthquakes will be 10 times more frequent than $M \geq 7$ earthquakes and 100 times more frequent than $M \geq 8$ earthquakes. In this instance, how meaningful is a single mean recurrence interval or COV? Does an $M \geq 6.2$ event reset the recurrence timer that includes $M \geq 8$ events (and vice versa), or should those be considered separately? These same questions can be applied to a scenario that explicitly includes multiple earthquake sources (i.e., multiple faults or subfaults that may rupture separately).

Appropriate statistical tools would include simplified metrics, capable of summarizing clustering from multiple sources, that would be sensitive to magnitude, as well as more comprehensive probability distributions (or structured collections of distributions) that describe these same parameters. The incorporation of multiple sources could be performed through the combination of terms for interevent time and interevent distance, perhaps, or distance from the hypocenter of each event to the centroid of the hypocenters, or distance measures that involve finite rupture geometries (as opposed to infinitesimal points of hypocenters). However, incorporating multiple variables with different units (time, distance, and magnitude) and vastly different scales is challenging. More accurate characterizations, comparisons (between data from different sources, models and data, or competing models), and simulations would be enabled through a statistical framework based around probability distributions that are mutually conditional, or linked and capable of mutual updates in some other manner.

The nature of these links and updates should reflect the nature of the processes driving spatiotemporal earthquake clustering and complex recurrence behavior. For example, models of earthquake triggering based on stress transfer may include explicit “clock advances” (or retreats) based on how stress from one earthquake modifies the current time variable in a stress-calibrated time-dependent recurrence probability distribution function (PDF) (e.g., Harris & Simpson, 1992). This could have a different statistical signature than epidemic-type aftershock sequence models (e.g., Field et al., 2017) that include the same faults. Instrumental and paleoseismic earthquake catalogs may also show statistical signatures that are consistent or inconsistent with these models.

Additionally, statistical sampling techniques applied to a structure of probability distributions would facilitate the creation of time-dependent regional PSHA models that incorporate fault interaction matching the degree of interaction present in the source catalogs used to calibrate the model, which is not trivial given

the current state of practice PSHA techniques. The UCERF3 time-dependent model (Field et al., 2017) is the only institutional PSHA model so far developed that includes finite faults, time dependence, and a statistical clustering model based on an epidemic-type aftershock sequence framework. Fortunately, and in contrast to many of the other challenges outlined in this paper, the development of these statistical tools does not require expensive field studies or laboratory measurements, and it is likely that analogous tools and techniques have been developed in other fields. Extensive catalogs of instrumental and paleoseismic data are readily available, and it is up to earthquake scientists to educate themselves in the methods of other fields and to collaborate with statisticians, to make progress on this front. For example, Biasi and Weldon (2009) propose a “stringing pearls” method to combine a large number of paleoseismic data from the San Andreas Fault into ensembles of probable scenarios. This type of analysis allows an objective approach to interpreting which event at a given paleoseismic site may or may not correlate with events identified at adjacent sites. These types of analyses are a necessary and underappreciated step that will enhance comparisons between regions, evaluations of the fits of physical models to data, and the statistical simulations of seismicity at the core of advanced PSHA.

4.7. Summary

In summary, more high-quality, long-term earthquake records are needed from a diversity of tectonic environments to develop a quantitative understanding of the temporal distribution of fault ruptures in different tectonic regimes. These records will involve the expansion of traditional paleoseismic techniques (i.e., trenching) to obtain earthquake records beyond what can be preserved and exposed in a trench. Robust statistical integration of diverse geological data sets is required to test alternative earthquake recurrence distributions based on available data and interpretations. Assuming quasiperiodic recurrence to calculate an average earthquake rate may lead to significantly biased hazard estimates, particularly in low-seismicity or peripheral plate boundary regions, such as the Otago basin and range province. Physics-based models, such as those that incorporate the effects of viscoelasticity of the lower crust and upper mantle, hold promise for understanding the fundamental processes underlying the temporal clustering of earthquakes and will likely be essential in future efforts aimed at accurately representing large earthquake behavior in PSHA.

5. Fault and Earthquake Complexity

Although faults are often treated as single planar features in three dimensions, it has long been obvious that seismogenic faults are instead a collection of smaller fault sections. For example, the main trace of the San Andreas Fault is highly segmented, with no section much longer than ~18 km and most less than ~10 km in length (Wallace, 1973, 1990). The 1906 M_w 7.9 San Francisco earthquake, which ruptured a total length distance of 477 on the San Andreas Fault, must therefore have involved rupture on multiple smaller fault segments (Lawson & Reid, 1908). These observations led early workers to describe the complexity of the 1906 San Andreas Fault rupture using fractals (e.g., Mandelbrot, 1977; Scholz et al., 1986) and to later suggestions that faults and fracture surfaces are fractal (rough) over 10 orders of magnitude in length scale (Candela et al., 2012; Renard et al., 2013; Renard & Candela, 2017; Power et al., 1987).

Several earthquake sequences throughout the past several decades further exemplify how complex fault rupture geometries can be. For example, the 1992 M_w 7.3 Landers, California, earthquake began on the Johnson Valley fault, then jumped progressively to the Kickapoo, Homestead Valley, and Emerson faults, until finally terminating on the Camp Rock fault, for a total rupture length of 85 km (Figure 8a) (Harris & Day, 1999). The 2012 M_w 8.6 Indian Ocean earthquake similarly involved four major ruptures, all with a M_w greater than 8.0 (Meng et al., 2012). The 2016 M_w 7.8 Kaikoura earthquake was one of the most complex ruptures ever recorded, involving a suite of at least 10–20 faults within the Marlborough fault system on the South Island of New Zealand (M. Adams, 2018; Hamling et al., 2017) (Figure 8b). In a recent example, the 2019 Ridgecrest earthquake sequence in Southern California ruptured across a network of complex and interlocking fault systems (Ross et al., 2019).

Large single fault ruptures can also trigger ruptures on faults separated from one another by substantial distance. The 1957 M_w 8.1 Gobi-Atay earthquake was one of the first known examples and involved meters of slip on both strike slip and thrust faults that were 25 km apart at the surface (although the fault planes are much closer at depth) (Bayarsayhan et al., 1996). The start of the 2008 M_w 7.9 Wenchuan earthquake involved rupture on the Pengguan and Beichuan faults, whose strikes are approximately parallel but are separated from one another by approximately 40 km (Fielding et al., 2013; Hartzell et al., 2013; Q. Liu, 2013).

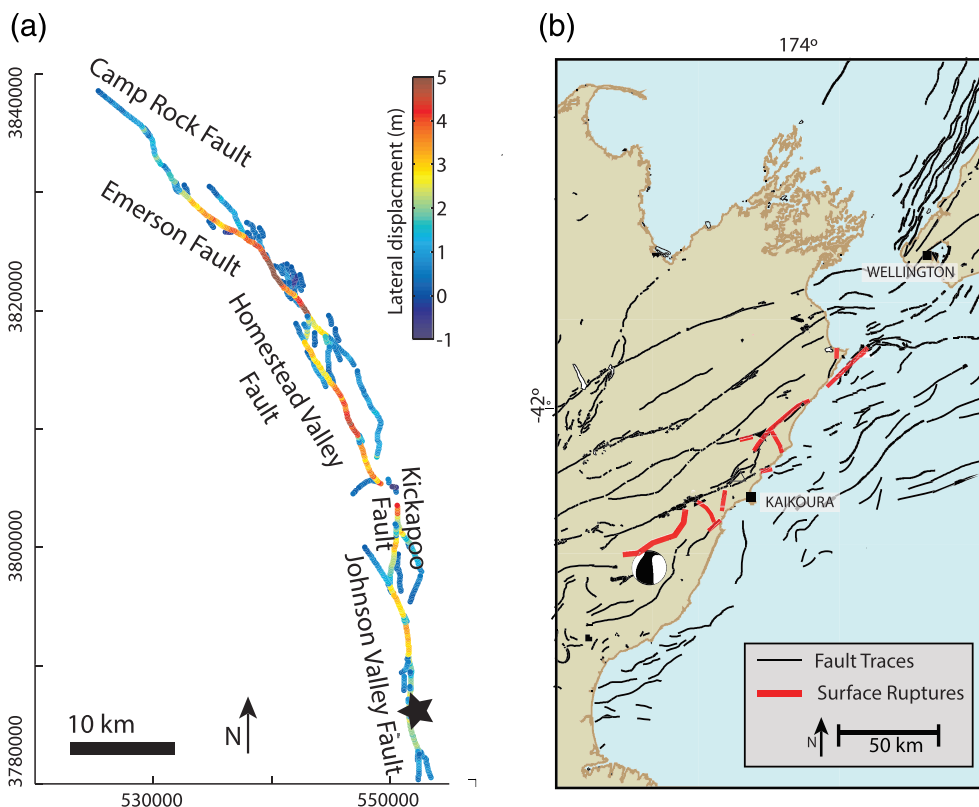


Figure 8. Examples of recent complex earthquake rupture. (a) Faults participating in the 1992 M_w 7.3 Landers earthquake (Harris & Day, 1999). Displacements color coded to show variation of slip even within the same fault taken from Milliner et al. (2015). UTM coordinates shown. (b) Surface ruptures associated with the 2016 M_w 7.8 Kaikoura earthquake, modified from Hamling et al. (2017). Focal mechanism shows epicentral location from USGS.

5.1. Implications for PSHA

Such complex fault and earthquake behavior can be problematic for PSHA models on several fronts, including estimating past or future earthquake magnitudes and recurrence intervals, deducing when a propagating rupture will or will not stop, and understanding how to estimate potential ground motions that may occur due to rupture on a fault. We discuss some of these implications in the following sections below.

5.1.1. Implications of Fault Triggering for PSHA

The observations that earthquake sequences are capable of triggering rupture on neighboring fault sections as part of the same rupture sequence leads to fundamental questions such as follows: Why does a propagating rupture stop? What are the roles of fault steps? Numerical simulations of dynamically propagating ruptures beginning with Harris et al. (1991) and followed by many others (e.g., Harris & Day, 1999; Kase & Kuge, 1998; Lozos et al., 2012; Oglesby, 2005) have tried to quantify the effect of discontinuous breaks in a fault, and Wesnousky (2006) provide an excellent review of geometrical conditions for the endpoints of 20 earthquakes ($M_w \geq 6.2$). In general, these studies suggest that fault sections separated by more than ~5 km will frequently stop a rupture from propagating (Biasi & Wesnousky, 2016).

These fundamentals were put into practice in UCERF3 (Field et al., 2014), which estimated seismic hazard for California, such that a rupture on one fault could jump to another only if the second fault was within 5 km of the first. Because California has a large number of faults, the possible combinations of fault segments rupturing allow for some very long earthquake ruptures and can reach greater than 500 km in about 20% of the possible ruptures, though the probabilities of these complex ruptures, in both an absolute sense, or relative to shorter and simpler ruptures, is extremely low.

5.1.2. Implications for Earthquake Magnitude Estimates

Paleoseismological chronologies of earthquakes are most often limited to a single geographical point. As such, this type of chronology reflects the timing and magnitude as if a fault ruptured independently of rupture on nearby faults. Given the limitations of radiocarbon dating on the South Island of New Zealand,

K. Clark et al. (2017) note that geological reconstructions based on highpoints of coastal uplift would likely have inferred two or four separate events for the 2016 Kaikoura earthquake sequence. If slip on each fault is treated independently of slip on other faults in a paleoseismological chronology, these data could therefore incorrectly affect the magnitude-frequency distribution ultimately used in the earthquake model.

While the Kaikoura earthquake (treated as a point source) was assigned a magnitude M_w 7.8 from teleseismic recordings (USGS, 2016), each of the faults that participated in the earthquake had much smaller magnitudes individually (e.g., M. Adams, 2018; Bradley et al., 2017; Wang et al., 2018). Although different magnitudes have been assigned to the faults depending on the data being analyzed, the magnitudes range between M_w 6.5 and 7.6 (M. Adams, 2018). With slip occurring on multiple faults, and in some cases with a different mechanism in a single event, the use of a single point measurement of slip therefore becomes questionable in ascertaining recurrence rates or possible magnitudes for input into a PSHA model.

5.1.3. Implications for Predicted Ground Motions

Given the possibly poor constraints on paleoearthquake magnitude presented by the Kaikoura example, one conundrum for PSHA is in assigning a magnitude that will directly affect the computation of ground motion intensity measures through the ground motion prediction equations. As discussed by Archuleta et al. (2018), the ground motion metrics such as peak ground acceleration and peak ground velocity in the case of the Kaikoura earthquake are dominated by the closest fault segment; that is, these intensity measures reflect a magnitude less than the M_w 7.8 assigned to the entire earthquake. Intensity measures related to duration would likely reflect the teleseismic-assigned magnitude.

5.2. Future Directions and Research Needs

Rich paleoseismic data sets are critical for determining the frequency of complex ruptures in a fault zone or network and are important for determining whether complex ruptures represent typical events. Recent paleoseismological work is challenging the ideas from the late twentieth century that large faults are persistently or completely segmented, where sections of the faults consistently rupture independently (e.g., Machette et al., 1991) and others (e.g., DuRoss et al., 2016; A. J. Elliott et al., 2018) have instead showed that ruptures sometimes penetrate segment boundaries in larger events and may apply multifault ruptures as well (e.g., DuRoss & Hylland, 2015). The frequencies of, and conditions for, multisegment and multifault ruptures are currently unknown but important for accurate PSHA. Making progress on these topics requires that expansive paleoseismic catalogs are created, which is a time-consuming and expensive process, and may not be possible in all locations. The combination of paleoseismic and neotectonic data with numerical modeling of rupture processes will likely greatly impact our understanding of when, where, and why complex ruptures occur (e.g., Duan et al., 2019; Lozos, 2016).

5.2.1. The Processes Behind Multifault Ruptures and Their Potential Relationship to Earthquake Triggering and Earthquake Clustering

It remains unclear whether temporally clustered earthquakes or multifault ruptures are similar expressions of the same underlying mechanical processes, differing only in the proximity of the secondary fault to their failure threshold, or whether they are less related. To take the idea that they are in fact closely related phenomena a bit farther, one may make a simple time-dependent model of the seismic cycle on each fault, where a “phase” variable represents the proximity to failure of a fault (it needs not be any particular physical quantity), starting from a minimum value immediately after an earthquake, and increasing until it reaches a failure threshold. At some random instant in time, each of the faults will be at its own phase which will probably be different than the other faults in the network. When one fault ruptures, it sends out dynamic stresses in the form of seismic waves, and static and elastic stress changes as displacement accumulates through its rupture time. These stresses will affect each receiver fault in the network differently, based primarily on the distance and orientation of the other faults with respect to the fault undergoing rupture. Some of these faults may be sufficiently close to failure that these instantaneous stresses are sufficient to cause them to fail, causing a multifault rupture. After this earthquake (regardless of the number of faults involved), postseismic processes such as afterslip, viscoelastic relaxation of the lower crust and upper mantle, and poroelastic relaxation within the crust will continue to modulate the stress field, and tectonic stresses on each fault will continue to increase as well. Additional faults in the network, perhaps those pushed close, but not all the way, to their failure thresholds during the earthquake may be pushed to failure in the minutes to decades following the initial rupture.

Fascinatingly, this type of earthquake triggering behavior may cause faults in a fault network to slowly become synchronized over tens to hundreds of seismic cycles (e.g., Bendick & Bilham, 2017; Chery et al., 2001; Hetland & Hager, 2006; Lynch et al., 2003; Scholz, 2010). As earthquakes on a fault advance or retard the timing of the proximal earthquakes on neighboring faults, these minor adjustments to the phase of the earthquake cycle on each fault may accumulate until the phases on some or all of the faults in the system are always similar, a situation known as “phase locking” in the applied mathematics and physics literature (e.g., Kuramoto, 1975; S. H. Strogatz, 2000). The degree of locking within a network of faults, and the time required for the locking to develop, depends on the similarity of the recurrence intervals for the faults and the amount of influence each fault has on its neighbors (Kuramoto, 1975), but it is not necessary that all of the faults in a network are locked (Scholz, 2010). Furthermore, synchronization is dependent on nonlinearity of the renewal process; systems in which phase variables increase more rapidly shortly after a discharge event may become synchronized, while other system phases that increase linearly do not (Lynch et al., 2003). The shear stress on faults is thought to increase somewhat more rapidly following an earthquake than later in its seismic cycle (Chery et al., 2001), which could indicate susceptibility of fault systems to phase locking. Finite element simulations of pairs of faults embedded in an elastic-viscoelastic crust display synchronization due to time-dependent viscoelastic postseismic stress transfer (Chery et al., 2001; Lynch et al., 2003).

Though phase locking is common in a wide range of physical and biological phenomena (S. H. Strogatz, 2000) (see S. Strogatz, 2004, for an introduction), it is difficult to demonstrate this phenomenon over earthquake timescales. Scholz (2010) presents an abundance of evidence of triggered earthquakes from the historical and instrumental records, and Bendick and Bilham (2017) statistically evaluate a global catalog of M 7+ earthquakes to identify groups or clusters of earthquakes on faults with similar estimated recurrence intervals spaced more closely in time than found in randomized catalogs (these earthquakes are generally not spatially proximal). Both of these sets of observations provide evidence for temporally linked fault ruptures, but synchrony and phase locking imply some degree of repetition of these temporally proximal events. Therefore, long paleoseismological records on many faults in a region are needed to evaluate the possibility of long-term fault synchronization and phase locking. Though these records are slowly accumulating, only a few studies have tested the hypotheses against sufficient data sets, and the results have been mixed. Sherrod and Gomberg (2014) found that despite a remarkable temporal cluster of earthquakes on distributed crustal faults in the Puget Lowland region of Washington State (USA), earthquakes farther back in the paleoseismic record were generally asynchronous, rejecting the hypothesis of phase locking. Benedetti et al. (2013), in contrast, found multiple episodes of temporally clustered seismicity separated by relatively quiet intervals on normal faults in Italy. Investigations that couple numerical modeling with rich paleoseismic data sets may reveal the prevalence of earthquake phase locking and the conditions that promote or inhibit it in the future.

6. Earthquake Scaling Relations

Earthquake magnitude scaling relations (hereafter referred to as scaling relations) are an integral component of a PSHA (Figure 1). They are used to estimate the maximum possible magnitude of earthquakes on faults that have not experienced a full-fault rupture historically. They are used to scale the size of each of the thousands to millions of possible ruptures in a PSHA so that ground motions at study sites may be calculated using distances to the closest point on the rupture surface, rather than the hypocenter (which may be tens to hundreds of kilometers away for large events). And fault-scaling relationships are also frequently used in paleoseismic studies to infer the size of paleoearthquakes, using measurements such as surface rupture or offset amounts that have been associated with a paleoseismic event (e.g., Biasi & Weldon, 2006).

Scaling relations are regression equations usually developed from historical earthquake data sets, in which magnitude is related to measurable parameters such as fault rupture length or rupture area. Scaling relations therefore provide earthquake magnitude estimates even in the absence of recorded earthquakes, so long as the length, rupture area, and/or geometry of a fault are known. In the following sections we describe the fundamentals of earthquake scaling, describe key factors that control differences in magnitude scaling, provide an overview of the main types of scaling relations that have been developed in the last couple decades, and provide some ideas as to where the general topic area is going in the future.

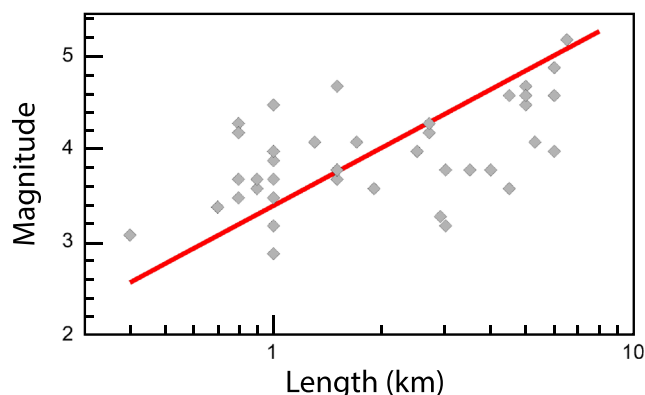


Figure 9. Magnitude-on-rupture-length scaling relation for the Etna region of Italy (Azzaro et al., 2017). The equation of the line is $M_w = 3.39 + 2.08\log(L)$, with a standard error of 0.39 on magnitude (M_w), and L represents length.

6.1. Fundamentals of Earthquake Scaling

Earthquake magnitude scales with earthquake source dimensions. The larger the earthquake rupture area and associated displacement, the larger the earthquake magnitude. For instance, the M_w 7.9 1906 San Francisco, California earthquake produced a 477-km-long rupture of the San Andreas Fault with an average slip of about 4 m (Lawson & Reid, 1908), whereas the M_w 6.9 1989 Loma Prieta, California, earthquake produced a 35-km subsurface rupture and average slip of about 1 m (e.g., Steidl et al., 1991). Scaling relations are typically developed as empirical regressions of instrumentally derived magnitude on measured fault dimensions. An example of a regression line and the associated data set is shown in Figure 9. What is obvious from this figure is the broadly linear trend of the data and the considerable data scatter.

6.2. The Importance of Rupture Size in Scaling Relations

Studies over the past several decades have shown that one of the most important factors affecting scaling relations relates to earthquake rupture size and more specifically the difference between width-unlimited and width-limited ruptures. Width-unlimited earthquakes refer to ruptures that are smaller than the full fault width, defined as the distance from the top to the bottom of the rupture along the fault plane surface. Width-limited earthquakes, by contrast, are larger events that rupture across the full width of the fault. The former can grow both laterally and vertically, whereas the latter can only grow laterally. Incorporating the differences in scaling between moderate (width-unlimited) and large (width-limited) earthquakes can result in a bilinear scaling relation as shown in Figure 10 (e.g., Allen & Hayes, 2017; Hanks & Bakun, 2008; Stafford, 2014), or even multilinear scaling relations, if very long earthquake ruptures are considered (Shaw, 2009, 2013).

These newer bilinear or multilinear scaling relations better incorporate earthquake physics into the scaling relations than previous linear relations such as those of Wells and Coppersmith (1994). As shown by the thin line in Figure 10, linear global scaling relations (e.g., Wells & Coppersmith, 1994) that use the entire suite of earthquake sizes can underestimate earthquake magnitude, especially for larger events (M. Stirling et al., 2002). The simpler example shown in Figure 9 with roughly linear scaling does not show this bias because the ruptures used in the regression were smaller in magnitude.

6.3. The Importance of Tectonic Environment

In addition to rupture size, recent work has also demonstrated that tectonic environments (e.g., slip type, slip rate, and proximity to the plate boundary) (Anderson et al., 1996; Kanamori & Allen, 1986; Scholz et al., 1986) present important factors to consider when choosing appropriate scaling relations (e.g., M. Stirling et al., 2013). For example, if rupture dimensions are comparable, earthquakes produced by reverse faults tend to be larger in magnitude than earthquakes produced by other slip types. Similarly, earthquakes in intraplate regions tend to be larger in magnitude than earthquakes in interplate regions for the same rupture dimensions (e.g., Scholz et al., 1986). These differences are likely a consequence of the differing stress regimes and fault strengths in the respective tectonic environments.

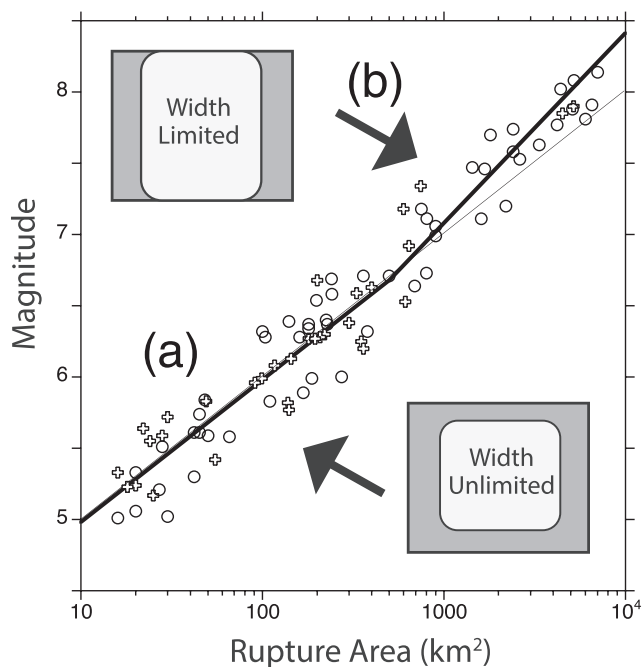


Figure 10. Magnitude-on-rupture-area scaling relations for continental strike-slip faults (Hanks & Bakun, 2008). Circles show global data, while crosses show data from the state of California, USA. Schematic faults shown as gray rectangles, and fault ruptures shown as white areas within the gray rectangles. The equation for part (a) (width unlimited, moderate earthquakes) of the scaling relation is $M_w = \log(A) + 3.98$, for $A \leq 537 \text{ km}^2$, and part (b) (width limited, large-to-great earthquakes) is $M_w = 4/3\log(A) + 3.07$, for $A > 537 \text{ km}^2$. The thin line of Wells and Coppersmith (1994) is shown for comparison. A represents rupture area.

Recent studies have pointed out that magnitude estimates for a given fault rupture length or area can differ by up to a full magnitude if inappropriate regression equations are used, or if the regression equation is developed based on combined data from multiple tectonic environments (M. Stirling et al., 2013). Table 1 shows a current classification scheme that could be used to select an appropriate scaling relation for a given study area.

6.4. Scaling Relation Equation Categories

Up-to-date scaling relations generally fall into the categories of magnitude-on-area, magnitude-on-length, magnitude-on-length-and-width, magnitude-on-area via seismic moment, and magnitude-on-length-and-slip rate. Examples of scaling relations for each of these categories (and more) are shown below, in which A , A_e , L , W , and M_o are rupture area, effective rupture area, length, width, and seismic moment, respectively.

Table 1
Tectonic Regime Classification Scheme Developed by M. Stirling et al. (2013) to Classify Scaling Relations

Plate Tectonic Setting	Subclass	Slip Type
Plate boundary crustal	Fast plate boundary faults ($> 10 \text{ mm/yr}$)	Strike-slip
Plate boundary crustal	Slow plate boundary faults ($< 10 \text{ mm/yr}$)	All types
Stable continental	–	Reverse
Stable continental	–	Strike-slip
Subduction	Continental megathrust	Thrust
Subduction	Marine megathrust	Thrust
Subduction	Intraslab subduction	Normal
Volcanic	Thin crust ($< 10 \text{ km}$)	Normal
Volcanic	Thick crust ($> 10 \text{ km}$)	Normal

Magnitude-on-area $M_w = \log A + 3.98$ (for $A \leq 537 \text{ km}^2$); Hanks and Bakun (2008) $M_w = 4/3 \log A + 3.07$ (for $A < 537 \text{ km}^2$); Hanks and Bakun (2008)

Applicable to continental strike-slip earthquakes.

Magnitude-on-length $M_w = 5.56 + 0.87 \log L$; Wesnousky (2008)

Applicable to continental strike-slip earthquakes.

Magnitude-on-length and width $M_w = 4.18 + 2/3 \log W + 4/3 \log L$; M. Stirling et al. (2008)

Applicable to oblique slip earthquakes in New Zealand.

Magnitude-on-area via seismic moment $\log A_e = -14.77 + 0.92 \log M_o$; Yen and Ma (2011)Applicable to strike-slip earthquakes. The equation $\log(M_o) = 16.05 + 1.5M_w$ (Hanks & Kanamori, 1979) is then used to convert from M_o to M_w .*Magnitude-on-length and slip rate* $M_w = c_0 + c_1 \log L_e + c_2 \log (S_f/S_0)$; Anderson et al. (2017)

Applicable to all slip types.

Magnitude on area and width

$$M_w = \log_{10} A + \frac{2}{3} \log_{10} \frac{\max(1, \sqrt{\frac{A}{W^2}})}{\left(1 + \max\left(1, \frac{A}{W^2 \beta}\right)\right)/2} + \text{const.}; \text{ Shaw (2013)}$$

Applicable to continental strike-slip earthquakes, in which β is a fitting parameter, and const. is an empirical constant.

6.5. Using Appropriate Scaling Relations

Linear global relations such as those of the Wells and Coppersmith (1994) can lead to misestimations of earthquake magnitude, by up to a full magnitude unit, in large part because they do not take into account known differences in scaling due to earthquake size or to tectonic environment (M. Stirling et al., 2013). Because the Wells and Coppersmith (1994) relations are now 25 years old, they exclude many of the major, well-instrumented earthquakes that have occurred since, and these larger earthquakes therefore have importance for accurate regressions at the highest magnitude range. Using up-to-date scaling relations (e.g., Anderson et al., 2017; Stafford, 2014) and relations that are specific to the study area is therefore critically important to consider in a seismic hazard assessment.

6.6. The Effect of Complex Earthquake Rupture on Earthquake Scaling

As already discussed in section 5, one of the lessons provided by recent well-instrumented major earthquakes is that earthquake events are often composed of subevents produced by multiple faults. The $M_w 7.1$ 2010 Darfield, New Zealand, earthquake ruptured several faults (Quigley et al., 2012), and the $M_w 7.8$ 2016 Kaikoura New Zealand earthquake ruptured over 20 distinct faults (e.g., Hamling et al., 2017; M. W. Stirling & Anderson, 2018). The Kaikoura earthquake in particular was considerably more complex than had been predicted from prior New Zealand seismic hazard models (e.g., M. Stirling et al., 2012).

This begs the question, are scaling relationships useful for characterizing complex multifault earthquake sources such as the 2016 Kaikoura earthquake? This question was addressed recently by comparing the estimates of magnitude derived from scaling relations to the observed magnitude of the Kaikoura earthquake in M. W. Stirling and Anderson (2018). The fault dimensions considered in this study included the combined length of all the faults involved in the earthquake, the mean width of all ruptures, and in the case of the Anderson et al. (2017) relation, the weighted mean slip rate of the faults. This and other studies (e.g., Quigley et al., 2012) showed that the earthquake scalings of both the Kaikoura and Darfield events were consistent

with magnitudes estimated from several modern scaling relations. This result implies that no unusual scaling occurred during these complex multifault earthquakes and gives confidence in the continued use of modern scaling relations to characterize complex earthquakes in a predictive sense in PSHA.

6.7. Conclusions and Future Directions

Scaling relations have progressed from simple linear relations of magnitude on fault rupture length or width to relations that consider additional earthquake physics-related parameters in the scaling. Some recent scaling relations include parameters such as slip rate and consider the differences between width-unlimited and width-limited scaling. One of the current issues associated with the use of scaling relations in seismic hazard analysis is choosing an appropriate relation for a given study area or magnitude range. Recognition of the importance of updated scaling relations has prompted at least one systematic effort to provide guidance on scaling relations usage in the last decade. The Global Earthquake Model (GEM) Foundation (globalquakemodel.org) was formed to develop a global seismic hazard and risk model, largely achieved by way of a number of global and regionally based efforts. A component of these efforts involved the compilation and assessment of the available scaling relations and provision of guidelines for the application of the scaling relations to different tectonic regimes. Some of the results of this effort were published in M. Stirling et al. (2013), which provides a suite of up-to-date scaling relations and also provides guidelines on their appropriate use.

Future scaling relation developments will likely progress on two fronts: (1) specific relations for a wider number of specific tectonic regimes and (2) globally relevant relations that incorporate key parameters relevant to earthquake physics (e.g., stress drop and slip rate). Of these topic areas, it is the latter that is seeing the greatest development at present, with the recent papers of Shaw (2013) and Anderson et al. (2017) as examples. Scaling relation developments in the last decade (e.g., Brengman et al., 2019; Thingbaijam et al., 2017) have been greatly facilitated through most of the recent large earthquakes being well instrumented and well studied and possessing multidisciplinary data sets. It is therefore not surprising that enhanced insights into the physics of earthquake scaling have resulted from these periodic injections of high quality data and will likely continue into the future.

On the practical side, the use of scaling relations in PSHA will need to improve significantly to keep up with the demands of industry end-users. PSHA is becoming increasingly complex as a result of official guidelines and regulations, requiring the full treatment of epistemic uncertainty. The demands of the industry for greater defensibility of PSHA will in turn require defensible selections of multiple scaling relations by the PSHA experts. These demands will also filter down to the scaling relation developers, who will need to provide (1) scaling relations based on the best-possible data, (2) clear recommendations regarding the appropriate use of their relations with respect to tectonic environment and magnitude range, and (3) standard deviations and/or standard errors for their relations. The next (fourth) version of the Unified California Earthquake Rupture Forecast (UCERF4) will likely see a renewed focus on scaling relations. A resolution of the differences and synergies between universal earthquake physics-based approaches to scaling relations (e.g., Shaw, 2013) and the more traditional empirical approaches (e.g., Anderson et al., 2017) will be one of the more significant tasks to address. Lastly, the innovative efforts to develop physics-based PSAs (e.g., Graves et al., 2011) have been heavily reliant on realistic estimates of all earthquake parameters. Obtaining the best-possible estimates of magnitude and a defensible quantification of magnitude epistemic uncertainty will be an important challenge in the future.

7. The Problem of Enigmatic Seismogenic Faults: Where Are They Located, and What Is Their Geometry and Rate of Activity?

The location, geometry, and slip rate of seismogenic faults represent some of the most basic data needed to construct an earthquake occurrence model (Figure 1). Although this type of information can sometimes be relatively easy to obtain, especially for large plate boundary faults such as the San Andreas, several recent, damaging, earthquakes have surprised us by occurring on inconspicuous, buried, unusual, or otherwise enigmatic fault systems. Recent examples include (1) the M_w 7.9 2008 Wenchuan earthquake, which ruptured the Yingxiu-Beichuan fault in the Sichuan Province of China and caused ~70,000 deaths (Figure 11); and (2) the 25 April 2015 M_w 7.8 Gorkha Nepal earthquake (Figure 11), which caused ~9,000 fatalities and extensive damage in Kathmandu (e.g., Avouac et al., 2015). In the Wenchuan case, seismic hazard maps did not anticipate a large event on the Yingxiu-Beichuan fault in particular (e.g., Shen et al., 2005). And

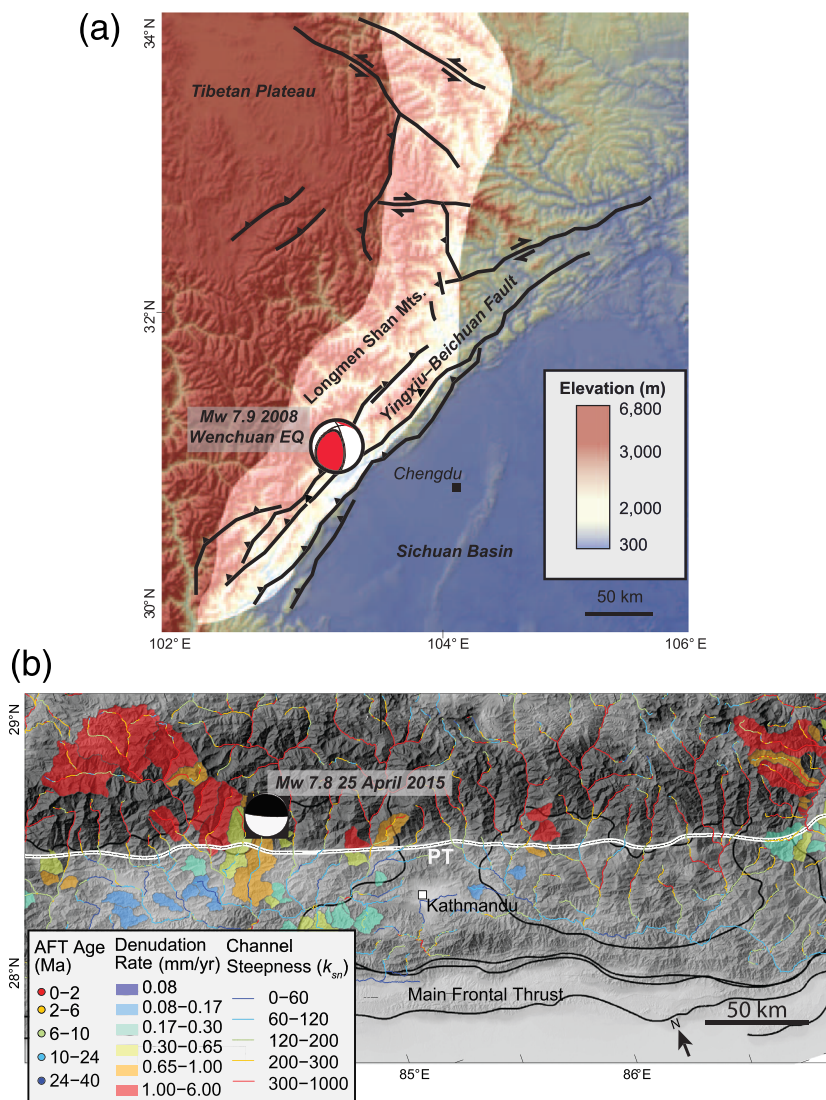


Figure 11. Examples of recent earthquakes in which the properties of the ruptured fault had been previously studied using topographic and geomorphic analyses. (a) Figure modified from Kirby et al. (2008) showing location of Wenchuan earthquake. Topographic analysis revealed a region of high rock uplift rate on the southeastern margin of the Tibetan Plateau (Kirby et al., 2003), despite low rates of GPS-derived convergence rates. The fault that hosted the Wenchuan earthquake ruptured within the region of high rock uplift rate, as highlighted in white. Black lines show surface traces of faults. (b) Figure modified from K. X. Whipple et al. (2016) showing normalized channel steepness values, denudation rates, and apatite fission track (AFT) ages, relative to the location of the M_w 7.8 2015 Gorkha earthquake. Black lines denote surface traces of faults. Focal mechanism from the USGS (USGS, 2015).

although the Gorkha earthquake was expected (e.g., Bilham et al., 2001), it did not release the total amount of estimated strain build up (Bilham et al., 2017; Mencin et al., 2016), it did not produce a surface rupture, and the geometry of the deeper seismogenic structure associated with this earthquake remains a topic of intense debate (J. Elliott et al., 2016; Whipple et al., 2017). Both of these earthquakes exemplify how traditional methods in seismic and geodetic monitoring or paleoseismic trenching alone cannot be used to deduce the long-term history, frequency, or size of earthquakes that might occur on all potentially damaging seismogenic faults, and they highlight the need to incorporate alternate approaches capable of estimating the locations, geometries, and slip rates of enigmatic fault systems. While there are many approaches to this problem, in the following sections we discuss some examples of how topography may be used to place constraints on the geometry, activity rate, and location of enigmatic faults and pose some ideas on how these

topic areas may progress in the future. In the first part of this section we focus on the application of geomorphic theory to topography, and in the second part we focus on technological advances and the increasing availability of high-resolution topography.

7.1. Topography and Geomorphic Theory Can Highlight Properties of Active Enigmatic Faults

Previous studies on the fault systems that ruptured during the Wenchuan and Gorkha earthquakes illustrate how topographic and geomorphic analyses can yield important insights into the properties of seismogenic faults. Despite the low rates of GPS convergence, long-term exhumation patterns and analyses of river channel steepness (k_{sn} , a proxy for rock uplift rate normalized for changes in basin area and shape) had already highlighted the Yingxiu-Beichuan fault as a potential seismic source prior to the Wenchuan rupture (Kirby et al., 2003, 2008). In the Himalaya, Seeber and Gornitz (1983) were the first to recognize that northward increases in topography and river steepness ~100 km from the frontal thrust (the Main Frontal Thrust) must delineate a major hidden tectonic boundary near where the Gorkha earthquake later ruptured (Figure 11). Although the details are vigorously debated, numerous subsequent studies have used topographic analyses in the form of river channel steepness (k_{sn}), relief, hillslope morphologies, and both millennial and multimillion-year erosion rates that generally corroborate Seeber and Gornitz's (1983) original hypothesis (Godard et al., 2014; Lavé & Avouac, 2001; Wobus et al., 2006). There is now broad consensus for a northward increase in rock uplift rate caused by either a change in the geometry of the décollement at depth or the presence of one or more buried active faults near the hypocenter of the Gorkha earthquake (Figure 11).

These are just two of a growing number of study areas where topographic and geomorphic analyses have been used to elucidate the properties of enigmatic seismogenic faults. For example, in the Po Valley of Italy, subtle changes in river channel morphology and plan view channel geometry have been used to pinpoint fault-related folding associated with buried seismogenic faults (Burrato et al., 2012). When combined with geodynamic modeling, balanced cross sections, and subsurface geophysical data, these tools placed constraints on the rates of fault slip beneath the Po Plain, that were later used in seismic hazard analyses (Maesano et al., 2015; Vannoli et al., 2015). In Northern California, along-strike increases in normalized river channel steepness were used to identify a region of heightened rock uplift created by a blind thrust fault beneath Mt. Tamalpais (Kirby et al., 2007). Coupled with geodynamic modeling, these data sets revealed the geometry of the blind fault, even though this proposed fault cuts through structures within the Franciscan melange and a fault cutting this unit would be difficult to image using geophysical techniques (C. B. Johnson et al., 2009). These studies highlight how topography and geomorphology have the potential to elucidate the location, activity, and geometry of enigmatic active faults, even in rapidly eroding landscapes where deformed young sediments are lacking or where fault-related features that can be important for paleoseismic studies (e.g., a fault scarp developed in Quaternary deposits) may be buried or erased from the geologic record. Below we describe some of the potential directions that we see this field to be taking in the future.

7.2. Future Directions

The inference that topography and geomorphology could elucidate the location and/or activity rate of active faults is based on the decades-old idea that actively uplifting landscapes should be equally balanced by erosion rates (e.g., Ahnert, 1970). Several decades of research have shown that increases in erosion rate and rock uplift rate in such landscapes will lead to steepening of hillslopes and river channels until a critical threshold is reached, so long as the effects of channel geometry, lithology, climate, and substrate erodibility can be accounted for (e.g., Wobus et al., 2006). For landscapes where erosion rates can be reasonably assumed to be balanced by rock uplift rates (i.e., topographic steady state) and where the effects of variations in lithology and rainfall rate can be taken into account, erosion rate and the elevation of river channels that incise bedrock have been used to infer spatiotemporal patterns of rock uplift rates due to active faulting in areas across the globe, including China (e.g., Kirby et al., 2008), California (e.g., C. B. Johnson et al., 2009; Kirby et al., 2007), and Italy (e.g., Burrato et al., 2012; Maesano et al., 2015; Vannoli et al., 2015), among many others. Many of these studies have taken advantage of the wide availability of topographic data sets from global digital elevation models (DEMs) derived from satellite data, such as the ASTER-derived global digital elevation model (GDEM) (e.g., Tachikawa et al., 2011) or the Shuttle Radar Topography Mission (SRTM) data sets (e.g., Farr et al., 2007).

Most previous studies that have aimed to constrain rock uplift rate or differential rock uplift in actively uplifting landscapes using these types of methods tend to assume spatially invariant rates of rock uplift (see Wobus et al., 2006). Although incorporating lateral advection of crust remains a challenge in most

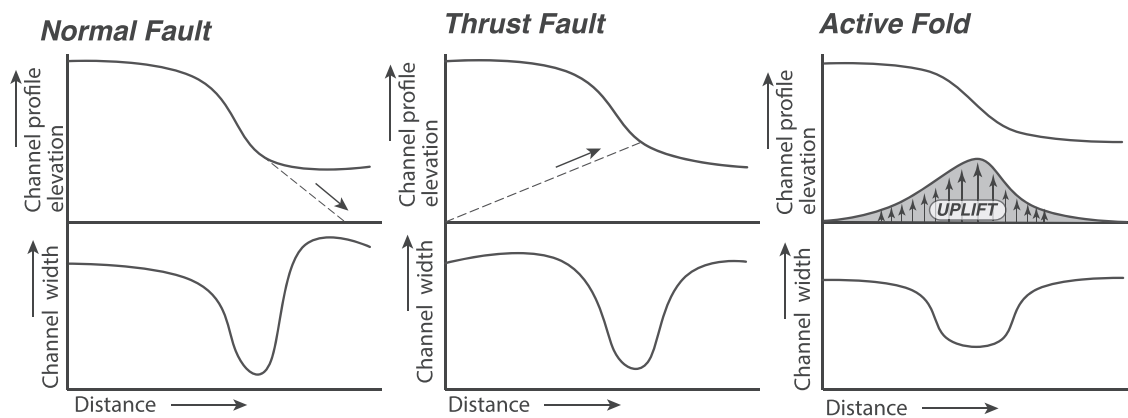


Figure 12. Figure modified from Fisher et al. (2013) showing how channel width is predicted to respond to changes in rock uplift rate across active faults or folds.

current landscape evolution models, several recent studies have demonstrated the utility in considering spatially irregular rock uplift rate patterns in the production of some uplifting and eroding landscapes. For example, B. Adams et al. (2016) show that the low-relief landscape of Central Bhutan in the eastern Himalaya can be explained by a northward gradient in rock uplift rate induced by recent duplexing at depth. These authors were able to place constraints on both the timing and the spatial variability of rock uplift rate along a blind portion of the Main Himalayan Thrust by combining topography with measurements of basin-wide erosion rates, landscape evolution models, and field data. Several recent studies have also used numerical models to simulate topographic and landscape development with the incorporation of horizontal motion across active faults (Gallen & Thigpen, 2018; Gray et al., 2017; Hallet & Molnar, 2001). For instance, Goren et al. (2015) show how sheared and rotated rivers out of disequilibrium can elucidate the rate of strike-slip faulting along the Dead Sea fault system. And Castelltort et al. (2012) place constraints on the long-term slip rate of the Alpine fault using sheared basins simulated with a landscape evolution model. Although both of these studied fault systems are emergent, these types of studies could have potential in elucidating strain that may occur across blind, buried, or poorly exposed fault systems or those that may have particularly long recurrence intervals or low slip rates.

Although it is widely accepted that river channels are more sensitive to changes in erosion or rock uplift rate than hillslopes (Ouimet et al., 2009), several recent studies suggest that hillslope morphology encodes information about tectonics that could be useful in elucidating the character of enigmatic faults, if sufficiently high-resolution topographic data are available (Hilley et al., 2010; Milodowski et al., 2015; Roering, 2008). Penserini et al. (2017) show that with adequate resolution, the topography of debris flow valley networks can scale with erosion or rock uplift rate in Cascadia. Hurst et al. (2012) demonstrate that although the relationships are complex (see Heimsath et al., 2012), hillslope curvature and roughness can yield information about the timing and spatial distribution of erosion rates, and by proxy rock uplift rates, in growing or decaying landscapes. With the increasing availability of high-resolution DEMs, these examples suggest that hillslope morphology could help in defining the timing and erosional response of landscapes to changes in rock uplift rates along blind or obscured seismogenic faults in the future.

The response of channel width to increases in rock uplift rate is often assumed constant, due to difficulties both in measurement and theory (see Wobus et al., 2006). However, a growing body of literature suggests that, under the right conditions, channel width could help elucidate spatial or temporal changes in rock uplift rate (Attal et al., 2008; Turowski et al., 2009; Yanites, 2018). Amos and Burbank (2007) use field data across active folds in New Zealand to show how channels initially adjust to an increase in rock uplift rate by narrowing their width, even before channel steepening begins. Fisher et al. (2013) point out that the channel width response to an increase in rock uplift rate is inversely proportional to channel steepness (so long as discharge, substrate erodibility, and climate can be accounted for). They show how channel width could be exploited to understand spatial or temporal patterns of rock uplift rate, such as those that can occur across active faults or folds (Figure 12). With the increasing availability of high-resolution imagery and topography from sources such as Google Earth®, channel width holds promise for elucidating properties of seismogenic faults in the future.

The chi metric (χ), which represents an integral form of the longitudinal profile of a river as described by the stream power model (Perron & Royden, 2013), has recently been used for a myriad of applications, including (1) to calculate normalized channel steepness (Perron & Royden, 2013), (2) to identify knickpoints and thus a deviation from topographic steady state, (3) to predict whether a drainage divide migrates in plan view, or (4) to calculate variations in rock uplift rate in space and time (Goren et al., 2014). Willett et al. (2014) show how sharp variations in χ across drainage divides can be a predictor of whether a divide migrates due to changes in drainage area between opposing basins. These studies highlight how future studies that wish to use erosion rate, incision rates, and river channel steepness to elucidate tectonics in actively uplifting landscapes will need to consider the influence of migrating drainage divides (Dahlquist et al., 2018; Forte & Whipple, 2018; K. Whipple et al., 2017). In a recent study, Goren et al. (2014) use χ maps to analyze a transient landscape in the Inyo Mountain Range of California and then use numerical solutions to directly invert for relative uplift rate. Although the Inyo Fault is an emergent fault, these types of analyses could be valuable in identifying the location of, and slip rates associated with, seismogenic faults under the right conditions.

Despite the promise shown by these examples, there remain many challenges and caveats to utilizing topography and geomorphology to understand the geometry and slip history of blind or hidden faults. In the case of the Himalaya, the wealth of topographic, erosion rate, GPS, seismicity, InSAR, and surficial geology data was not able to lay to rest the ongoing debate about the geometry and kinematics of the seismogenic faults near the location of the Gorkha earthquake (Avouac et al., 2015; K. X. Whipple et al., 2016). Moreover, our ability to deduce tectonic information from topography is complicated by an incomplete understanding about many processes, including incision thresholds (e.g., Lague, 2014), nontectonic factors (e.g., Sklar & Dietrich, 2001), channel geometry (e.g., Finnegan et al., 2005), the influence of glacial processes (e.g., Brocklehurst & Whipple, 2002), the effects of precipitation and/or climate (e.g., K. X. Whipple, 2009), and many others. It has long been recognized that there is not a straightforward relationship between incision and rock uplift rate across all study areas, and there are complicated potential feedbacks between factors such as local climate, sediment supply, rock strength, and grain size that hinder our ability to interpret tectonics from topography (Hurst et al., 2013; Molnar et al., 2007; Sklar & Dietrich, 2001). In particular, it has been difficult to isolate the effects of mass strength, grain size, or fracture density on erosion rate and incision rate. However, several recent studies have made headway in understanding these complications (e.g., S. Roy et al., 2016). For example, DiBiase et al. (2018) show that lower fracture density leads to larger grain size and therefore steeper channels without large changes in rock uplift rate. Future studies aimed at teasing out these various effects will help in our ability to interpret topography and geomorphology in terms of data that are valuable for PSHA, including longer-term records of slip rate, and the location, kinematics, and geometry of potentially active faults that may be difficult to analyze using traditional techniques.

7.3. Enigmatic Faults Revealed by Increasing Topographic Resolution

The growing availability of high-resolution topography as a consequence of new technologies, such as lidar and photogrammetry (including structure from motion techniques; e.g., K. Johnson et al., 2014), represents one of the most important recent advances in facilitating the identification and location of previously unknown active faults (Haddad et al., 2012; Kondo et al., 2008; Meigs, 2013; Oskin et al., 2012; Zielke et al., 2010). Bare-earth DEMs derived from lidar data, which now routinely have a resolution of $<1\text{--}2\text{ m}$ in the horizontal and $<10\text{ cm}$ in the vertical directions, have provided an unprecedented view of the elevation of the Earth's surface beneath vegetation (e.g., Haugerud et al., 2003). Bare-earth lidar DEMs have been used to elucidate previously unidentified Quaternary-active faults in the Pacific Northwest of North America (e.g., Haugerud et al., 2003; Morell et al., 2017), California, USA (e.g., Arrowsmith & Zielke, 2009), Slovenia (e.g., Cunningham et al., 2006), New Zealand (Barth et al., 2012), and many other areas across the globe. In addition to coseismic surface ruptures, lidar data have also been used to identify previously unknown geomorphic surfaces (e.g., Meigs, 2013), quantify off-fault deformation (e.g., Oskin et al., 2012), identify microscale geomorphic or tectonic features, map fault zone structure (e.g., DeLong et al., 2010), and estimate rupture size or paleorecurrence interval on individual fault strands (e.g., Zielke et al., 2010), among many other applications. In the same way, high-resolution multibeam bathymetry is providing insights into submarine faults that were previously unknown (D. D. Brothers et al., 2020). For example, Pow-nall et al. (2016) used high-resolution multibeam data to discover Earth's largest known normal fault, the 450-km-long Banda Detachment in eastern Indonesia, now considered the likely source of several damaging historical earthquakes and tsunamis (Cummins et al., 2020).

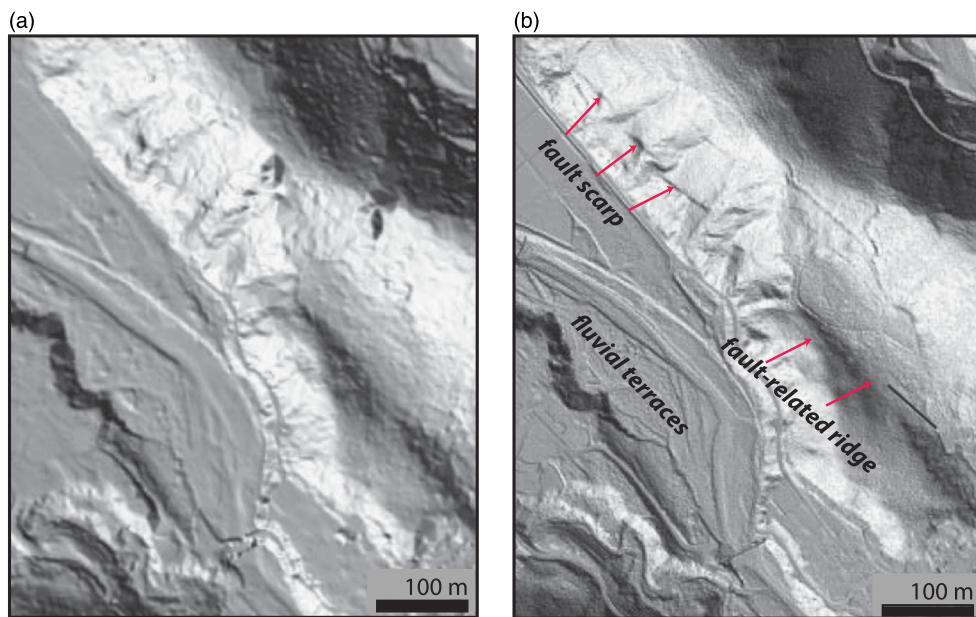


Figure 13. Figure modified from Lin et al. (2013) showing a 2-m bare-earth lidar DEM in a forested region of Japan (a), compared with a 0.25-m-resolution lidar DEM (b). Note how the higher-resolution topography in part (b) highlights fault-related features that are not clearly visible in part (a).

7.4. Future Directions

Currently, bare-earth lidar DEMs that are often used in tectonic-geomorphic studies are commonly 1–2 m in horizontal resolution, due in large part to the ground point density of the point cloud (<~8 ground points per m^2 Heidemann, 2012). However, several recent studies suggest that even higher-resolution topography (<0.5 m), which is becoming more easily available, could be necessary for identifying some types of seismogenic faults in the future. For example, Lin et al. (2013) show that 2-m lidar DEMs derived from a density of ~1.2 ground points per m^2 were insufficient to detect subtle fault-related features in a densely forested region of Japan (Figure 13). These authors show that a 0.25-m-resolution DEM produced from a high-resolution lidar survey with density as high as ~12.7 ground points per m^2 was instead necessary to reveal tectonic-geomorphic features that would otherwise have been concealed beneath vegetation in this study area. The high ground point density was achieved by scanning the study area three or more times from varying angles during a number of flight passes.

New photogrammetry techniques and structure from motion software (e.g., Agisoft PhotoScan[®]) that allow the production of high-resolution 3-D models and point clouds show great promise in facilitating the identification of new enigmatic faults, potentially at a much cheaper price than the average lidar collection campaign (e.g., K. Johnson et al., 2014). The accuracy and precision of a 3-D model produced from photogrammetry depends on a wide variety factors, such as the scale and resolution of the input images, the distribution and accuracy of control data, and the overlap and view angles between images (Bemis et al., 2014; James & Robson, 2012; K. Johnson et al., 2014). However, in the absence of vegetation, a DEM produced by photogrammetry software using photographs taken by relatively inexpensive unmanned aerial vehicles (UAVs), balloons, or cameras can routinely yield submeter horizontal resolution and subcentimeter vertical resolution, in a manner similar to (or with much higher resolution than) a bare-earth lidar data set. Moreover, given the increasing availability of relatively high-resolution stereopair satellite data, such as imagery recently acquired by Digital Globe[®], these types of technologies will provide rich data sets for future researchers searching for locations to place a paleoseismic trench or to conduct additional field campaigns aimed at elucidating previously unknown faults.

7.5. Summary and Future Challenges

We have outlined a few examples that show how topography can help identify the location and activity of enigmatic faults and how it may be used to constrain the activity rate of enigmatic seismogenic structures in the future. We envision that the increasing availability of higher-resolution topography and the

progress in understanding geomorphic theory will continue to advance the capabilities. We also envision that our growing understanding of the linkages between topography and geomorphology hold promise in acquiring longer-term rates of fault motion than is currently the norm based on techniques such as paleoseismic trenching. However, there are cases where potentially seismogenic faults do not have a topographic expression, which might occur for a number of reasons. Such was the case for the M_w 7.1 mainshock of the 2010–2012 Canterbury earthquake sequence that occurred on the previously unidentified Greendale fault (Gledhill et al., 2011). In these instances, secondary paleoseismic evidence in the form of paleoliquefaction features, rockfall, fragile geologic features, or other earthquake-induced environmental effects may be required to constrain properties of buried faults such as the Greendale fault (e.g., Quigley et al., 2016). The implementation of distributed seismicity into PSHA models continues to be an important effort to capture these types of events.

8. Conclusions and Future Directions

The proper incorporation of geologic data into PSHA models ideally requires specification of the geometry, location, and kinematics of active faults and a detailed spatial and temporal record of paleoseismic events on these faults and their rates of slip over long (many thousands of years) time periods. But a number of factors present challenges in acquiring these data sets or implementing them properly into PSHA. Creative new methods and advances in the fundamental science behind triggering, complex rupture, earthquake clustering, fault scaling, and enigmatic fault systems are needed. Although we have outlined many of the contemporary challenges faced within many of subdisciplines involved in seismic hazard analysis, the greatest progress may be made through connections between methods of investigation. For example, statistical methods can be used to combine a large number of existing paleoseismic data to interpret which event at a given paleoseismic site may or may not correlate with events identified at adjacent sites. Analyses such as these will enhance comparisons between regions, improve evaluations of the fits of physical models to data, and refine the statistical simulations of seismicity at the core of advanced PSHA. Making connections across subfields will improve our ability to incorporate geologic and geomorphic data of sufficient quantity and quality into PSHA models and ultimately aid in the development of seismically safe building codes and in the mitigation of economic losses due to seismic events.

Data Availability Statement

All data are cited and referenced in the text.

Acknowledgments

K. M. thanks NSF-EAR-1756943 for support. We thank Trevor Allen, Kendra Johnson, and Robin Gee for discussions about this contribution. We thank Ned Field, Mark Quigley and two anonymous reviewers for their comments. Jonathan Griffin publishes with the permission of the CEO, Geoscience Australia.

References

- Adams, M. (2018). Subject-oriented finite fault inversions and their applications, PhD dissertation (Ph.D. Thesis), University of California, Santa Barbara.
- Adams, B. A., Whipple, K. X., Hodges, K. V., & Heimsath, A. M. (2016). In situ development of high-elevation, low-relief landscapes via duplex deformation in the Eastern Himalayan hinterland, Bhutan. *Journal of Geophysical Research: Earth Surface*, 121, 294–319. <https://doi.org/10.1002/2015JF003508>
- Ahnert, F. (1970). Functional relationships between denudation, relief, and uplift in large, mid-latitude drainage basins. *American Journal of Science*, 268(3), 243–263. <https://doi.org/10.2475/ajs.268.3.243>
- Aitken, M. (1998). *An introduction to optical dating: The dating of Quaternary sediments by the use of photon-stimulated luminescence*. Oxford, UK: Oxford University Press.
- Akaike, H. (1981). Likelihood of a model and information criteria. *Journal of Econometrics*, 16(1), 3–14. [https://doi.org/10.1016/0304-4076\(81\)90071-3](https://doi.org/10.1016/0304-4076(81)90071-3)
- Allen, T. I., & Hayes, G. P. (2017). Alternative rupture-scaling relationships for subduction interface and other offshore environments. *Bulletin of the Seismological Society of America*, 107(3), 1240–1253. <http://doi.org/10.1785/0120160255>
- Amos, C. B., & Burbank, D. W. (2007). Channel width response to differential uplift. *Journal of Geophysical Research*, 112, F02010. <https://doi.org/10.1029/2006JF000672>
- Amos, C. B., Burbank, D. W., Nobes, D. C., & Read, S. A. L. (2007). Geomorphic constraints on listric thrust faulting: Implications for active deformation in the Mackenzie Basin, South Island, New Zealand. *Journal of Geophysical Research*, 112, B03S11. <https://doi.org/10.1029/2006JB004291>
- Amos, C. B., Kelso, K. I., Rood, D. H., Simpson, D. T., & Rose, R. S. (2010). Late Quaternary slip rate on the Kern Canyon fault at Soda Spring, Tulare County, California. *Lithosphere*, 2(6), 411–417. <https://doi.org/10.1130/L100.1>
- Anderson, J. G., Biasi, G. P., & Wesnousky, S. G. (2017). Fault-scaling relationships depend on the average fault-slip rate. *Bulletin of the Seismological Society of America*, 107(6), 2561–2577.
- Anderson, J. G., Wesnousky, S. G., & Stirling, M. W. (1996). Earthquake size as a function of fault slip rate. *Bulletin of the Seismological Society of America*, 86(3), 683–690.
- Archuleta, R. J., Ji, C., & Adams, M. N. (2018). Strong ground motion from earthquakes with multiple faults. SMIP18 Seminar Proceedings, https://www.conservation.ca.gov/cgs/Pages/Program-SMIP/Seminar/smip18_toc.aspx

- Argus, D. F., Gordon, R. G., Heflin, M. B., Ma, C., Eanes, R. J., Willis, P., et al. (2010). The angular velocities of the plates and the velocity of Earth's centre from space geodesy. *Geophysical Journal International*, 180(3), 913–960. <https://doi.org/10.1111/j.1365-246X.2009.04463.x>
- Arrowsmith, J. R., & Zielke, O. (2009). Tectonic geomorphology of the San Andreas Fault zone from high resolution topography: An example from the Cholame segment. *Geomorphology*, 113(1–2), 70–81.
- Attal, M., Tucker, G. E., Whittaker, A. C., Cowie, P. A., & Roberts, G. P. (2008). Modeling fluvial incision and transient landscape evolution: Influence of dynamic channel adjustment. *Journal of Geophysical Research*, 113, F03013. <https://doi.org/10.1029/2007JF000893>
- Avouac, J.-P., Meng, L., Wei, S., Wang, T., & Ampuero, J.-P. (2015). Lower edge of locked Main Himalayan Thrust unzipped by the 2015 Gorkha earthquake. *Nature Geoscience*, 8(9), 708–711.
- Azzaro, R., Barberi, G., D'Amico, S., Pace, B., Peruzza, L., & Tuvè, T. (2017). When probabilistic seismic hazard climbs volcanoes: The Mt. Etna case, Italy—Part 1: Model components for sources parameterization. *Natural Hazards and Earth System Sciences*, 17, 1981–1998.
- Balco, G. (2011). Contributions and unrealized potential contributions of cosmogenic-nuclide exposure dating to glacier chronology, 1990–2010. *Quaternary Science Reviews*, 30(1–2), 3–27.
- Barnhart, W. D. (2017). Fault creep rates of the Chaman fault (Afghanistan and Pakistan) inferred from InSAR. *Journal of Geophysical Research: Solid Earth*, 122, 372–386. <https://doi.org/10.1002/2016JB013656>
- Barth, N. C., Toy, V. G., Langridge, R. M., & Norris, R. J. (2012). Scale dependence of oblique plate-boundary partitioning: New insights from LiDAR, central Alpine fault, New Zealand. *Lithosphere*, 4(5), 435–448.
- Bayarsayhan, C., Bayasgalan, A., Enhtuvshin, B., Hudnut, K. W., Kurushin, R. A., Molnar, P., & Olziyat, M. (1996). 1957 Gobi-Altay, Mongolia, earthquake as a prototype for Southern California's most devastating earthquake. *Geology*, 24(7), 579–582.
- Beanland, S., & Barrow-Hurlbert, S. A. (1988). The Nevis-Cardrona fault system, central Otago, New Zealand: Late Quaternary tectonics and structural development. *New Zealand Journal of Geology and Geophysics*, 31(3), 337–352.
- Beanland, S., & Berryman, K. R. (1989). Style and episodicity of late Quaternary activity on the Pisa-Grandview fault zone, Central Otago, New Zealand. *New Zealand Journal of Geology and Geophysics*, 32(4), 451–461.
- Behr, W. M., Rood, D. H., Fletcher, K. E., Guzman, N., Finkel, R., Hanks, T. C., et al. (2010). Uncertainties in slip-rate estimates for the Mission Creek strand of the southern San Andreas Fault at Biskra Palms Oasis, southern California. *Bulletin*, 122(9–10), 1360–1377.
- Bell, J. W., Caskey, S. J., Ramelli, A. R., & Guerrieri, L. (2004). Pattern and rates of faulting in the central Nevada seismic belt, and paleoseismic evidence for prior beltlike behavior. *Bulletin of the Seismological Society of America*, 94(4), 1229–1254. <https://doi.org/10.1785/012003226>
- Bernis, S. P., Micklethwaite, S., Turner, D., James, M. R., Akciz, S., Thiele, S. T., & Bangash, H. A. (2014). Ground-based and UAV-based photogrammetry: A multi-scale, high-resolution mapping tool for structural geology and paleoseismology. *Journal of Structural Geology*, 69, 163–178.
- Bendick, R., & Bilham, R. (2017). Do weak global stresses synchronize earthquakes? *Geophysical Research Letters*, 44, 8320–8327. <https://doi.org/10.1002/2017GL074934>
- Bendick, R., Bilham, R., Freymueller, J., Larson, K., & Yin, G. (2000). Geodetic evidence for a low slip rate in the Altyn Tagh fault system. *Nature*, 404(6773), 69–72. <https://doi.org/10.1038/35003555>
- Benedetti, L., Manighetti, I., Gaudemer, Y., Finkel, R., Malavieille, J., Pou, K., et al. (2013). Earthquake synchrony and clustering on Fucino faults (central Italy) as revealed from in situ ^{36}Cl exposure dating. *Journal of Geophysical Research: Solid Earth*, 118, 4948–4974. [https://doi.org/10.1002/jgrb.50299/abstract](https://doi.org/10.1002/jgrb.50299)
- Bennett, S. E. K., DuRoss, C. B., Gold, R. D., Briggs, R. W., Personius, S. F., Reitman, N. G., et al. (2018). Paleoseismic results from the Alpine site, Wasatch fault zone: Timing and displacement data for six Holocene earthquakes at the Salt Lake City-Provo segment boundary. *Bulletin of Seismological Society of America*, 108, 3202–3224.
- Berryman, K. R., Cochran, U. A., Clark, K. J., Biasi, G. P., Langridge, R. M., & Villamor, P. (2012). Major earthquakes occur regularly on an isolated plate boundary fault. *Science*, 336(6089), 1690–1693.
- Bi, H., Zheng, W., Ge, W., Zhang, P., Zeng, J., & Yu, J. (2018). Constraining the distribution of vertical slip on the South Heli Shan Fault (northeastern Tibet) from high-resolution topographic data. *Journal of Geophysical Research: Solid Earth*, 123, 2484–2501. <https://doi.org/10.1002/2017JB014901>
- Biasi, G. P., Langridge, R. M., Berryman, K. R., Clark, K. J., & Cochran, U. A. (2015). Maximum-likelihood recurrence parameters and conditional probability of a ground-rupturing earthquake on the Southern Alpine Fault, South Island, New Zealand. *Bulletin of the Seismological Society of America*, 105(1), 94–106.
- Biasi, G. P., & Thompson, S. C. (2018). Estimating time-dependent seismic hazard of faults in the absence of an earthquake recurrence record. *Bulletin of the Seismological Society of America*, 108(1), 39–50.
- Biasi, G. P., & Weldon, R. J. (2006). Estimating surface rupture length and magnitude of paleoearthquakes from point measurements of rupture displacement. *Bulletin of the Seismological Society of America*, 96(5), 1612–1623.
- Biasi, G. P., & Weldon, R. J. (2009). San Andreas Fault rupture scenarios from multiple paleoseismic records: Stringing pearls. *Bulletin of the Seismological Society of America*, 99(2A), 471–498.
- Biasi, G. P., Weldon, R. J., Fumal, T. E., & Seitz, G. G. (2002). Paleoseismic event dating and the conditional probability of large earthquakes on the southern San Andreas Fault, California. *Bulletin of the Seismological Society of America*, 92(7), 2761–2781.
- Biasi, G. P., & Wesnousky, S. G. (2016). Steps and gaps in ground ruptures: Empirical bounds on rupture propagation. *Bulletin of the Seismological Society of America*, 106(3), 1110–1124.
- Bilham, R., & Gaur, V. (2013). Buildings as weapons of mass destruction. *Science*, 341(6146), 618–619.
- Bilham, R., Gaur, V. K., & Molnar, P. (2001). Himalayan seismic hazard. *Science*, 293, 1442–1444.
- Bilham, R., Mencin, D., Bendick, R., & Bürgmann, R. (2017). Implications for elastic energy storage in the Himalaya from the Gorkha 2015 earthquake and other incomplete ruptures of the Main Himalayan Thrust. *Quaternary International*, 462, 3–21.
- Bird, P. (2009). Long-term fault slip rates, distributed deformation rates, and forecast of seismicity in the western United States from joint fitting of community geologic, geodetic, and stress direction data sets. *Journal of Geophysical Research*, 114, B11403. <https://doi.org/10.1029/2009JB006317>
- Bommer, J. J. (2002). Deterministic vs. probabilistic seismic hazard assessment: an exaggerated and obstructive dichotomy. *Journal of Earthquake Engineering*, 6(spec01), 43–73.
- Bormann, J. M., Hammond, W. C., Kreemer, C., & Blewitt, G. (2016). Accommodation of missing shear strain in the Central Walker Lane, western North America: Constraints from dense GPS measurements. *Earth and Planetary Science Letters*, 440, 169–177. <https://doi.org/10.1016/j.epsl.2016.01.015>
- Bradley, B. A., Razafindrakoto, H. N. T., & Polak, V. (2017). Ground-motion observations from the 14 November 2016 Mw 7.8 Kaikoura, New Zealand, earthquake and insights from broadband simulations. *Seismological Research Letters*, 88(3), 740–756.

- Brengman, C. M. J., Barnhart, W. D., Mankin, E. H., & Miller, C. N. (2019). Earthquake-scaling relationships from geodetically derived slip distributions. *Bulletin of the Seismological Society of America*, 109(5), 1701–1715.
- Brocklehurst, S. H., & Whipple, K. X. (2002). Glacial erosion and relief production in the Eastern Sierra Nevada, California. *Geomorphology*, 42(1–2), 1–24.
- Bronk Ramsey, C. (2009). Bayesian analysis of radiocarbon dates. *Radiocarbon*, 51(1), 337–360.
- Brothers, D., Kilb, D., Luttrell, K., Driscoll, N., & Kent, G. (2011). Loading of the San Andreas fault by flood-induced rupture of faults beneath the Salton Sea. *Nature Geoscience*, 4(7), 486–492. <https://doi.org/10.1038/ngeo1184>
- Brothers, D. S., Miller, N. C., Barrie, J. V., Haeussler, P. J., Greene, H. G., Andrews, B. D., et al. (2020). Plate boundary localization, slip-rates and rupture segmentation of the Queen Charlotte Fault based on submarine tectonic geomorphology. *Earth and Planetary Science Letters*, 530, 115882. <https://doi.org/10.1016/j.epsl.2019.115882>
- Burgette, R. J., Hanson, A. M., Scharer, K. M., Rittenour, T. M., & McPhillips, D. (2020). Late Quaternary slip rate of the Central Sierra Madre fault, Southern California: Implications for slip partitioning and earthquake hazard. *Earth and Planetary Science Letters*, 530, 115907. <https://doi.org/10.1016/j.epsl.2019.115907>
- Burnham, K. P., & Anderson, D. R. (2004). Multimodel inference: Understanding AIC and BIC in model selection. *Sociological Methods & Research*, 33(2), 261–304. <https://doi.org/10.1177/0049124104268644>
- Burrato, P., Vannoli, P., Fracassi, U., Basili, R., & Valensise, G. (2012). Is blind faulting truly invisible? Tectonic-controlled drainage evolution in the epicentral area of the May 2012, Emilia-Romagna earthquake sequence (northern Italy). *Annals of Geophysics*, 55(4), 525–531.
- Busschers, F. S., Wesselingh, F., Kars, R. H., Verslujs-Helder, M., Wallinga, J., Bosch, J. H. A., et al. (2014). Radiocarbon dating of late Pleistocene marine shells from the Southern North Sea. *Radiocarbon*, 56(3), 1151–1166.
- Calais, E., Camelbeeck, T., Stein, S., Liu, M., & Craig, T. J. (2016). A new paradigm for large earthquakes in stable continental plate interiors. *Geophysical Research Letters*, 43, 10,621–10,637. <https://doi.org/10.1002/2016GL070815>
- Candela, T., Renard, F., Klinger, Y., Mair, K., Schmittbuhl, J., & Brodsky, E. E. (2012). Roughness of fault surfaces over nine decades of length scales. *Journal of Geophysical Research*, 117, B08409. <https://doi.org/10.1029/2011JB009041>
- Castelltort, S., Goren, L., Willett, S. D., Champagnac, J.-D., Herman, F., & Braun, J. (2012). River drainage patterns in the New Zealand alps primarily controlled by plate tectonic strain. *Nature Geoscience*, 5(10), 744.
- Chery, J., Carretier, S., & Ritz, J.-F. (2001). Postseismic stress transfer explains time clustering of large earthquakes in Mongolia. *Earth and Planetary Science Letters*, 194(1–2), 277–286. [https://doi.org/10.1016/S0012-821X\(01\)00552-0](https://doi.org/10.1016/S0012-821X(01)00552-0)
- Clark, D. A., & Allen, T. (2018). What have we learnt of cratonic earthquakes in the fifty years since Meckering? Perth, Western Australia.
- Clark, D. J., Brennan, S., Brenn, G., Garthwaite, M. C., Dimech, J., Allen, T. I., & Standen, S. (2020). Surface deformation relating to the 2018 Lake Muir earthquake sequence, southwest Western Australia: New insight into stable continental region earthquakes. *Solid Earth*, 11(2), 691–717.
- Clark, K. J., Cochran, U. A., Berryman, K. R., Biasi, G., Langridge, R., Villamor, P., et al. (2013). Deriving a long paleoseismic record from a shallow-water Holocene basin next to the Alpine fault, New Zealand. *Bulletin*, 125(5–6), 811–832.
- Clark, D., Dentith, M., Wyrwoll, K.-H., Yanchou, L., Dent, V., & Featherstone, W. (2008). The Hyden fault scarp, Western Australia: Paleoseismic evidence for repeated Quaternary displacement in an intracratonic setting. *Australian Journal of Earth Sciences*, 55(3), 379–395.
- Clark, D., McPherson, A., Cupper, M., Collins, C. D. N., & Nelson, G. (2015). The Cadell Fault, southeastern Australia: A record of temporally clustered morphogenic seismicity in a low-strain intraplate region. *Geological Society, London, Special Publications*, 432(1), 163–185.
- Clark, D., McPherson, A., & Van Dissen, R. (2012). Long-term behaviour of Australian stable continental region (SCR) faults. *Tectonophysics*, 566, 1–30.
- Clark, K. J., Nissen, E. K., Howarth, J. D., Hamling, I. J., Mountjoy, J. J., Ries, W. F., et al. (2017). Highly variable coastal deformation in the 2016 $Mw7.8$ Kaikōura earthquake reflects rupture complexity along a transpressional plate boundary. *Earth and Planetary Science Letters*, 474, 334–344.
- Cocco, M., Nostro, C., & Ekström, G. (2000). Static stress changes and fault interaction during the 1997 Umbria-Marche earthquake sequence. *Journal of Seismology*, 4(4), 501–516.
- Cochran, U. A., Clark, K. J., Howarth, J. D., Biasi, G. P., Langridge, R. M., Villamor, P., et al. (2017). A plate boundary earthquake record from a wetland adjacent to the Alpine fault in New Zealand refines hazard estimates. *Earth and Planetary Science Letters*, 464, 175–188.
- Cohen, S. C., & Kramer, M. J. (1984). Crustal deformation, the earthquake cycle, and models of viscoelastic flow in the asthenosphere. *Geophysical Journal International*, 78(3), 735–750. <https://doi.org/10.1111/j.1365-246X.1984.tb05068.x>
- Cornell, C. A. (1968). Engineering seismic risk analysis. *Bulletin of the Seismological Society of America*, 58(5), 1583–1606.
- Cortés, A. J., González, L. G., Binnie, S. A., Robinson, R., Freeman, S. P. H. T., & Vargas E, G. (2012). Paleoseismology of the Mejillones Fault, northern Chile: Insights from cosmogenic ^{10}Be and optically stimulated luminescence determinations. *Tectonics*, 31, TC2017. <https://doi.org/10.1029/2011TC002877>
- Cowgill, E., Gold, R. D., Xuanhua, C., Xiao-Feng, W., Arrowsmith, J. R., & Southon, J. (2009). Low Quaternary slip rate reconciles geodetic and geologic rates along the Altyn Tagh fault, northwestern Tibet. *Geology*, 37(7), 647–650. <https://doi.org/10.1130/G25623A.1>
- Cox, R. T., Cherryhomes, J., Harris, J. B., Larsen, D., Van Arsdale, R. B., & Forman, S. L. (2006). Paleoseismology of the southeastern Reelfoot rift in western Tennessee and implications for intraplate fault zone evolution. *Tectonics*, 25, TC3019. <https://doi.org/10.1029/2005TC001829>
- Craig, T. J., Calais, E., Fleitout, L., Bollinger, L., & Scotti, O. (2016). Evidence for the release of long-term tectonic strain stored in continental interiors through intraplate earthquakes. *Geophysical Research Letters*, 43, 6826–6836. <https://doi.org/10.1002/2016GL069359>
- Crone, A. J., De Martini, P. M., Machette, M. N., Okumura, K., & Prescott, J. R. (2003). Paleoseismicity of two historically quiescent faults in Australia: Implications for fault behavior in stable continental regions. *Bulletin of the Seismological Society of America*, 93(5), 1913–1934.
- Crone, A. J., Machette, M. N., & Bowman, J. R. (1997). Episodic nature of earthquake activity in stable continental regions revealed by palaeoseismicity studies of Australian and North American Quaternary faults. *Australian Journal of Earth Sciences*, 44(2), 203–214.
- Cummins, P. R., Pranantyo, I. R., Pownall, J. M., Griffin, J. D., Meilano, I., & Zhao, S. (2020). Earthquakes and tsunamis caused by low-angle normal faulting in the Banda Sea, Indonesia. *Nature Geoscience*, 13(4), 312–318. <https://doi.org/10.1038/s41561-020-0545-x>
- Cunningham, D., Grebby, S., Tansey, K., Gosar, A., & Kastelic, V. (2006). Application of airborne LiDAR to mapping seismogenic faults in forested mountainous terrain, southeastern Alps, Slovenia. *Geophysical Research Letters*, 33, L20308. <https://doi.org/10.1029/2006GL027014>
- Dahlquist, M. P., West, A. J., & Li, G. (2018). Landslide-driven drainage divide migration. *Geology*, 46(5), 403–406.

- DeLong, S. B., Hilley, G. E., Rymer, M. J., & Prentice, C. (2010). Fault zone structure from topography: Signatures of en echelon fault slip at Mustang Ridge on the San Andreas Fault, Monterey County, California. *Tectonics*, 29, TC5003. <https://doi.org/10.1029/2010TC002673>
- DeVries, P. M. R., Krastev, P. G., Dolan, J. F., & Meade, B. J. (2017). Viscoelastic block models of the North Anatolian Fault: A unified earthquake cycle representation of pre- and postseismic geodetic observations. *Bulletin of the Seismological Society of America*, 107(1), 403–417. <https://doi.org/10.1785/0120160059>
- DiBiase, R. A., Rossi, M. W., & Neely, A. B. (2018). Fracture density and grain size controls on the relief structure of bedrock landscapes. *Geology*, 46(5), 399–402.
- DiCaprio, C. J., Simons, M., Kenner, S. J., & Williams, C. A. (2008). Post-seismic reloading and temporal clustering on a single fault. *Geophysical Journal International*, 172(2), 581–592.
- Dixon, T. H. (1991). An introduction to the global positioning system and some geological applications. *Reviews of Geophysics*, 29(2), 249–276. <https://doi.org/10.1029/91RG00152>
- Dolan, J. F., Bowman, D. D., & Sammis, C. G. (2007). Long-range and long-term fault interactions in Southern California. *Geology*, 35(9), 855–858. <https://doi.org/10.1130/G23789A.1>
- Dolan, J. F., McAuliffe, L. J., Rhodes, E. J., McGill, S. F., & Zinke, R. (2016). Extreme multi-millennial slip rate variations on the Garlock fault, California: Strain super-cycles, potentially time-variable fault strength, and implications for system-level earthquake occurrence. *Earth and Planetary Science Letters*, 446(Supplement C), 123–136. <https://doi.org/10.1016/j.epsl.2016.04.011>
- Dolan, J. F., & Meade, B. J. (2017). A comparison of geodetic and geologic rates prior to large strike-slip earthquakes: A diversity of earthquake-cycle behaviors? *Geochemistry, Geophysics, Geosystems*, 18, 4426–4436. <https://doi.org/10.1002/2017GC007014>
- DuRoss, C. B., Bennett, S. E. K., Briggs, R. W., Personius, S. F., Gold, R. D., Reitman, N. G., et al. (2018). Combining conflicting Bayesian models to develop paleoseismic records: An example from the Wasatch fault zone, Utah. *Bulletin of the Seismological Society of America*, 108(6), 3180–3201.
- DuRoss, C. B., Gold, R. D., Briggs, R. W., Delano, J. E., Ostendar, D. A., Zellman, M. S., et al. (2019). Holocene earthquake history and slip rate of the southern Teton fault, Wyoming, USA. *Geological Society of America Bulletin*.
- DuRoss, C. B., & Hylland, M. D. (2015). Synchronous ruptures along a major graben-forming fault system: Wasatch and West Valley fault zones, Utah. *Bulletin of the Seismological Society of America*, 105(1), 14–37.
- DuRoss, C. B., Personius, S. F., Crone, A. J., Olig, S. S., Hylland, M. D., Lund, W. R., & Schwartz, D. P. (2016). Fault segmentation: New concepts from the Wasatch fault zone, Utah, USA. *Journal of Geophysical Research: Solid Earth*, 121, 1131–1157. <https://doi.org/10.1002/2015JB012519>
- DuRoss, C. B., Personius, S. F., Crone, A. J., Olig, S. S., & Lund, W. R. (2011). Integration of paleoseismic data from multiple sites to develop an objective earthquake chronology: Application to the Weber segment of the Wasatch fault zone, Utah. *Bulletin of the Seismological Society of America*, 101(6), 2765–2781.
- Duan, B., Liu, Z., & Elliott, A. J. (2019). Multicycle dynamics of the Aksay Bend along the Altyn Tagh fault in Northwest China: 2. The realistically complex fault geometry. *Tectonics*, 38(3), 1120–1137.
- Elliott, J. R., Biggs, J., Parsons, B., & Wright, T. J. (2008). InSAR slip rate determination on the Altyn Tagh Fault, northern Tibet, in the presence of topographically correlated atmospheric delays. *Geophysical Research Letters*, 35, L12309. <https://doi.org/10.1029/2008GL033659>
- Elliott, J. R., Jolivet, R., González, P. J., Avouac, J.-P., Hollingsworth, J., Searle, M. P., & Stevens, V. L. (2016). Himalayan megathrust geometry and relation to topography revealed by the Gorkha earthquake. *Nature Geoscience*, 9(2), 174–180.
- Elliott, A. J., Osokin, M. E., Liu-zeng, J., & Shao, Y. X. (2018). Persistent rupture terminations at a restraining bend from slip rates on the eastern Altyn Tagh fault. *Tectonophysics*, 733, 57–72.
- Evans, E. L., Loveless, J. P., & Meade, B. J. (2015). Total variation regularization of geodetically and geologically constrained block models for the Western United States. *Geophysical Journal International*, 202(2), 713–727.
- Farr, T. G., Rosen, P. A., Caro, E., Crippen, R., Duren, R., Hensley, S., et al. (2007). The Shuttle Radar Topography Mission. *Reviews of geophysics*, 45, RG2004. <https://doi.org/10.1029/2005RG000183>
- Ferry, M., Meghraoui, M., Karaki, N. A., Al-Taj, M., Amoush, H., Al-Dhaisat, S., & Barjous, M. (2007). A 48-kyr-long slip rate history for the Jordan Valley segment of the Dead Sea Fault. *Earth and Planetary Science Letters*, 260(3), 394–406.
- Fialko, Y., Sandwell, D., Simons, M., & Rosen, P. (2005). Three-dimensional deformation caused by the Bam, Iran, earthquake and the origin of shallow slip deficit. *Nature*, 435(7040), 295–299. <https://doi.org/10.1038/nature03425>
- Field, E. H. (2015). Computing elastic-rebound-motivated earthquake probabilities in unsegmented fault models: A new methodology supported by physics-based simulators. *Bulletin of the Seismological Society of America*, 105(2A), 544–559.
- Field, E. H., Arrowsmith, R. J., Biasi, G. P., Bird, P., Dawson, T. E., Felzer, K. R., et al. (2014). Uniform California earthquake rupture forecast, version 3 (UCERF3)—The time-independent model. *Bulletin of the Seismological Society of America*, 104(3), 1122–1180.
- Field, E. H., & Jordan, T. H. (2015). Time-dependent renewal-model probabilities when date of last earthquake is unknown. *Bulletin of the Seismological Society of America*, 105(1), 459–463.
- Field, E. H., Milner, K. R., Hardebeck, J. L., Page, M. T., van der Elst, N., Jordan, T. H., et al. (2017). A spatiotemporal clustering model for the third Uniform California Earthquake Rupture Forecast (UCERF3-ETAS): Toward an operational earthquake forecast. *Bulletin of the Seismological Society of America*, 107(3), 1049–1081. <https://doi.org/10.1785/0120160173>
- Fielding, E. J., Sladen, A., Li, Z., Avouac, J.-P., Bürgmann, R., & Ryder, I. (2013). Kinematic fault slip evolution source models of the 2008 M7. 9 Wenchuan earthquake in China from SAR interferometry, GPS and teleseismic analysis and implications for Longmen Shan tectonics. *Geophysical Journal International*, 194(2), 1138–1166.
- Finnegan, N. J., Roe, G., Montgomery, D. R., & Hallet, B. (2005). Controls on the channel width of rivers: Implications for modeling fluvial incision of bedrock. *Geology*, 33(3), 229–232.
- Fisher, G. B., Bookhagen, B., & Amos, C. (2013). Channel planform geometry and slopes from freely available high-spatial resolution imagery and DEM fusion: Implications for channel width scalings, erosion proxies, and fluvial signatures in tectonically active landscapes. *Geomorphology*, 194, 46–56.
- Fitzenz, D. D., Ferry, M. A., & Jalobeanu, A. (2010). Long-term slip history discriminates among occurrence models for seismic hazard assessment. *Geophysical Research Letters*, 37, L20307. <https://doi.org/10.1029/2010GL044071>
- Flesch, L., & Bendick, R. (2007). Present-day kinematics at the India-Asia collision zone: Comment and reply: Comment. *Geology*, 35(1), e160–e160. <https://doi.org/10.1130/G24443.C.1>
- Flesch, L., Bendick, R., & Bischoff, S. (2018). Limitations on inferring 3D architecture and dynamics from surface velocities in the India-Eurasia collision zone. *Geophysical Research Letters*, 45, 1379–1386. <https://doi.org/10.1002/2017GL076503/abstract>

- Forman, S. L., Nelson, A. R., & McCalpin, J. P. (1991). Thermoluminescence dating of fault-scarp-derived colluvium: Deciphering the timing of paleoearthquakes on the Weber Segment of the Wasatch fault zone, north central Utah. *Journal of Geophysical Research*, 96(B1), 595–605.
- Forte, A. M., & Whipple, K. X. (2018). Criteria and tools for determining drainage divide stability. *Earth and Planetary Science Letters*, 493, 102–117.
- Franco, A., Lasserre, C., Lyon-Caen, H., Kostoglodov, V., Molina, E., Guzman-Speziale, M., et al. (2012). Fault kinematics in northern Central America and coupling along the subduction interface of the Cocos Plate, from GPS data in Chiapas (Mexico), Guatemala and El Salvador: Kinematics in northern Central America. *Geophysical Journal International*, 189(3), 1223–1236. <https://doi.org/10.1111/j.1365-246X.2012.05390.x>
- Frankel, K. L., Dolan, J. F., Finkel, R. C., Owen, L. A., & Hoeft, J. S. (2007). Spatial variations in slip rate along the Death Valley-Fish Lake Valley fault system determined from LiDAR topographic data and cosmogenic ^{10}Be geochronology. *Geophysical Research Letters*, 34, L18303. <https://doi.org/10.1029/2007GL030549>
- Friedrich, A. M., Wernicke, B. P., Niemi, N. A., Bennett, R. A., & Davis, J. L. (2003). Comparison of geodetic and geologic data from the Wasatch region, Utah, and implications for the spectral character of Earth deformation at periods of 10 to 10 million years. *Journal of Geophysical Research: Solid Earth*, 108(B4), 2199. <https://doi.org/10.1029/2001JB000682>
- Gallen, S. F., Clark, M. K., & Godt, J. W. (2015). Coseismic landslides reveal near-surface rock strength in a high-relief, tectonically active setting. *Geology*, 43(1), 11–14.
- Gallen, S. F., & Thigpen, J. R. (2018). Lithologic controls on focused erosion and intraplate earthquakes in the eastern Tennessee seismic zone. *Geophysical Research Letters*, 45, 9569–9578. <https://doi.org/10.1029/2018GL079157>
- Gao, M., Xu, X., Klinger, Y., Van Der Woerd, J., & Tapponnier, P. (2017). High-resolution mapping based on an unmanned aerial vehicle (UAV) to capture paleoseismic offsets along the Altyn Tagh fault, China. *Scientific Reports*, 7(1), 1–11.
- Gavin, D. G. (2001). Estimation of inbuilt age in radiocarbon ages of soil charcoal for fire history studies. *Radiocarbon*, 43(1), 27–44.
- Gledhill, K., Ristau, J., Reyners, M., Fry, B., & Holden, C. (2011). The Darfield (Canterbury, New Zealand) Mw 7.1 earthquake of September 2010: A preliminary seismological report. *Seismological Research Letters*, 82(3), 378–386.
- Godard, V., Bourles, D. L., Spinabellia, F., Burbank, D. W., Bookhagen, B., Fisher, G. B., et al. (2014). Dominance of tectonics over climate in Himalayan denudation. *Geology*, 42(3), 243–246.
- Goes, S. D. B., & Ward, S. N. (1994). Synthetic seismicity for the San Andreas Fault. *Annali di Geofisica*, XXXVII (6).
- Gold, R. D., Cowgill, E., Arrowsmith, J. R., & Friedrich, A. M. (2017). Pulsed strain release on the Altyn Tagh fault, northwest China. *Earth and Planetary Science Letters*, 459, 291–300.
- Gold, R. D., Cowgill, E., Arrowsmith, J. R., Gosse, J., Chen, X., & Wang, X. F. (2009). Riser diachroneity, lateral erosion, and uncertainty in rates of strike slip faulting: A case study from Tuzidun along the Altyn Tagh Fault, NW China. *Journal of Geophysical Research*, 114, B04401. <https://doi.org/10.1029/2008JB005913>
- Gold, R. D., DuRoss, C. B., Delano, J. E., Gibson, R. W., Briggs, R. W., Mahan, S. A., et al. (2019). Four major Holocene earthquakes on the Reelfoot fault recorded by sackungen in the New Madrid seismic zone, USA. *Journal of Geophysical Research: Solid Earth*, 124, 3105–3126. <https://doi.org/10.1029/2018JB016806>
- Goldfinger, C. (2011). Submarine paleoseismology based on turbidite records. *Annual Review of Marine Science*, 3, 35–66.
- Goldfinger, C., Nelson, C. H., Morey, A. E., Johnson, J. E., Patton, J. R., Karabanov, E., et al. (2012). Turbidite event history—Methods and implications for Holocene paleoseismicity of the Cascadia Subduction zone. *Earthquake Hazards of the Pacific Northwest Coastal and Marine Regions*, US Geological Survey Professional Paper 1661-F, Profession, 170.
- Goren, L., Castelltort, S., & Klinger, Y. (2015). Modes and rates of horizontal deformation from rotated river basins: Application to the Dead Sea fault system in Lebanon. *Geology*, 43(9), 843–846.
- Goren, L., Fox, M., & Willett, S. D. (2014). Tectonics from fluvial topography using formal linear inversion: Theory and applications to the Inyo Mountains, California. *Journal of Geophysical Research: Earth Surface*, 119, 1651–1681. <https://doi.org/10.1002/2014JF003079>
- Gosse, J. C., & Phillips, F. M. (2001). Terrestrial in situ cosmogenic nuclides: Theory and application. *Quaternary Science Reviews*, 20(14), 1475–1560. [https://doi.org/10.1016/S0277-3791\(00\)00171-2](https://doi.org/10.1016/S0277-3791(00)00171-2)
- Granger, D. E., Lifton, N. A., & Willenbring, J. K. (2013). A cosmic trip: 25 years of cosmogenic nuclides in geology. *Geological Society of America Bulletin*, 125(9–10), 1379–1402.
- Grant Ludwig, L., Akçiz, S. O., Arrowsmith, J. R., & Salisbury, J. B. (2019). Reproducibility of San Andreas fault slip rate measurements at Wallace Creek in the Carrizo Plain, CA. *Earth and Space Science*, 6(1), 156–165. <https://doi.org/10.1029/2017EA000360>
- Grant, L. B., & Sieh, K. (1994). Paleoseismic evidence of clustered earthquakes on the San Andreas Fault in the Carrizo Plain, California. *Journal of Geophysical Research*, 99(B4), 6819. <https://doi.org/10.1029/94JB00125>
- Graves, R., Jordan, T. H., Callaghan, S., Deelman, E., Field, E., Juve, G., et al. (2011). CyberShake: A physics-based seismic hazard model for southern California. *Pure and Applied Geophysics*, 168(3–4), 367–381.
- Gray, H. J., Mahan, S. A., Nelson, M. S., & Rittenour, T. M. (2015). Guide to luminescence dating techniques and their application for paleoseismic research in Western States Seismic Policy Council: Basin and Range Province Seismic Hazards Summit III, Utah Geological Survey Miscellaneous Publication. Proceedings Volume, 15–5.
- Gray, H. J., Shobe, C. M., Hobley, D. E. J., Tucker, G. E., Duvall, A. R., Harbert, S. A., & Owen, L. A. (2017). Off-fault deformation rate along the southern San Andreas Fault at Mecca Hills, Southern California, inferred from landscape modeling of curved drainages. *Geology*, 46(1), 59–62.
- Grezio, A., Babeyko, A., Baptista, M. A., Behrens, J., Costa, A., Davies, G., et al. (2017). Probabilistic tsunami hazard analysis: Multiple sources and global applications. *Reviews of Geophysics*, 55, 1158–1198. <https://doi.org/10.1002/2017RG000579>
- Griffin, J. D., Allen, T. I., & Gerstenberger, M. C. (2020). Seismic hazard assessment in Australia: Can structured expert elicitation achieve consensus in the “land of the fair go” *Seismological Research Letters*.
- Gutenberg, B., & Richter, C. F. (1944). Frequency of earthquakes in California. *Bulletin of the Seismological Society of America*, 34(4), 185–188.
- Haddad, D. E., Akçiz, S. O., Arrowsmith, J. R., Rhodes, D. D., Oldow, J. S., Zielke, O., et al. (2012). Applications of airborne and terrestrial laser scanning to paleoseismology. *Geosphere*, 8(4), 771–786.
- Haddon, E. K., Amos, C. B., Zielke, O., Jayko, A. S., & Bürgmann, R. (2016). Surface slip during large Owens Valley earthquakes. *Geochemistry, Geophysics, Geosystems*, 17, 2239–2269. <https://doi.org/10.1002/2015GC006033>
- Hallet, B., & Molnar, P. (2001). Distorted drainage basins as markers of crustal strain east of the Himalaya. *Journal of Geophysical Research*, 106(B7), 13,697–13,709.
- Hamling, I. J., Hreinsdóttir, S., Clark, K., Elliott, J., Liang, C., Fielding, E., et al. (2017). Complex multifault rupture during the 2016 Mw 7.8 Kaikōura earthquake, New Zealand. *Science*, 356(6334), eaam7194.

- Hanks, T. C., & Bakun, W. H. (2008). M-log A observations for recent large earthquakes. *Bulletin of the Seismological Society of America*, 98(1), 490–494.
- Hanks, T. C., & Kanamori, H. (1979). A moment magnitude scale. *Journal of Geophysical Research*, 84(B5), 2348–2350.
- Hardebeck, J. L. (2004). Stress triggering and earthquake probability estimates. *Journal of Geophysical Research*, 109, B04310. <https://doi.org/10.1029/2003JB002437>
- Hardebeck, J. L., & Hauksson, E. (2001). Crustal stress field in Southern California and its implications for fault mechanics. *Journal of Geophysical Research*, 106(B10), 21,859–21,882. <https://doi.org/10.1029/2001JB000292/abstract>
- Harkins, N., Kirby, E., Shi, X., Wang, E., Burbank, D., & Chun, F. (2010). Millennial slip rates along the eastern Kunlun fault: Implications for the dynamics of intracontinental deformation in Asia. *Lithosphere*, 2(4), 247–266.
- Harris, R. A., Archuleta, R. J., & Day, S. M. (1991). Fault steps and the dynamic rupture process: 2-D numerical simulations of a spontaneously propagating shear fracture. *Geophysical Research Letters*, 18(5), 893–896.
- Harris, R. A., & Day, S. M. (1999). Dynamic 3D simulations of earthquakes on en echelon faults. *Geophysical Research Letters*, 26(14), 2089–2092.
- Harris, R. A., & Simpson, R. W. (1992). Changes in static stress on Southern California faults after the 1992 Landers earthquake. *Nature*, 360(6401), 251–254.
- Hartzell, S., Mendoza, C., Ramirez-Guzman, L., Zeng, Y., & Mooney, W. (2013). Rupture history of the 2008 M_w 7.9 Wenchuan, China, earthquake: Evaluation of separate and joint inversions of geodetic, teleseismic, and strong-motion data. *Bulletin of the Seismological Society of America*, 103(1), 353–370.
- Hatem, A. E., Dolan, J. F., Zinke, R. W., Van Dissen, R. J., McGuire, C. M., & Rhodes, E. J. (2019). A 2000 Yr paleoearthquake record along the Conway segment of the Hope fault: Implications for patterns of earthquake occurrence in northern South Island and Southern North Island, New Zealand. *Bulletin of the Seismological Society of America*, 109(6), 2216–2239.
- Haugerud, R., Harding, D., Johnson, S., Harless, J., & Weaver, C. (2003). High-resolution lidar topography of the Puget Lowland, Washington. *GSA Today*, 12(6), 4–10.
- Heidemann, H. K. (2012). Lidar base specification. US Geological Survey.
- Heimpel, M., & Olson, P. (1996). A seismodynamical model of lithosphere deformation: Development of continental and oceanic rift networks. *Journal of Geophysical Research*, 101(B7), 16,155–16,176.
- Heimsath, A. M., DiBiase, R. A., & Whipple, K. X. (2012). Soil production limits and the transition to bedrock-dominated landscapes. *Nature Geoscience*, 5(3), 210–214.
- Hemphill-Haley, M. A., & Weldon, R. J. (1999). Estimating prehistoric earthquake magnitude from point measurements of surface rupture. *Bulletin of the Seismological Society of America*, 89(5), 1264–1279.
- Herbert, J. W., Cooke, M. L., & Marshall, S. T. (2014). Influence of fault connectivity on slip rates in Southern California: Potential impact on discrepancies between geodetic derived and geologic slip rates. *Journal of Geophysical Research: Solid Earth*, 119, 2342–2361. <https://doi.org/10.1002/2013JB010472>
- Herbert, J. W., Cooke, M. L., Oskin, M., & Difo, O. (2014). How much can off-fault deformation contribute to the slip rate discrepancy within the Eastern California Shear Zone? *Geology*, 42(1), 71–75.
- Hetland, E. A., & Hager, B. H. (2006). Interseismic strain accumulation: Spin-up, cycle invariance, and irregular rupture sequences. *Geochemistry, Geophysics, Geosystems*, 7, Q05004. <https://doi.org/10.1029/2005GC001087>
- Hetland, E. A., Mus, P., Simons, M., Lin, Y. N., Agram, P. S., & DiCaprio, C. J. (2012). Multiscale InSAR Time Series (MInTS) analysis of surface deformation. *Journal of Geophysical Research*, 117, B02404. <https://doi.org/10.1029/2011JB008731>
- Hetzler, R., & Hampel, A. (2005). Slip rate variations on normal faults during glacial interglacial changes in surface loads. *Nature*, 435(7038), 81–84. <https://doi.org/10.1038/nature03562>
- Heyman, J., Stroeven, A. P., Harbor, J. M., & Caffee, M. W. (2011). Too young or too old: Evaluating cosmogenic exposure dating based on an analysis of compiled boulder exposure ages. *Earth and Planetary Science Letters*, 302(1-2), 71–80.
- Hidy, A. J., Gosse, J. C., Pederson, J. L., Mattern, J. P., & Finkel, R. C. (2010). A geologically constrained Monte Carlo approach to modeling exposure ages from profiles of cosmogenic nuclides: An example from Lees Ferry, Arizona. *Geochemistry Geophysics Geosystems*, 11, Q0AA10. <https://doi.org/10.1029/2010GC003084>
- Hilley, G. E., DeLong, S., Prentice, C., Blisniuk, K., & Arrowsmith, J. R. (2010). Morphologic dating of fault scarps using airborne laser swath mapping (ALSM) data. *Geophysical Research Letters*, 37, L04301. <https://doi.org/10.1029/2009GL042044>
- Hooper, A. (2008). A multi-temporal InSAR method incorporating both persistent scatterer and small baseline approaches. *Geophysical Research Letters*, 35, L16302. <https://doi.org/10.1029/2008GL034654>
- Howarth, J. D., Cochran, U. A., Langridge, R. M., Clark, K., Fitzsimons, S. J., Berryman, K., et al. (2018). Past large earthquakes on the Alpine Fault: Paleoseismological progress and future directions. *New Zealand Journal of Geology and Geophysics*, 61(3), 309–328.
- Hurst, M. D., Mudd, S. M., Attal, M., & Hilley, G. (2013). Hillslopes record the growth and decay of landscapes. *Science*, 341(6148), 868–871.
- Hurst, M. D., Mudd, S. M., Walcott, R., Attal, M., & Yoo, K. (2012). Using hilltop curvature to derive the spatial distribution of erosion rates. *Journal of Geophysical Research*, 117, F02017. <https://doi.org/10.1029/2011JF002057>
- James, M. R., & Robson, S. (2012). Straightforward reconstruction of 3D surfaces and topography with a camera: Accuracy and geoscience application. *Journal of Geophysical Research*, 117, F03017. <https://doi.org/10.1029/2011JF002289>
- Jobe, J. A. T., Li, T., Chen, J., Burbank, D. W., & Bufe, A. (2017). Quaternary tectonic evolution of the Pamir-Tian Shan convergence zone, Northwest China. *Tectonics*, 36, 2748–2776. <https://doi.org/10.1002/2017TC004541>
- Johnson, C. B., Furlong, K. P., & Kirby, E. (2009). Integrated geomorphic and geodynamic modeling of a potential blind thrust in the San Francisco Bay area, California. *Tectonophysics*, 471(3-4), 319–328.
- Johnson, K. M., Hilley, G. E., & Brigmann, R. (2007). Influence of lithosphere viscosity structure on estimates of fault slip rate in the Mojave region of the San Andreas fault system. *Journal of Geophysical Research*, 112, B07408. <https://doi.org/10.1029/2006JB004842>
- Johnson, K., Nissen, E., Saripalli, S., Arrowsmith, J. R., McGarey, P., Scherer, K., et al. (2014). Rapid mapping of ultrafine fault zone topography with structure from motion. *Geosphere*, 10(5), 969–986.
- Johnson, S. Y., Watt, J. T., Hartwell, S. R., & Kluesner, J. W. (2018). Neotectonics of the Big Sur Bend, San Gregorio-Hosgri Fault System, Central California. *Tectonics*, 37(7), 1930–1954. <https://doi.org/10.1029/2017TC004724>
- Jolivet, R., Agram, P. S., Lin, N. Y., Simons, M., Doin, M.-P., Peltzer, G., & Li, Z. (2014). Improving InSAR geodesy using Global Atmospheric Models. *Journal of Geophysical Research: Solid Earth*, 119, 2324–2341. <https://doi.org/10.1002/2013JB010588>
- Jull, A. J. T., Scott, E. M., & Bierman, P. (2015). The CRONUS-Earth inter-comparison for cosmogenic isotope analysis. *Quaternary Geochronology*, 26, 3–10.
- Kagan, Y. Y., Jackson, D. D., & Geller, R. J. (2012). Characteristic earthquake model, 1884–2011, RIP. *Seismological Research Letters*, 83(6), 951–953.

- Kanamori, H., & Allen, C. R. (1986). Earthquake repeat time and average stress drop. In *Earthquake source mechanics. geophysical monograph. no. 37*, American Geophysical Union, pp. 227–235.
- Kase, Y., & Kuge, K. (1998). Numerical simulation of spontaneous rupture processes on two non-coplanar faults: The effect of geometry on fault interaction. *Geophysical Journal International*, 135(3), 911–922.
- Kenner, S. J., & Simons, M. (2005). Temporal clustering of major earthquakes along individual faults due to post-seismic reloading. *Geophysical Journal International*, 160(1), 179–194.
- Kilb, D., Gomberg, J., & Bodin, P. (2002). Aftershock triggering by complete Coulomb stress changes. *Journal of Geophysical Research*, 107(B4), ESE–2.
- King, T. R., Quigley, M., & Clark, D. (2019). Surface-rupturing historical earthquakes in Australia and their environmental effects: New insights from re-analyses of observational data. *Geosciences*, 9(10), 408.
- King, G. C. P., Stein, R. S., & Lin, J. (1994). Static stress changes and the triggering of earthquakes. *Bulletin of the Seismological Society of America*, 84(3), 935–953.
- Kirby, E., Johnson, C., Furlong, K., & Heimsath, A. (2007). Transient channel incision along Bolinas Ridge, California: Evidence for differential rock uplift adjacent to the San Andreas Fault. *Journal of Geophysical Research*, 112, F03S07. <https://doi.org/10.1029/2006JF000559>
- Kirby, E., Whipple, K., & Harkins, N. (2008). Topography reveals seismic hazard. *Nature Geoscience*, 1, 485–487.
- Kirby, E., Whipple, K. X., Tang, W., & Chen, Z. (2003). Distribution of active rock uplift along the eastern margin of the Tibetan Plateau: Inferences from bedrock channel longitudinal profiles. *Journal of Geophysical Research*, 108(2217), 2217.
- Koehn, D., Lindenfeld, M., Rmpker, G., Aanyu, K., Haines, S., Passchier, C. W., & Sachau, T. (2010). Active transsection faults in rift transfer zones: Evidence for complex stress fields and implications for crustal fragmentation processes in the western branch of the East African Rift. *International Journal of Earth Sciences*, 99(7), 1633–1642. <https://doi.org/10.1007/s00531-010-0525-2>
- Kondo, H., Toda, S., Okumura, K., Takada, K., & Chiba, T. (2008). A fault scarp in an urban area identified by LiDAR survey: A case study on the Itoigawa-Shizuoka Tectonic Line, central Japan. *Geomorphology*, 101(4), 731–739.
- Korup, O. (2012). Earth's portfolio of extreme sediment transport events. *Earth-Science Reviews*, 112(3–4), 115–125. <https://doi.org/10.1016/j.earscirev.2012.02.006>
- Kuramoto, Y. (1975). Self-entrainment of a population of coupled non-linear oscillators. In H. Araki (Ed.), *International symposium on mathematical problems in theoretical physics* (Vol. 39, pp. 420–422). Berlin/Heidelberg: Springer-Verlag. <https://doi.org/10.1007/BFb0013365>
- Lague, D. (2014). The stream power river incision model: Evidence, theory and beyond. *Earth Surface Processes and Landforms*, 39(1), 38–61.
- Lal, D. (1991). Cosmic ray labeling of erosion surfaces: In situ nuclide production rates and erosion models. *Earth and Planetary Science Letters*, 104, 424–439.
- Lavé, J., & Avouac, J.-P. (2000). Active folding of fluvial terraces across the Siwaliks Hills, Himalayas of central Nepal. *Journal of Geophysical Research*, 105(B3), 5735–5770.
- Lavé, J., & Avouac, J. P. (2001). Fluvial incision and tectonic uplift across the Himalayas of central Nepal. *Journal of Geophysical Research*, 106(B11), 26,561–26,591.
- Lawson, A. C., & Reid, H. F. (1908). *The california earthquake of April 18, 1906: Report of the state earthquake investigation commission...* Washington: Carnegie institution of Washington.
- Leonard, M. (2010). Earthquake fault scaling: Self-consistent relating of rupture length, width, average displacement, and moment release. *Bulletin of the Seismological Society of America*, 100(5A), 1971–1988.
- Lienkaemper, J. J., & Ramsey, C. B. (2009). OxCal: Versatile tool for developing paleoearthquake chronologies—A primer. *Seismological Research Letters*, 80(3), 431–434.
- Lifton, Z. M., Frankel, K. L., & Newman, A. V. (2015). Latest Pleistocene and Holocene slip rates on the Lone Mountain fault: Evidence for accelerating slip in the Silver Peak-Lone Mountain extensional complex. *Tectonics*, 34(3), 449–463. <https://doi.org/10.1002/2013TC003512>
- Lin, Z., Kaneda, H., Mukoyama, S., Asada, N., & Chiba, T. (2013). Detection of subtle tectonic-geomorphic features in densely forested mountains by very high-resolution airborne lidar survey. *Geomorphology*, 182, 104–115.
- Lindsey, E. O., & Fialko, Y. (2013). Geodetic slip rates in the southern San Andreas Fault system: Effects of elastic heterogeneity and fault geometry. *Journal of Geophysical Research: Solid Earth*, 118, 689–697. <https://doi.org/10.1029/2012JB009358>
- Litchfield, N. J. (2001). The Titiri Fault System: Quaternary-active faults near the leading edge of the Otago reverse fault province. *New Zealand Journal of Geology and Geophysics*, 44(4), 517–534.
- Litchfield, N. J., & Norris, R. J. (2000). Holocene motion on the Akatore fault, south Otago coast, New Zealand. *New Zealand Journal of Geology and Geophysics*, 43(3), 405–418.
- Liu, Q. (2013). *Broadband simulation with physics-based seismic source models*. Santa Barbara: University of California.
- Liu, M., Shen, Y., & Yang, Y. (2000). Gravitational collapse of orogenic crust: A preliminary three-dimensional finite element study. *Journal of Geophysical Research*, 105(B2), 3159–3173.
- Liu, M., & Stein, S. (2016). Mid-continental earthquakes: Spatiotemporal occurrences, causes, and hazards. *Earth-Science Reviews*, 162, 364–386.
- Liu, M., Stein, S., & Wang, H. (2011). 2000 years of migrating earthquakes in North China: How earthquakes in midcontinents differ from those at plate boundaries. *Lithosphere*, 3(2), 128–132.
- Loveless, J. P., & Meade, B. J. (2011). Partitioning of localized and diffuse deformation in the Tibetan Plateau from joint inversions of geologic and geodetic observations. *Earth and Planetary Science Letters*, 303(1–2), 11–24. <https://doi.org/10.1016/j.epsl.2010.12.014>
- Lovon, H., Tarque, N., Silva, V., & Yépez-Estrada, C. (2018). Development of fragility curves for confined masonry buildings in Lima, Peru. *Earthquake Spectra*, 34(3), 1339–1361.
- Lozos, J. C. (2016). A case for historic joint rupture of the San Andreas and San Jacinto faults. *Science Advances*, 2(3), e1500621. <https://doi.org/10.1126/sciadv.1500621>
- Lozos, J. C., Oglesby, D. D., Brune, J. N., & Olsen, K. B. (2012). Small intermediate fault segments can either aid or hinder rupture propagation at stepovers. *Geophysical Research Letters*, 39, L18305. <https://doi.org/10.1029/2012GL053005>
- Luttrell, K., & Sandwell, D. (2010). Ocean loading effects on stress at near shore plate boundary fault systems. *Journal of Geophysical Research*, 115, B08411. <https://doi.org/10.1029/2009JB006541>
- Lyakhovsky, V., Ben-Zion, Y., & Agnon, A. (2001). Earthquake cycle, fault zones, and seismicity patterns in a rheologically layered lithosphere. *Journal of Geophysical Research*, 106(B3), 4103–4120. <https://doi.org/10.1029/2000JB900218>

- Lynch, J. C., Brigmann, R., Richards, M. A., & Ferencz, R. M. (2003). When faults communicate: Viscoelastic coupling and earthquake clustering in a simple two-fault system. *Geophysical Research Letters*, 30(6), 1270. <https://doi.org/10.1029/2002GL016765>
- Machette, M. N. (1984). Preliminary investigations of late Quaternary slip rates along the southern part of the Wasatch fault zone, central Utah. In *Proceedings of Conference XXVI; A Workshop on Evaluation of Regional and Urban Earthquake Hazards and Risk in Utah, Conference XXVI*, Citeseer, pp. 391–406.
- Machette, M. N., Personius, S. F., Nelson, A. R., Schwartz, D. P., & Lund, W. R. (1991). The Wasatch fault zone, Utah—Segmentation and history of Holocene earthquakes. *Journal of Structural Geology*, 13(2), 137–149. [https://doi.org/10.1016/0191-8141\(91\)90062-N](https://doi.org/10.1016/0191-8141(91)90062-N)
- Mackenzie, D., & Elliott, A. (2017). Untangling tectonic slip from the potentially misleading effects of landform geometry. *Geosphere*, 13(4), 1310–1328.
- Maesano, F. E., D'Ambrogi, C., Burrato, P., & Toscani, G. (2015). Slip-rates of blind thrusts in slow deforming areas: Examples from the Po Plain (Italy). *Tectonophysics*, 643, 8–25.
- Main, I. G., Leonard, T., Papasouliotis, O., Hatton, C. G., & Meredith, P. G. (1999). One slope or two? Detecting statistically significant breaks of slope in geophysical data, with application to fracture scaling relationships. *Geophysical Research Letters*, 26(18), 2801–2804. <https://doi.org/10.1029/1999GL005372>
- Mandelbrot, B. B. (1977). *Fractals: Form, chance, and dimension*, vol. 706. San Francisco: WH Freeman San Francisco.
- Mann, P., Demets, C., & Wiggins-Grandison, M. (2007). Toward a better understanding of the Late Neogene strike-slip restraining bend in Jamaica: Geodetic, geological, and seismic constraints. *Geological Society, London, Special Publications*, 290(1), 239–253. <https://doi.org/10.1144/SP290.8>
- Marrero, S. M., Phillips, F. M., Borchers, B., Lifton, N., Aumer, R., & Balco, G. (2016). Cosmogenic nuclide systematics and the CRONUScal program. *Quaternary Geochronology*, 31, 160–187. <https://doi.org/10.1016/j.quageo.2015.09.005>
- Massonnet, D., & Feigl, K. L. (1998). Radar interferometry and its application to changes in the Earth's surface. *Reviews of Geophysics*, 36(4), 441–500. <https://doi.org/10.1029/97RG03139>
- Matthews, M. V., Ellsworth, W. L., & Reasenberg, P. A. (2002). A Brownian model for recurrent earthquakes. *Bulletin of the Seismological Society of America*, 92(6), 2233–2250.
- McCalpin, J. P. (2009). *Paleoseismology*, vol. 95. San Diego: Academic press.
- McGuire, R. K. (2004). Seismic hazard and risk analysis. Earthquake Engineering Research Institute.
- Meade, B. J., DeVries, P. M. R., Faller, J., Viegas, F., & Wattenberg, M. (2017). What is better than Coulomb failure stress? A ranking of scalar static stress triggering mechanisms from 105 mainshock-aftershock pairs. *Geophysical Research Letters*, 44, 11,409–11,416. <https://doi.org/10.1002/2017GL075875>
- Meade, B. J., Hager, B. H., McClusky, S. C., Reilinger, R. E., Ergintav, S., Lenk, O., et al. (2002). Estimates of seismic potential in the Marmara Sea region from block models of secular deformation constrained by Global Positioning System measurements. *Bulletin of the Seismological Society of America*, 92(1), 208–215. <https://doi.org/10.1785/0120000837>
- Meigs, A. (2013). Active tectonics and the LiDAR revolution. *Lithosphere*, 5(2), 226–229.
- Mencin, D., Bendick, R., Upadhyay, B. N., Adhikari, D. P., Gajurel, A. P., Bhattacharai, R. R., et al. (2016). Himalayan strain reservoir inferred from limited afterslip following the Gorkha earthquake. *Nature Geoscience*, 9(7), 533.
- Meng, L., Ampuero, J.-P., Stock, J., Duputel, Z., Luo, Y., & Tsai, V. C. (2012). Earthquake in a maze: Compressional rupture branching during the 2012 Mw 8.6 Sumatra earthquake. *Science*, 337(6095), 724–726.
- Mildon, Z. K., Roberts, G. P., Faure Walker, J. P., & Iezzi, F. (2017). Coulomb stress transfer and fault interaction over millennia on non-planar active normal faults: The Mw 6.5–5.0 seismic sequence of 2016–2017, central Italy. *Geophysical Journal International*, 210(2), 1206–1218.
- Milliner, CWD, Dolan, J. F., Hollingsworth, J., Leprince, S., Ayoub, F., & Sammis, C. G. (2015). Quantifying near-field and off-fault deformation patterns of the 1992 Mw 7.3 Landers earthquake. *Geochemistry, Geophysics, Geosystems*, 16, 1577–1598. <https://doi.org/10.1002/2014GC005693>
- Milodowski, D. T., Mudd, S. M., & Mitchard, E. T. A. (2015). Topographic roughness as a signature of the emergence of bedrock in eroding landscapes. *Earth Surface Dynamics*, 3(4), 483–499.
- Minster, J. B., & Jordan, T. H. (1987). Vector constraints on western U.S. deformation from space geodesy, neotectonics, and plate motions. *Journal of Geophysical Research*, 92(B6), 4798. <https://doi.org/10.1029/JB092iB06p04798>
- Mitchell, S. G., Matmon, A., Bierman, P. R., Enzel, Y., Caffee, M., & Rizzo, D. (2001). Displacement history of a limestone normal fault scarp, northern Israel, from cosmogenic ^{36}Cl . *Journal of Geophysical Research*, 106(B3), 4247–4264.
- Moernaut, J., Van Daele, M., Fontijn, K., Heirman, K., Kempf, P., Pino, M., et al. (2018). Larger earthquakes recur more periodically: New insights in the megathrust earthquake cycle from lacustrine turbidite records in south-central Chile. *Earth and Planetary Science Letters*, 481, 9–19.
- Mohadjer, S., Ehlers, T. A., Bendick, R., & Mutz, S. G. (2017). Review of GPS and Quaternary fault slip rates in the Himalaya-Tibet orogen. *Earth-Science Reviews*, 174(Supplement C), 39–52.
- Molnar, P., Anderson, R. S., & Anderson, S. P. (2007). Tectonics, fracturing of rock, and erosion. *Journal of Geophysical Research*, 112, F03014. <https://doi.org/10.1029/2005JF000433>
- Morell, K. D., Regalla, C., Amos, C., Bennett, S., Leonard, L., Graham, A., et al. (2018). Holocene surface rupture history of an active forearc fault redefines seismic hazard in southwestern British Columbia, Canada. *Geophysical Research Letters*, 45, 11,605–11,611. <https://doi.org/10.1029/2018GL078711>
- Morell, K. D., Regalla, C., Leonard, L. J., Amos, C., & Levson, V. (2017). Quaternary rupture of a crustal fault beneath Victoria, British Columbia, Canada. *GSA Today*, 27(3), 4–10.
- Mouslopoulou, V., Nicol, A., Walsh, J. J., Begg, J. G., Townsend, D. B., & Hristopulos, D. T. (2012). Fault-slip accumulation in an active rift over thousands to millions of years and the importance of paleoearthquake sampling. *Journal of Structural Geology*, 36, 71–80.
- Mouslopoulou, V., Oncken, O., Hainzl, S., & Nicol, A. (2016). Uplift rate transients at subduction margins due to earthquake clustering. *Tectonics*, 35(10), 2370–2384.
- Mouslopoulou, V., Walsh, J. J., & Nicol, A. (2009). Fault displacement rates on a range of timescales. *Earth and Planetary Science Letters*, 278(3–4), 186–197.
- Nicol, A., Walsh, J., Mouslopoulou, V., & Villamor, P. (2009). Earthquake histories and Holocene acceleration of fault displacement rates. *Geology*, 37(10), 911–914.
- Nicol, A., Walsh, J. J., Villamor, P., Seebeck, H., & Berryman, K. R. (2010). Normal fault interactions, paleoearthquakes and growth in an active rift. *Journal of Structural Geology*, 32(8), 1101–1113. <https://doi.org/10.1016/j.jsg.2010.06.018>
- Nicol, A., Walsh, J. J., Watterson, J., & Underhill, J. R. (1997). Displacement rates of normal faults. *Nature*, 390(6656), 157–159. <https://doi.org/10.1038/36548>

- Nishenko, S. P., & Buland, R. (1987). A generic recurrence interval distribution for earthquake forecasting. *Bulletin of the Seismological Society of America*, 77(4), 1382–1399.
- Nocquet, J.-M., Jarrin, P., Vallée, M., Mothes, P. A., Grandin, R., Rolandone, F., et al. (2017). Supercycle at the Ecuadorian subduction zone revealed after the 2016 Pedernales earthquake. *Nature Geoscience*, 10(2), 145–149.
- Nomura, S., Ogata, Y., Komaki, F., & Toda, S. (2011). Bayesian forecasting of recurrent earthquakes and predictive performance for a small sample size. *Journal of Geophysical Research*, 116, B04315. <https://doi.org/10.1029/2010JB007917>
- Norris, R. J. (2004). Strain localisation within ductile shear zones beneath active faults. *Earth, planets and space*, 56(12), 1095–1101.
- Obermeier, S. F. (1996). Use of liquefaction-induced features for paleoseismic analysis? an overview of how seismic liquefaction features can be distinguished from other features and how their regional distribution and properties of source sediment can be used to infer the location and strength of holocene paleo-earthquakes. *Engineering Geology*, 44(1–4), 1–76.
- Ogata, Y. (1999). Estimating the hazard of rupture using uncertain occurrence times of paleoearthquakes. *Journal of Geophysical Research*, 104(B8), 17,995–18,014.
- Oglesby, D. D. (2005). The dynamics of strike-slip step-overs with linking dip-slip faults. *Bulletin of the Seismological Society of America*, 95(5), 1604–1622.
- Ortuño, M., Masana, E., García-Meléndez, E., Martínez-Díaz, J., Štěpánčíková, P., Cunha, P. P., et al. (2012). An exceptionally long paleoseismic record of a slow-moving fault: The Alhama de Murcia fault (Eastern Betic shear zone, Spain). *Bulletin*, 124(9–10), 1474–1494.
- Oskin, M. E., Arrowsmith, J. R., Corona, A. H., Elliott, A. J., Fletcher, J. M., Fielding, E. J., et al. (2012). Near-field deformation from the El Mayor–Cucapah earthquake revealed by differential LIDAR. *Science*, 335(6069), 702–705.
- Oskin, M., Perg, L., Blumentritt, D., Mukhopadhyay, S., & Iriondo, A. (2007). Slip rate of the Calico fault: Implications for geologic versus geodetic rate discrepancy in the Eastern California Shear Zone. *Journal of Geophysical Research*, 112, B03402. <https://doi.org/10.1029/2006JB004451>
- Oskin, M., Perg, L., Shelef, E., Strane, M., Gurney, E., Singer, B., & Zhang, X. (2008). Elevated shear zone loading rate during an earthquake cluster in eastern California. *Geology*, 36(6), 507. <https://doi.org/10.1130/G24814A.1>
- Ouimet, W. B., Whipple, K., & Granger, D. (2009). Beyond threshold hillslopes: Channel adjustment to base-level fall in tectonically active mountain ranges. *Geology*, 37(9), 579–582.
- Pérouse, E., & Wernicke, B. P. (2017). Spatiotemporal evolution of fault slip rates in deforming continents: The case of the Great Basin region, northern Basin and Range province. *Geosphere*, 13(1), 112–135.
- Page, M. T., Field, E. H., Milner, K. R., & Powers, P. M. (2014). The UCERF3 grand inversion: Solving for the long-term rate of ruptures in a fault system. *Bulletin of the Seismological Society of America*, 104(3), 1181–1204.
- Palumbo, L., Benedetti, L., Bourles, D., Cinque, A., & Finkel, R. (2004). Slip history of the Magnola fault (Apennines, Central Italy) from ^{36}Cl surface exposure dating: Evidence for strong earthquakes over the Holocene. *Earth and Planetary Science Letters*, 225(1–2), 163–176.
- Pérouse, E., & Wernicke, B. P. (2017). Spatiotemporal evolution of fault slip rates in deforming continents: The case of the Great Basin region, northern Basin and Range province. *Geosphere*, 13(1), 112–135. <https://doi.org/10.1130/GES01295.1>
- Penarubia, C., Kendra, J., Styron, R. H., Sevilla, W. I. G., Perez, J. S., Bonita, J. D., et al. (2019). Probabilistic seismic hazard analysis model for the Philippines. *Earthquake Spectra*.
- Penserini, B. D., Roering, J. J., & Streig, A. (2017). A morphologic proxy for debris flow erosion with application to the earthquake deformation cycle, Cascadia Subduction Zone, USA. *Geomorphology*, 282, 150–161.
- Perfettini, H., & Avouac, J.-P. (2007). Modeling afterslip and aftershocks following the 1992 Landers earthquake. *Journal of Geophysical Research*, 112, B07409. <https://doi.org/10.1029/2006JB004399>
- Perron, J. T., & Royden, L. (2013). An integral approach to bedrock river profile analysis. *Earth Surface Processes and Landforms*, 38(6), 570–576.
- Personius, S. F., Briggs, R. W., Nelson, A. R., Schermer, E. R., Maharry, J. Z., Sherrod, B. L., et al. (2014). Holocene earthquakes and right-lateral slip on the left-lateral Darrington–Devils Mountain fault zone, northern Puget Sound, Washington. *Geosphere*, 10(6), 1482–1500.
- Petersen, M. D., Moschetti, M. P., Powers, P. M., Mueller, C. S., Haller, K. M., Frankel, A. D., et al. (2015). The 2014 United States national seismic hazard model. *Earthquake Spectra*, 31(S1), S1–S30.
- Petersen, M. D., Zeng, Y., Haller, K. M., McCaffrey, R., Hammond, W. C., Bird, P., et al. (2014). Geodesy- and geology-based slip-rate models for the Western United States (excluding California) national seismic hazard maps (2013–2023). Reston, VA: U.S. Geological Survey.
- Peterson, C. D., Carver, G. A., Cruikshank, K. M., Abramson, H. F., Garrison-Laney, C. E., & Dengler, L. A. (2011). Evaluation of the use of paleotsunami deposits to reconstruct inundation distance and runup heights associated with prehistoric inundation events, Crescent City, southern Cascadia margin. *Earth Surface Processes and Landforms*, 36(7), 967–980.
- Philibosian, B., & Meltzner, A. J. (2020). Segmentation and supercycles: A catalog of earthquake rupture patterns from the Sumatran Sunda Megathrust and other well-studied faults worldwide. *Quaternary Science Reviews*, 241, 106,390.
- Philibosian, B., Sieh, K., Avouac, J.-P., Natawidjaja, D. H., Chiang, H.-W., Wu, C.-C., et al. (2017). Earthquake supercycles on the Mentawai segment of the Sunda megathrust in the seventeenth century and earlier. *Journal of Geophysical Research: Solid Earth*, 122, 642–676. <https://doi.org/10.1002/2016JB013560>
- Phillips, F. M., Argento, D. C., Balco, G., Caffee, M. W., Clem, J., Dunai, T. J., et al. (2016). The CRONUS-Earth project: A synthesis. *Quaternary Geochronology*, 31, 119–154. <https://doi.org/10.1016/j.quageo.2015.09.006>
- Pollitz, F., Vergnolle, M., & Calais, E. (2003). Fault interaction and stress triggering of twentieth century earthquakes in Mongolia. *Journal of Geophysical Research*, 108(B10), 2503. <https://doi.org/10.1029/2002JB002375>
- Power, W. L., Tullis, T. E., Brown, S. R., Boitnott, G. N., & Scholz, C. H. (1987). Roughness of natural fault surfaces. *Geophysical Research Letters*, 14(1), 29–32.
- Pownall, J. M., Hall, R., & Lister, G. S. (2016). Rolling open Earth's deepest forearc basin. *Geology*, 44(11), 947–950.
- Prawirodirjo, L., Bocel, Y., McCaffrey, R., Genrich, J., Calais, E., Stevens, C., et al. (1997). Geodetic observations of interseismic strain segmentation at the Sumatra subduction zone. *Geophysical Research Letters*, 24(21), 2601–2604. <https://doi.org/10.1029/97GL52691>
- Prush, V., & Oskin, M. E. (2020). A mechanistic erosion model for cosmogenic nuclide inheritance in fluvial single-clast exposure ages. *Earth and Planetary Science Letters*.
- Quigley, M. C., Hughes, M. W., Bradley, B. A., van Ballegooij, S., Reid, C., Morgenroth, J., et al. (2016). The 2010–2011 Canterbury earthquake sequence: Environmental effects, seismic triggering thresholds and geologic legacy. *Tectonophysics*, 672, 228–274.
- Quigley, M., Van Dissen, R., Litchfield, N., Villamor, P., Duffy, B., Barrell, D., et al. (2012). Surface rupture during the 2010 M_w 7.1 Darfield (Canterbury) earthquake: Implications for fault rupture dynamics and seismic-hazard analysis. *Geology*, 40(1), 55–58.

- Reid, H. F. (1910). The mechanics of the earthquake. The California Earthquake of April 18, 1906, Report of the State Earthquake Investigation Commission.
- Reitman, N. G., Mueller, K. J., Tucker, G. E., Gold, R. D., Briggs, R. W., & Barnhart, K. R. (2019). Offset channels may not accurately record strike-slip fault displacement: Evidence from landscape evolution models. *Journal of Geophysical Research: Solid Earth*, 124, 13,427–13,451. <https://doi.org/10.1029/2019JB018596>
- Ren, J., Xu, X., Yeats, R. S., & Zhang, S. (2013). Latest Quaternary paleoseismology and slip rates of the Longriba fault zone, eastern Tibet: Implications for fault behavior and strain partitioning. *Tectonics*, 32(2), 216–238. <https://doi.org/10.1002/tect.20029>
- Renard, F., & Candela, T. (2017). Scaling of fault roughness and implications for earthquake mechanics. *Fault Zone Dynamic Processes: Evolution of Fault Properties During Seismic Rupture*, 227, 197–216.
- Renard, F., Candela, T., & Bouchaud, E. (2013). Constant dimensionality of fault roughness from the scale of micro-fractures to the scale of continents. *Geophysical Research Letters*, 40, 83–87. <https://doi.org/10.1029/2012GL054143>
- Rhoades, D. A., Van Dissen, R. J., & Dowrick, D. J. (1994). On the handling of uncertainties in estimating the hazard of rupture on a fault segment. *Journal of Geophysical Research*, 99(B7), 13,701–13,712.
- Rockwell, T. (2010). The non-regularity of earthquake recurrence in California: Lessons from long paleoseismic records from the San Andreas and San Jacinto faults in Southern California, and the north Anatolian fault in Turkey.
- Rockwell, T. K., Dawson, T. E., Ben-Horin, J. Y., & Seitz, G. (2015). A 21-event, 4,000-year history of surface ruptures in the Anza seismic gap, San Jacinto Fault, and implications for long-term earthquake production on a major plate boundary fault. *Pure and Applied Geophysics*, 172(5), 1143–1165.
- Rodríguez Pascua, M. A., Abad Casal, L., Pérez López, R., Gamo Parras, B., Silva Barroso, P. G., Garduño Monroy, V. H., et al. (2013). Roman, Visigothic and Islamic evidence of earthquakes recorded in the archaeological site of “El Tolmo de Minateda” (Prebetic Zone, southeast of Spain). *Cuaternario y Geomorfología*, 27, 83–90.
- Roering, J. J. (2008). How well can hillslope evolution models ‘explain’ topography? Simulating soil transport and production with high-resolution topographic data. *Geological Society of America Bulletin*, 120(9–10), 1248–1262.
- Rosen, P. A., Hensley, S., Joughin, I. R., Li, F. K., Madsen, S. N., Rodriguez, E., & Goldstein, R. M. (2000). Synthetic aperture radar interferometry. *Proceedings of the IEEE*, 88(3), 333–382.
- Ross, Z. E., Idini, B., Jia, Z., Stephenson, O. L., Zhong, M., Wang, X., et al. (2019). Hierarchical interlocked orthogonal faulting in the 2019 Ridgecrest earthquake sequence. *Science*, 366(6463), 346–351.
- Roy, M. (1998). Evolution of fault systems at a strike-slip plate boundary: A viscoelastic model. *Geophysical Research Letters*, 25(15), 2881–2884. <https://doi.org/10.1029/98GL02184>
- Roy, S. G., Tucker, G. E., Koons, P. O., Smith, S. M., & Upton, P. (2016). A fault runs through it: Modeling the influence of rock strength and grain-size distribution in a fault-damaged landscape. *Journal of Geophysical Research: Earth Surface*, 121, 1911–1930. <https://doi.org/10.1002/2015JF003662>
- Rubin, C. M., Horton, B. P., Sieh, K., Pilarczyk, J. E., Daly, P., Ismail, N., & Parnell, A. C. (2017). Highly variable recurrence of tsunamis in the 7,400 years before the 2004 Indian Ocean tsunami. *Nature Communications*, 8, 16,019.
- Ryder, I., Brägmann, R., & Fielding, E. (2012). Static stress interactions in extensional earthquake sequences: An example from the South Lunggar Rift, Tibet. *Journal of Geophysical Research*, 117, B09405. <https://doi.org/10.1029/2012JB009365>
- Salditch, L., Stein, S., Neely, J., Spencer, B. D., Brooks, E. M., Agnon, A., & Liu, M. (2020). Earthquake supercycles and Long-Term Fault Memory. *Tectonophysics*, 774, 228,289.
- Sandiford, M. I. K. E. (2003). Neotectonics of southeastern Australia: Linking the Quaternary faulting record with seismicity and in situ stress. Special Papers—Geological Society of America, 107–120.
- Savage, J. C., & Prescott, W. H. (1978). Asthenosphere readjustment and the earthquake cycle. *Journal of Geophysical Research*, 83, 3369–3376. <https://doi.org/10.1029/JB083iB07p03369>
- Scharer, K. M., Biasi, G. P., Weldon, R. J., & Fumal, T. E. (2010). Quasi-periodic recurrence of large earthquakes on the southern San Andreas Fault. *Geology*, 38(6), 555–558.
- Scharer, K. M., Weldon, R. J., Fumal, T. E., & Biasi, G. P. (2007). Paleoearthquakes on the southern San Andreas Fault, Wrightwood, California, 3000 to 1500 BC: A new method for evaluating paleoseismic evidence and earthquake horizons. *Bulletin of the Seismological Society of America*, 97(4), 1054–1093.
- Scholz, C. H. (2010). Large earthquake triggering, clustering, and the synchronization of faults. *Bulletin of the Seismological Society of America*, 100(3), 901–909. <https://doi.org/10.1785/0120090309>
- Scholz, C. H., Aviles, C. A., & Wesnousky, S. G. (1986). Scaling differences between large interplate and intraplate earthquakes. *Bulletin of the Seismological Society of America*, 76(1), 65–70.
- Seeber, L., & Gornitz, V. (1983). River profiles along the Himalayan arc as indicators of active tectonics. *Tectonophysics*, 92(4), 335–367.
- Shaw, B. E. (2009). Constant stress drop from small to great earthquakes in magnitude-area scaling. *Bulletin of the Seismological Society of America*, 99(2A), 871–875.
- Shaw, B. E. (2013). Earthquake surface slip-length data fit by constant stress drop and is useful for seismic hazard analysis. *Bulletin of the Seismological Society of America*, 103(2A), 876–893.
- Shen, Z.-K., Lü, J., Wang, M., & Bürgmann, R. (2005). Contemporary crustal deformation around the southeast borderland of the Tibetan Plateau. *Journal of Geophysical Research*, 110, B11409. <https://doi.org/10.1029/2004JB003421>
- Sherrod, B. L., Blakely, R. J., Lasher, J. P., Lamb, A., Mahan, S. A., Foit Jr, F. F., & Barnett, E. A. (2016). Active faulting on the Wallula fault zone within the Olympic-Wallowa lineament, Washington State, USA. *Bulletin*, 128(11–12), 1636–1659.
- Sherrod, B., & Gomberg, J. (2014). Crustal earthquake triggering by pre-historic great earthquakes on subduction zone thrusts. *Journal of Geophysical Research: Solid Earth*, 119, 1273–1294. <https://doi.org/10.1002/2013JB010635>
- Shirzaei, M., & Brägmann, R. (2013). Time-dependent model of creep on the Hayward fault from joint inversion of 18 years of InSAR and surface creep data. *Journal of Geophysical Research: Solid Earth*, 118, 1733–1746. <https://doi.org/10.1002/jgrb.50149>
- Sieh, K. E. (1978). Prehistoric large earthquakes produced by slip on the San Andreas fault at Pallett Creek, California. *Journal of Geophysical Research*, 83(B8), 3907–3939.
- Sieh, K. E., & Jahns, R. H. (1984). Holocene activity of the San Andreas Fault at Wallace Creek, California. *Geological Society of America Bulletin*, 95(8), 883–896.
- Sieh, K., Natawidjaja, D. H., Meltzner, A. J., Shen, C.-C., Cheng, H., Li, K.-S., et al. (2008). Earthquake supercycles inferred from sea-level changes recorded in the corals of west Sumatra. *Science*, 322(5908), 1674–1678.
- Sklar, L. S., & Dietrich, W. E. (2001). Sediment and rock strength controls on river incision into bedrock. *Geology*, 29(12), 1087–1090.
- Speth, G. T., Amos, C. B., Amidon, W. H., Balco, G., Meigs, A. J., & Graf, S. (2019). Glacial chronology and slip rate on the west Klamath Lake fault zone, Oregon. *Geological Society of America Bulletin*, 131(3–4), 444–460. <https://doi.org/10.1130/B31961.1>

- Stafford, P. J. (2014). Source-scaling relationships for the simulation of rupture geometry within probabilistic seismic-hazard analysis. *Bulletin of the Seismological Society of America*, 104(4), 1620–1635.
- Stahl, T., Quigley, M. C., McGill, A., & Bebbington, M. S. (2016). Modeling earthquake moment magnitudes on imbricate reverse faults from paleoseismic data: Fox peak and forest creek faults, South Island, New Zealand. *Bulletin of the Seismological Society of America*, 106(5), 2345–2363.
- Steidl, J. H., Archuleta, R. J., & Hartzell, S. H. (1991). Rupture history of the 1989 Loma Prieta, California, earthquake. *Bulletin of the Seismological Society of America*, 81(5), 1573–1602.
- Stein, R. S., Barka, A. A., & Dieterich, J. H. (1997). Progressive failure on the North Anatolian fault since 1939 by earthquake stress triggering. *Geophysical Journal International*, 128(3), 594–604. <https://doi.org/10.1111/j.1365-246X.1997.tb05321.x>
- Stein, S., Geller, R. J., & Liu, M. (2012). Why earthquake hazard maps often fail and what to do about it. *Tectonophysics*, 562, 1–25.
- Stirling, M. W., & Anderson, J. G. (2018). Magnitude as a function of rupture length and slip rate for recent large New Zealand Earthquakes – Magnitude as a function of rupture length and slip rate. *Bulletin of the Seismological Society of America*, 108(3B), 1623–1629.
- Stirling, M., Gerstenberger, M., Litchfield, N., McVerry, G., Smith, W., Pettinga, J., & Barnes, P. (2008). Seismic hazard of the Canterbury region, New Zealand: New earthquake source model and methodology. *Bulletin of the New Zealand Society for Earthquake Engineering*, 41(2), 51–67.
- Stirling, M., Goded, T., Berryman, K., & Litchfield, N. (2013). Selection of earthquake scaling relationships for seismic-hazard analysis. *Bulletin of the Seismological Society of America*, 103(6), 2993–3011.
- Stirling, M., McVerry, G., Gerstenberger, M., Litchfield, N., Van Dissen, R., Berryman, K., et al. (2012). National seismic hazard model for New Zealand: 2010 update. *Bulletin of the Seismological Society of America*, 102(4), 1514–1542.
- Stirling, M., Rhoades, D., & Berryman, K. (2002). Comparison of earthquake scaling relations derived from data of the instrumental and preinstrumental era. *Bulletin of the Seismological Society of America*, 92(2), 812–830.
- Stirling, M. W., Wesnousky, S. G., & Shimazaki, K. (1996). Fault trace complexity, cumulative slip, and the shape of the magnitude-frequency distribution for strike-slip faults: A global survey. *Geophysical Journal International*, 124(3), 833–868.
- Strogatz, S. H. (2000). From Kuramoto to Crawford: Exploring the onset of synchronization in populations of coupled oscillators. *Physica D: Nonlinear Phenomena*, 143(1), 1–20. [https://doi.org/10.1016/S0167-2789\(00\)00094-4](https://doi.org/10.1016/S0167-2789(00)00094-4)
- Strogatz, S. (2004). *Sync: The emerging science of spontaneous order*. UK: Penguin.
- Stucchi, M., Meletti, C., Montaldo, V., Crowley, H., Calvi, G. M., & Boschi, E. (2011). Seismic hazard assessment (2003–2009) for the Italian building code. *Bulletin of the Seismological Society of America*, 101(4), 1885–1911.
- Styron, R. (2019). The impact of earthquake cycle variability on neotectonic and paleoseismic slip rate estimates. *Solid Earth*, 10(1), 15–25. <https://doi.org/10.5194/se-10-15-2019>
- Swan III, F. H., Schwartz, D. P., & Cluff, L. S. (1980). Recurrence of moderate to large magnitude earthquakes produced by surface faulting on the Wasatch fault zone, Utah. *Bulletin of the Seismological Society of America*, 70(5), 1431–1462.
- Tachikawa, T., Hato, M., Kaku, M., & Iwasaki, A. (2011). Characteristics of ASTER GDEM version 2. In *2011 IEEE international geoscience and remote sensing symposium*, IEEE, pp. 3657–3660.
- Tamura, Y., Sato, T., Ooe, M., & Ishiguro, M. (1991). A procedure for tidal analysis with a Bayesian information criterion. *Geophysical Journal International*, 104(3), 507–516. <https://doi.org/10.1111/j.1365-246X.1991.tb05697.x>
- Taylor-Silva, B. I., Stirling, M. W., Litchfield, N. J., Griffin, J. D., van den Berg, E. J., & Wang, N. (2019). Paleoseismology of the Akatore Fault, Otago, New Zealand. *New Zealand Journal of Geology and Geophysics*, 1–17.
- Thackray, G. D., & Staley, A. E. (2017). Systematic variation of Late Pleistocene fault scarp height in the Teton Range, Wyoming, USA: Variable fault slip rates or variable landform ages? *Geosphere*, 13(2), 287–300.
- Thingbaijam, K. K. S., Martin Mai, P., & Goda, K. (2017). New empirical earthquake source-scaling laws. *Bulletin of the Seismological Society of America*, 107(5), 2225–2246.
- Thompson, S. C., Weldon, R. J., Rubin, C. M., Abdulkhamatov, K., Molnar, P., & Berger, G. W. (2002). Late Quaternary slip rates across the central Tien Shan, Kyrgyzstan, central Asia. *Journal of Geophysical Research*, 107(B9), ETG 7-1-ETG 7-32.
- Townend, J., & Zoback, M. D. (2006). Stress, strain, and mountain building in central Japan. *Journal of Geophysical Research*, 111, B03411. <https://doi.org/10.1029/2005JB003759>
- Tsodoulos, I. M., Stamoulis, K., Caputo, R., Koukouvelas, I., Chatzipetros, A., Pavlides, S., et al. (2016). Middle-Late Holocene earthquake history of the Gyrtoni Fault, Central Greece: Insight from optically stimulated luminescence (OSL) dating and paleoseismology. *Tectonophysics*, 687, 14–27.
- Turowski, J. M., Yager, E. M., Badoux, A., Rickenmann, D., & Molnar, P. (2009). The impact of exceptional events on erosion, bedload transport and channel stability in a step-pool channel. *Earth Surface Processes and Landforms*, 34(12), 1661–1673.
- USGS (2015). M 7.8–36 km E of Khudi, Nepal. USGS, http://earthquake.usgs.gov/earthquakes/eventpage/us20002926/#general_summary
- USGS (2016). USGS, executive summary of M7.8 Amberley, New Zealand earthquake. USGS, <https://earthquake.usgs.gov/earthquakes/eventpage/us1000778i-executive>
- Vallage, A., & Bollinger, L. (2019). Testing fault models in intraplate settings: A potential for challenging the seismic hazard assessment inputs and hypothesis? *Pure and Applied Geophysics*, 117, 1879–1889.
- van Der Woerd, J., Tappouner, P., Ryerson, F. J., Meriaux, A.-S., Meyer, B., Gaudemer, Y., et al. (2002). Uniform postglacial slip-rate along the central 600 km of the Kunlun Fault (Tibet), from ^{26}Al , ^{10}Be , and ^{14}C dating of riser offsets, and climatic origin of the regional morphology. *Geophysical Journal International*, 148(3), 356–388.
- Van Dissen, R., Barrell, D., Langridge, R., Litchfield, N., Villamor, P., & Tonkin, P. (2006). Reassessment of seismic hazard at the Clyde Dam, Central Otago: Earthquake geology field investigations and determination of Dunstan Fault rupture characteristics. GNS Science Consultancy Report, 147.
- Vannoli, P., Burrato, P., & Valensise, G. (2015). The seismotectonics of the Po Plain (northern Italy): Tectonic diversity in a blind faulting domain. *Pure and Applied Geophysics*, 172(5), 1105–1142.
- Veloza, G., Taylor, M., Mora, A., & Gosse, J. (2015). Active mountain building along the eastern Colombian Subandes: A folding history from deformed terraces across the Tame anticline, Llanos Basin. *Geological Society of America Bulletin*, 127(9–10), 1155–1173. <https://doi.org/10.1130/B31168.1>
- Wallace, R. E. (1973). Surface fracture patterns along the San Andreas Fault. In *Proc. conf. on tectonic problems of the San Andreas Fault system*, 13, School of Earth Sciences, Stanford University Stanford, California, pp. 248–250.
- Wallace, R. E. (1987). A perspective of paleoseismology. *Direction in paleoseismology*, 7–16.
- Wallace, R. E. (1990). *The San Andreas Fault system*. California: US Government Printing Office.
- Walters, R. J., Gregory, L. C., Wedmore, L. N. J., Craig, T. J., McCaffrey, K., Wilkinson, M., et al. (2018). Dual control of fault intersections on stop-start rupture in the 2016 central Italy seismic sequence. *Earth and Planetary Science Letters*, 500, 1–14.

- Wang, T., Wei, S., Shi, X., Qiu, Q., Li, L., Peng, D., et al. (2018). The 2016 Kaikōura earthquake: Simultaneous rupture of the subduction interface and overlying faults. *Earth and Planetary Science Letters*, 482, 44–51.
- Wechsler, N., Rockwell, T. K., Klinger, Y., Štěpančíková, P., Kanari, M., Marco, S., & Agnon, A. (2014). A paleoseismic record of earthquakes for the Dead Sea transform fault between the first and seventh centuries CE: Nonperiodic behavior of a plate boundary fault. *Bulletin of the Seismological Society of America*, 104(3), 1329–1347.
- Weldon, R. J. (2011). To what extent does earthquake variability affect slip rate estimates; A test using San Andreas fault paleoseismology. *AGU Fall Meeting Abstracts*, 43, T43I-04.
- Wells, D. L., & Coppersmith, K. J. (1994). New empirical relationships among magnitude, rupture length, rupture width, rupture area, and surface displacement. *Bulletin of the Seismological Society of America*, 84(4), 974–1002.
- Wesnousky, S. G. (1994). The Gutenberg-Richter or characteristic earthquake distribution, which is it? *Bulletin of the Seismological Society of America*, 84(6), 1940–1959.
- Wesnousky, S. G. (2006). Predicting the endpoints of earthquake ruptures. *Nature*, 444(7117), 358.
- Wesnousky, S. G. (2008). Displacement and geometrical characteristics of earthquake surface ruptures: Issues and implications for seismic-hazard analysis and the process of earthquake rupture. *Bulletin of the Seismological Society of America*, 98(4), 1609–1632.
- Wesnousky, S. G., Bormann, J. M., Kreemer, C., Hammond, W. C., & Brune, J. N. (2012). Neotectonics, geodesy, and seismic hazard in the Northern Walker Lane of Western North America: Thirty kilometers of crustal shear and no strike-slip? *Earth and Planetary Science Letters*, 329–330, 133–140.
- Wesnousky, S. G., Scholz, C. H., Shimazaki, K., & Matsuda, T. (1984). Integration of geological and seismological data for the analysis of seismic hazard: A case study of Japan. *Bulletin of the Seismological Society of America*, 74(2), 687–708.
- Whipple, K. X. (2009). The influence of climate on the tectonic evolution of mountain belts. *Nature Geoscience*, 2(2), 97–104.
- Whipple, K. X., Forte, A. M., DiBiase, R. A., Gasparini, N. M., & Ouimet, W. B. (2017). Timescales of landscape response to divide migration and drainage capture: Implications for the role of divide mobility in landscape evolution. *Journal of Geophysical Research: Earth Surface*, 122, 248–273. <https://doi.org/10.1002/2016JF003973>
- Whipple, K. X., Shirzaei, M., Hodges, K. V., & Arrowsmith, J. R. (2016). Active shortening within the Himalayan orogenic wedge implied by the 2015 Gorkha earthquake. *Nature Geoscience*, 9, 711–716.
- White, B. J. P., Smith, R. B., Husen, S., Farrell, J. M., & Wong, I. (2009). Seismicity and earthquake hazard analysis of the Teton-Yellowstone region, Wyoming. *Journal of Volcanology and Geothermal Research*, 188(1–3), 277–296.
- Wilkinson, M., Roberts, G. P., McCaffrey, K., Cowie, P. A., Faure Walker, J. P., Papanikolaou, I., et al. (2015). Slip distributions on active normal faults measured from LiDAR and field mapping of geomorphic offsets: An example from L'Aquila, Italy, and implications for modelling seismic moment release. *Geomorphology*, 237, 130–141. <https://doi.org/10.1016/j.geomorph.2014.04.026>
- Willett, S. D., McCoy, S. W., Perron, J. T., Goren, L., & Chen, C.-Y. (2014). Dynamic reorganization of river basins. *Science*, 343(6175), 1248765.
- Williams, R. T., Beard, B. L., Goodwin, L. B., Sharp, W. D., Johnson, C. M., & Mozley, P. S. (2019). Radiogenic isotopes record a ‘drop in a bucket’—A fingerprint of multi-kilometer-scale fluid pathways inferred to drive fault-valve behavior. *Journal of Structural Geology*, 125, 262–269.
- Williams, R. T., Davis, J. R., & Goodwin, L. B. (2019). Do large earthquakes occur at regular intervals through time? A perspective from the geologic record. *Geophysical Research Letters*, 46, 8074–8081. <https://doi.org/10.1029/2019GL083291>
- Williams, R. T., Goodwin, L. B., Sharp, W. D., & Mozley, P. S. (2017). Reading a 400,000-year record of earthquake frequency for an intraplate fault. *Proceedings of the National Academy of Sciences*, 114(19), 4893–4898.
- Wobus, C., Whipple, K., & Hodges, K. (2006). Neotectonics of the central Nepalese Himalaya: Constraints from geomorphology, detrital $^{40}\text{Ar}/^{39}\text{Ar}$ thermochronology, and thermal modeling. *Tectonics*, 25, TC4011. <https://doi.org/10.1029/2005TC001935>
- Wobus, C., Whipple, K., Kirby, E., Snyder, N., Johnson, J., Spyropoulou, K., et al. (2006). Tectonics from topography: Procedures, promise, and pitfalls. In S. D. Willett, N. Hovius, M. T. Brandon, D. M. Fisher (Eds.), *Tectonics, climate, and landscape evolution: Geological society of america special paper 398, penrose conference series* (pp. 55–74). USA: Geological Society of America.
- Wright, T. J. (2004). InSAR observations of low slip rates on the major faults of western Tibet. *Science*, 305(5681), 236–239. <https://doi.org/10.1126/science.1096388>
- Yang, W., Qi, W., & Zhou, J. (2018). Decreased post-seismic landslides linked to vegetation recovery after the 2008 Wenchuan earthquake. *Ecological Indicators*, 89, 438–444.
- Yanites, B. J. (2018). The dynamics of channel slope, width, and sediment in actively eroding bedrock river systems. *Journal of Geophysical Research: Earth Surface*, 123, 1504–1527. <https://doi.org/10.1029/2017JF004405>
- Yen, Y.-T., & Ma, K.-F. (2011). Source-scaling relationship for M 4.6–8.9 earthquakes, specifically for earthquakes in the collision zone of Taiwan. *Bulletin of the Seismological Society of America*, 101(2), 464–481.
- Yepes-Estrada, C., Silva, V., Valcárcel, J., Acevedo, A. B., Tarque, N., Hube, M. A., et al. (2017). Modeling the residential building inventory in South America for seismic risk assessment. *Earthquake spectra*, 33(1), 299–322.
- Youngs, R. R., & Coppersmith, K. J. (1985). Implications of fault slip rates and earthquake recurrence models to probabilistic seismic hazard estimates. *Bulletin of the Seismological Society of America*, 75(4), 939–964.
- Yuan, Z., Liu-Zeng, J., Wang, W., Weldon II, R. J., Oskin, M. E., Shao, Y., et al. (2018). A 6000-year-long paleoseismologic record of earthquakes along the Xorkoli section of the Altyn Tagh fault, China. *Earth and Planetary Science Letters*, 497, 193–203.
- Zechar, J. D., & Frankel, K. L. (2009). Incorporating and reporting uncertainties in fault slip rates. *Journal of Geophysical Research*, 114, B12407. <https://doi.org/10.1029/2009JB006325>
- Zielke, O., Arrowsmith, J. R., Gran Ludwig, L., & Akçiz, S. O. (2012). High-resolution topography-derived offsets along the 1857 Fort Tejon earthquake rupture trace, San Andreas Fault. *Bulletin of the Seismological Society of America*, 102(3), 1135–1154.
- Zielke, O., Arrowsmith, J. R., Ludwig, L. G., & Akçiz, S. O. (2010). Slip in the 1857 and earlier large earthquakes along the Carrizo Plain, Aan Andreas Fault. *Science*, 327(5969), 1119–1122.
- Zinke, R., Dolan, J. F., Rhodes, E. J., Van Dissen, R., McGuire, C. P., Hatem, A. E., et al. (2019). Multimillennial incremental slip rate variability of the Clarence fault at the Tophouse Road site, Marlborough fault system, New Zealand. *Geophysical Research Letters*, 46, 717–725. <https://doi.org/10.1029/2018GL080688>